Ultimate Tensile Deformation and Strength Capacity of Shear Tab Connections

by

Chen Zhang

A thesis
submitted to the Faculty of Graduate Studies
in partial fulfillment of requirements for the
Degree of Master of Science
in
Civil Engineering

Supervisor
Yanglin Gong, Ph.D., P.Eng.
Professor, Dept. of Civil Engineering

Co-Supervisor
Jian Deng, Ph.D., P.Eng.
Associate Professor, Dept. of Civil Engineering

Lakehead University
Thunder Bay, Ontario
June 2019

Declaration

I hereby declare that I am the sole author of this thesis. This is a true copy of the thesis, including any required final revisions, as accepted by my examiners. I understand that my thesis may be made electronically available to the public.

Abstract

Single plate or shear tab is a common simple connection to connect steel beams to columns. The connection is traditionally designed for the shear load transferred from the supported beam only, while it has long been recognized that the shear connection can resist a certain amount of tensile force in the longitudinal direction of the supported beam which is critical to preserve the integrity of a structure. Canadian standard CSA/S16-14 explicitly states that connections shall be designed to provide resistance to progressive collapse as a consequence of a local failure. However, few specific design requirements are provided in the standard. Hence, the main objective of this research is to quantify the deformation and strength capacities of shear-tab connections when subjected to a pure tension or a combined tension and shear load in the context of progressive collapse resistance.

First, a set of full-scale shear tab connection specimens were tested under a pure tension load. The results from the experiments are then used to verify and calibrate a finite element model of the connections. Thirdly, the finite element model is used to conduct a parametric study to determine the impact of tab thickness, tab edge distance, bolt diameter and the combined effect of tension and shear load. Finally, a formulation describing the relationship between the tensile force and the axial deformation for the shear tab connections is developed.

Acknowledgements

This research would not be successful without the help of many people that I owe a debt of gratitude. I would like to express my gratitude to all those who helped me during the course of this thesis.

First, my deepest gratitude goes to Professor Yanglin Gong, my supervisor, for his constant encouragement and guidance. Dr. Gong has walked me through all the stages of this research. Without his patient instruction, insight criticism and expert guidance, the completion of this thesis would not have been possible. Also, I would like to thank my co-supervisor, Professor Jian Deng, whose support, knowledge and experience helped me tremendously during the research.

I would like to thank Professor Sam Salem for serving as a thesis committee member. My gratitude is also due to Professor Hao Bai for serving as the external thesis examiner.

I would like to thank students Blake Peters, Daniel Leung, Thomas Wipf and Asparukh Akanayev, for assistance in executing the laboratory work. Thank you for spending your reading week by my side at Lakehead University Structure Laboratory.

I would like to extend my appreciation to my parents who gave me their love and support throughout my studies. Last, but not least, a special thanks to my fiancée, with her support, patience and understanding throughout this research, I have completed this thesis.

Contents

List of Tables

List of Figures

Chapter 1 Introduction

This chapter provides a general background about shear tab connections and the reasons of this study. Research objectives and literature review are listed, and the outline of the thesis is presented.

1.1 Research considerations and objectives

Shear tab connection is one of the most popular and common simple connections used in steel construction industry because of its cost efficiency, easy fabrication, and rapid erection capabilities. It usually consists of a single steel plate and several bolts to connect a beam to a column or a girder. The connecting plate is welded to the supporting member in shop, while the connection between the supported beam and the steel plate is achieved with the use of bolts on site. There are two kinds of shear tab connections: one is called the shear tab connection (or the conventional shear tab connection), the other is the extended shear tab connection. Figure 1.1 shows the two types of shear tab connections for beam-to-column and beam-to-girder joints.

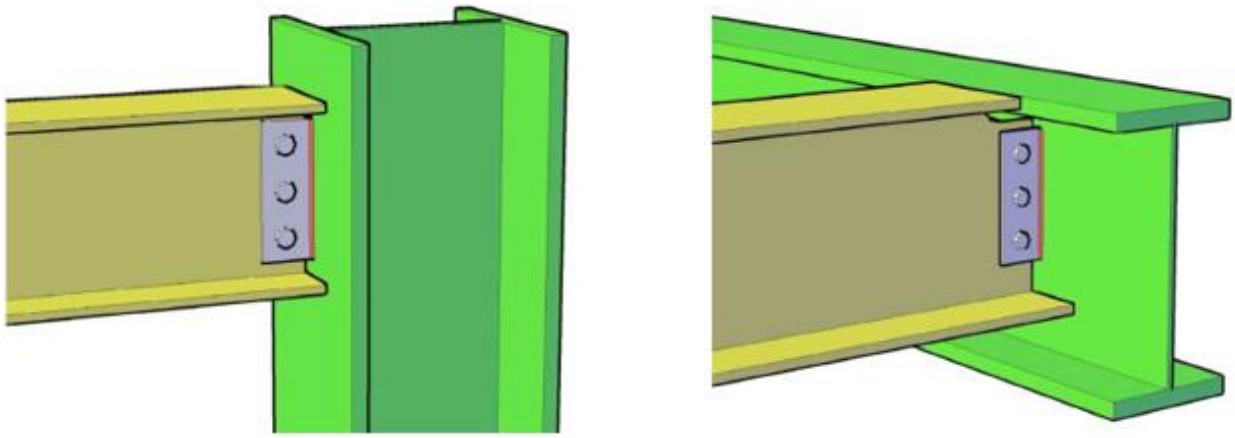

(a) shear tab connection

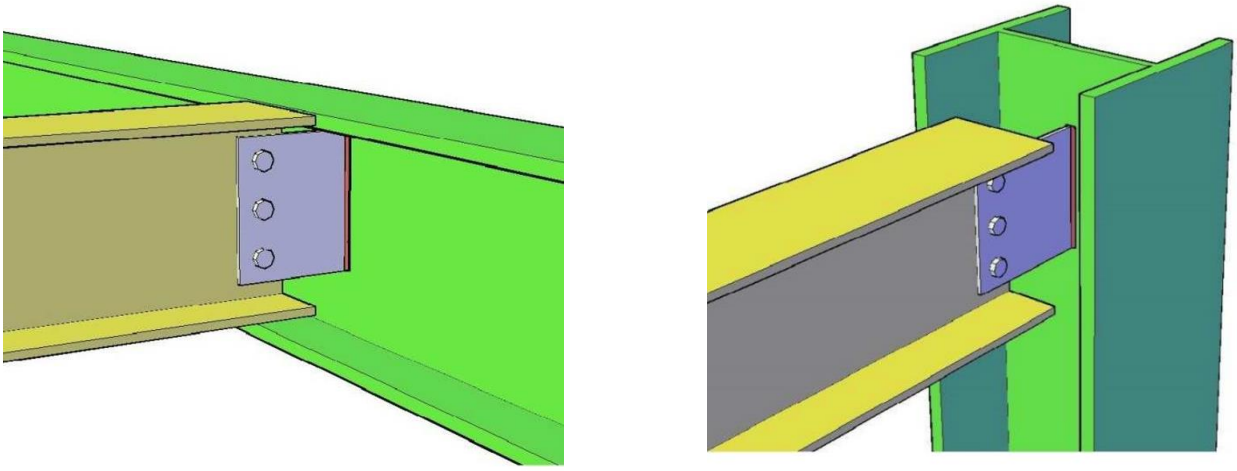

(b) extended shear tab connection

Figure 1.1 Two types of shear tab connections

Shear connections of steel structures are traditionally designed for the shear load transferred from the supported beam only, while it was long been recognized that these shear connections can resist a certain amount of tensile force in the longitudinal direction of the supported beam. This tensile force resistance allows the development of a horizontal tying force (called catenary action) which helps to preserve the integrity of the structures. In Canada, the steel structure standard CSA/S16-14 (CSA 2014) explicitly states that connections shall be designed to provide resistance to progressive collapse as a consequence of a local failure (Clause 6.1.2). However, few specific design requirements are provided in the standard. Instead, the standard states that "the requirements of this standard generally provide a satisfactory level of structural integrity for steel structures".

Recent research found that when assessing the integrity of a steel structure against progressive collapse, the scenario of a sudden column loss could impose a very large tension force on the shear connections, as the girders or beams need to structurally span two bays under the sustained gravity loads. Thus, the modeling of steel connections under a tensile load is essential for evaluating the behaviors of a steel structure under such an abnormal loading.

The main objective of this research is to develop formulas to predict the deformation and strength capacities of conventional shear tab connections subjected to a tension load. In order to achieve this goal, we need to finish the sub-objectives as follows:

1) A set of experimental tests are conducted to quantify the ultimate strength and deformation

capacities of shear tab connections subjected to a pure tension load.

2) The results from the experiments will be used to verify a finite element model of the connections.

3) The finite element model will be used to conduct a parametric study.

4) Finally, a formulation describing the relationship between the tensile force and the tensile deformation of the shear tab connections will be developed.

1.2 Lab tests of shear tab connection

Lipson (1968) conducted a study on the performance of three kinds of simple connections, including the welded bolted single plate which is now commonly referred to as a shear tab. The shear tab was welded to a supporting beam and bolted to the web of the supported beam .

A single vertical row of bolts (2 to 6 A325 bolts) were used for a series of 12 full-scale tests. Three types of loading were conducted: pure moment, moment-shear with no rotation, and moment-shear with rotation. Figure 1.2 shows the two setups in the study.

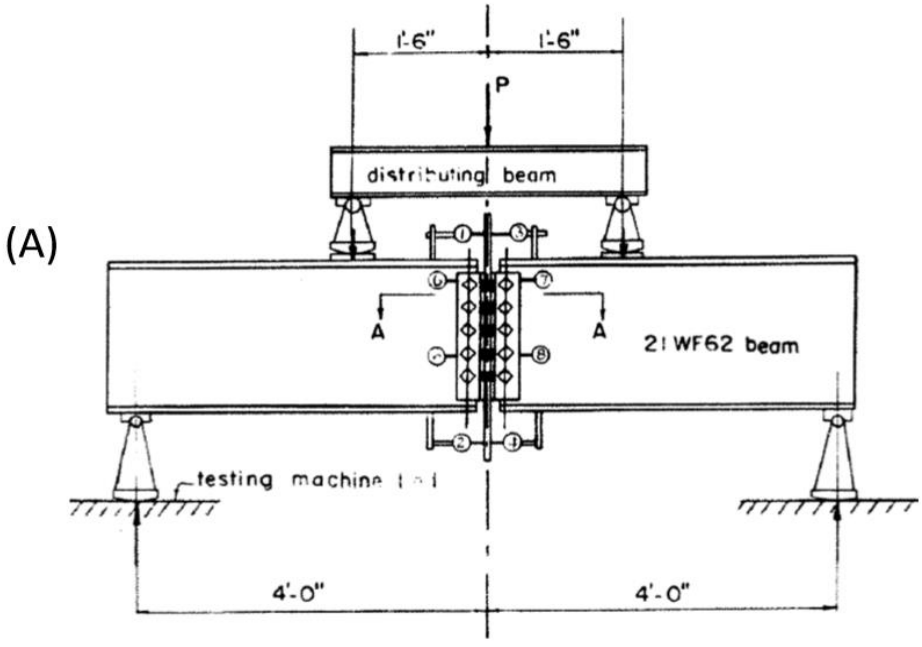

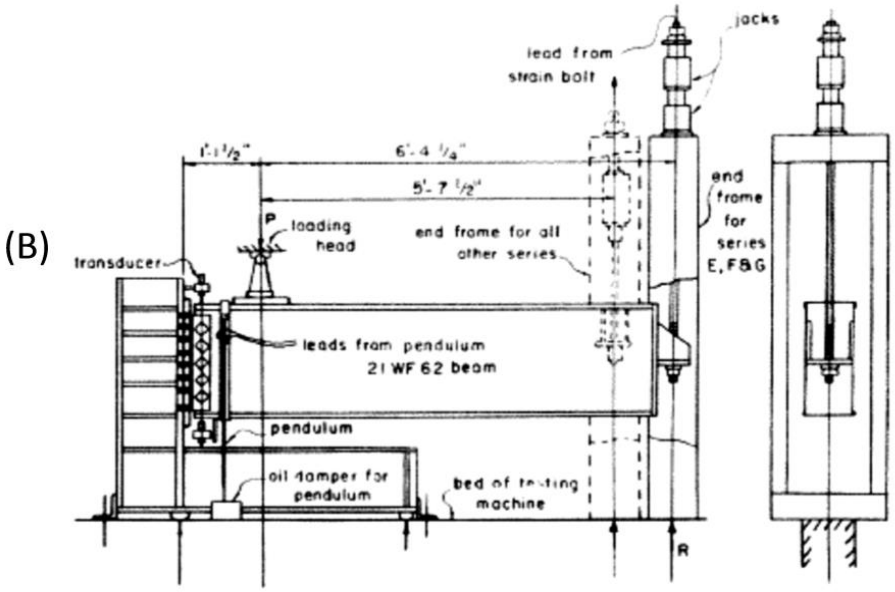

Figure 1.2 Lipson's test setups (Mirzaei, A., 2014)

In Figure 1.2(a), the two test beams were spliced together in the middle at the point of zero shear, and for the setup in Figure 1.2(b) , two hydraulic jacks were used to control rotation.

The purposes of the Lipson's work were to observe the behavior of shear tab connections under the loads, to find the maximum rotational capacities of the connections, to determine a safety factor for the ultimate load, and to evaluate the feasibility of the shear tabs. Lipson observed three kinds of failure modes: weld rupture, bolt tear-out and plate yielding. His investigation showed that the centre of rotation, which was close to the centre of bolt group, was not more than 20mm from the centre in the direction of the compression edge of the shear tab. Also, the test results showed that bolt slip occurred at a rotation of less than 0.04 radians. He concluded that it was feasible to use these connections in reality.

Astaneh et al.(1993) presented a strength-based design guideline for shear tabs, and the guideline was later adopted by the American Institute of Steel Construction (AISC) manual. There were 5 strength limits in the guideline: plate yielding, bearing failure of bolt holes, fracture of the net section of the plate, bolt fracture, and weld fracture. This design approach was applicable with both ASTM A325 and A490 bolts, either fully tightened or snug tightened. The procedure was not applicable to oversized or long-slotted bolt holes. The requirements of the guidelines are: the connection has only one vertical row of bolts, and the number of bolts is not less than 2 and more

than 7; bolt spacing is equal to 76 mm; edge distances are equal to or greater than 1.5d, where d is the diameter of the bolts, and the vertical edge distance for the lowest bolt is preferred not to be less than 38 mm; thickness of the single plate should be less than or equal to $d/2 + {}^{1}/_{16}$ in; the ratio of c/d of the plate should be greater than or equal to 2 to prevent local buckling of the plate, where c is edge distance; the distance between the bolt line and the weld line was limited to 64-76 mm; the size of the connecting fillet weld was required to be greater than 0.75t, where t is the thickness of the shear tab.

A series of test specimens was designed with this approach, and the test results showed that the ductile and tolerated rotations was from 0.026 to 0.061 radians at the point of the maximum shear. The number of bolts influenced the rotational ductility; i.e., the higher the number of bolts, the lower the rotational ductility that could be achieved. At last, the experimental studies indicated that considerable shear and bearing yielding occurred in the plate before the failure. The yielding would decrease the rotational stiffness which would cause the reduction of the end moments of the supported beam.

Guravich and Dawe (2006) tested 108 full-scale shear tab connections. Their main goal was to investigate the performance of shear tab connections under the effect of combined shear, moment and tension force.

They used a single row of 3 bolts (3/4 inch ASTM A325) to connect the shear tab (7.9mm thickness), which was commonly used at that time. Figure 1.3 shows the test setup.

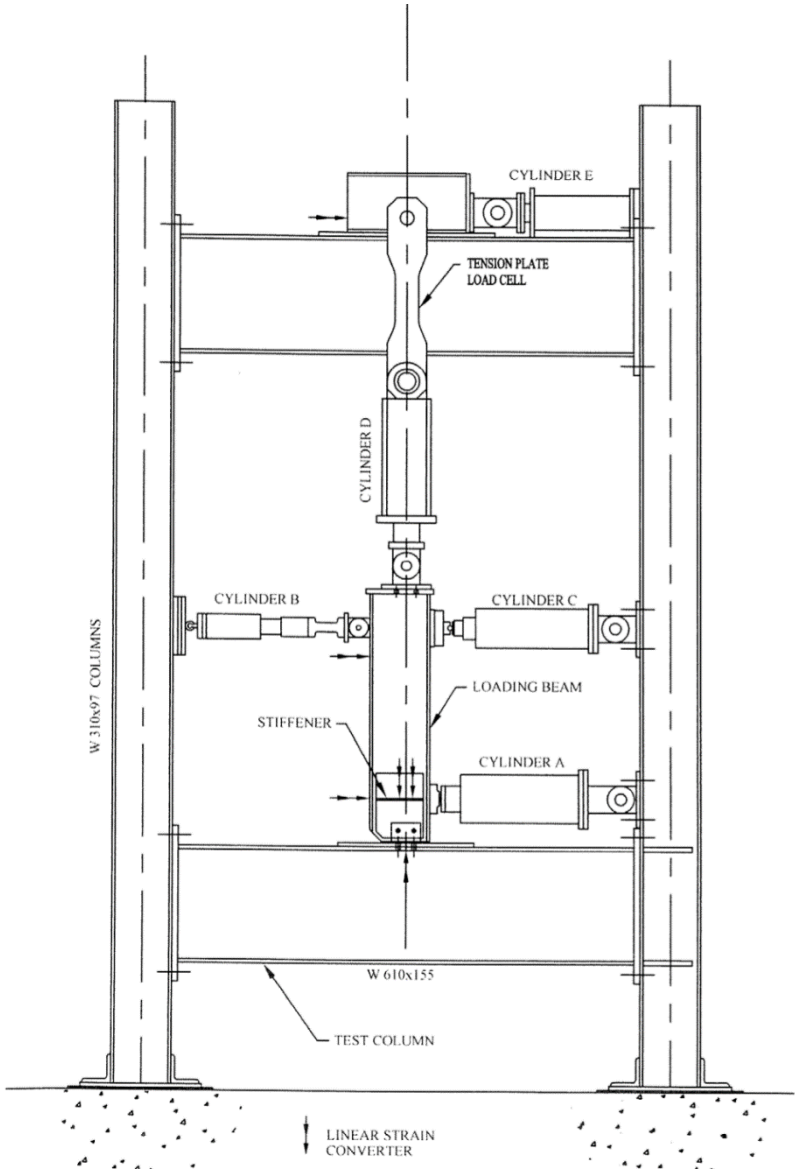

Figure 1.3 Guravich and Dawe's test setup (Mirzaei, A., 2014)

Two vertical W310 × 97 reaction columns were fixed to the rigid ground while two horizontal W610 × 155 reaction beams were framed to the two columns. The upper beam was the support for cylinder D, and the lower beam acted as a rigid support for the specimens. Shear tabs were welded to a steel plate which was bolted onto the lower beam. Five hydraulic cylinders were used: A applied the main shear force to the connection; B and C controlled the rotation of the connection; D applied the tension force; E controlled the position of cylinder D to keep the force perpendicular to the beams . The test procedures were as follows:

1) rotated the test beam to 0.03 radians and applied the desired value of shear force (either half

or total of the factored bolt shear capacity)

2) applied the axial tension to the test beam (the rotation and shear force remain unchanged during the testing)

Table 1.1 shows the results of 11 shear tab connection tests.

Table 1.1 Results of 11 shear tab connection tests.

Specimen	F_y (MPa)	F_u (MPa)	V_{test} (kN)	T_{ult} (kN)	Failure mode[a]	V_{res} (kN)	B_p (kN)	V_{res}/B_p
T308-1	260	321	380	0	H	380	—	—
T308-2	260	321	337	0	H	337	—	—
T308-4	260	321	89	384	G	394	402	0.98
T308-5	260	321	104	370	G	384	411	0.94
T308-9	260	321	102	382	G	395	414	0.96
T308-8	260	321	213	321	G	385	403	0.96
T308-10	260	321	253	310	G	400	401	1.00
T308-11	260	321	245	284	G	375	401	0.94
T308-6	260	321	0	360	G	360	401	0.90
T308-7	260	321	0	374	G	374	412	0.91
T308-12	260	321	0	386	G	386	412	0.94
Avg.								0.94
COV								0.03

Note: —, buckled prematurely.
[a]G, shear fracture through tab plate; H, plate buckling

Notes: V_{test}: Applied shear load; T_{ult}: ultimate tension load; V_{res}: Resultant shear force; B_p: Bearing resistance of shear tabs.

From Table 1.1, T308-1 and T308-2 failed with plate buckling failure under pure shear load, and all other tests failed with steel plate shear fracture. Also, from the average ratio of V_{res}/B_p of 0.94, they concluded that B_p was a key factor to determine the ultimate resistance capacity of shear tab connection under combined shear and tension load.

Thompson (2009) investigated 9 full-scale tests of shear tab connections under a scenario of column removal. His main goal was to determine the stability of the shear tab connections and their ability for the catenary action. Figure 1.4 shows the test setup.

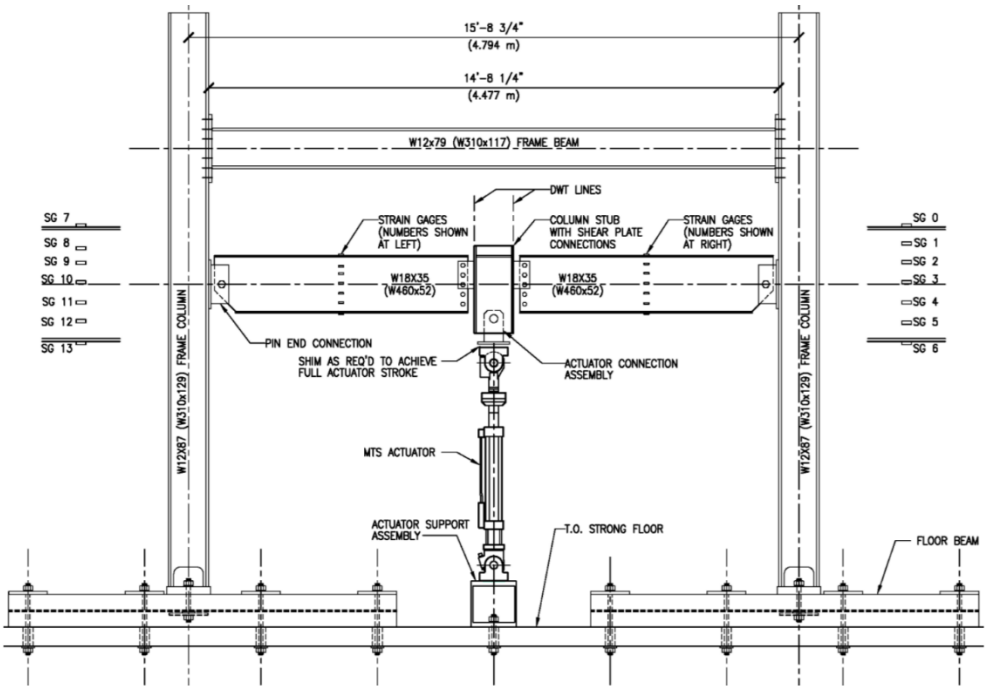

Figure 1.4 Thompson's test setup (Mirzaei, A., 2014)

Two identical shear tabs were connected to the test beams in the middle of the setup. The other ends of the test beams were pin-connected to the frame columns. A hydraulic cylinder below the test specimen was used to apply a force to the shear tab connections .

The test results gave three failure modes: bolt shear, localized net section tensile rupture, and localized block shear rupture at the bottom bolt location. Thompson concluded that the shear tab connections had the ability to resist the unexpected forces because of the loss of a column.

Oosterhof and Driver (2011) tested 45 full scale specimens of various kinds of simple connections, including 9 shear tabs, under combined shear, moment and axial forces to simulate a column removal scenario.

Two kinds of shear tab specimens were used: a 230 x 110 x 6.4 mm shear tab connected by three 19.05mm diameter ASTM A325 bolts to a W310x143 test beam; a 390 x 110 x 9.5 mm shear tab connected by five 22.2mm diameter ASTM A325 bolts to a W530 x 165 test beam. Figure 1.5 shows the test setup.

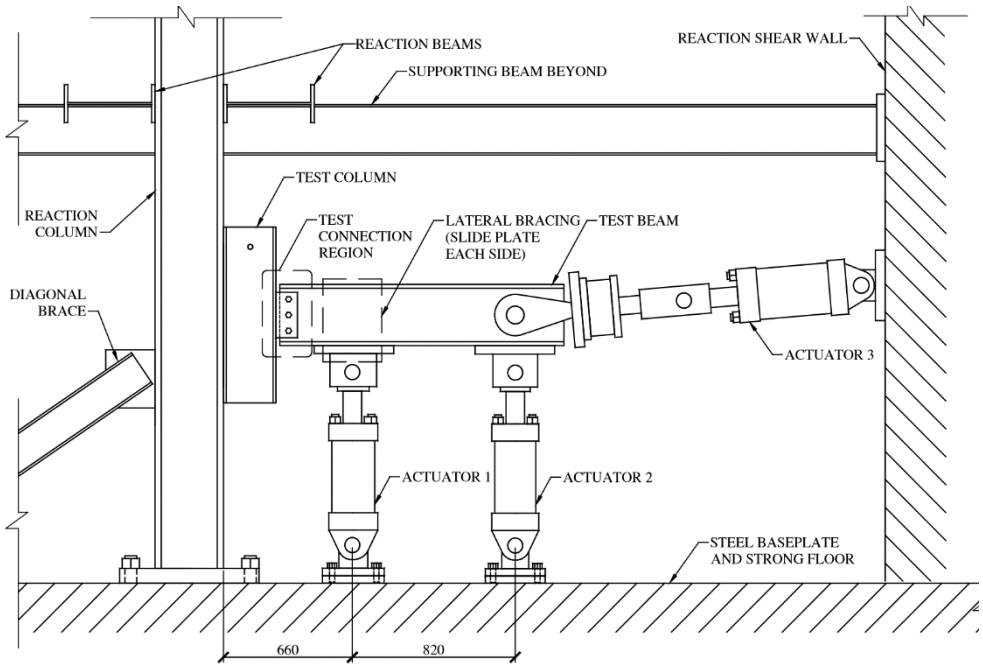

Figure 1.5 Oosterhof and Driver's test setup (Mirzaei, A., 2014)

The setup was different from Thomson's (2009), as it only used one test beam and one shear tab connection on a W250x89 test column. Three actuators were used to apply any combination of shear, moment and axial forces to the connection. Actuators 1 and 2 applied the moment and shear, while actuator 3 applied the axial force.

Oosterhof and Driver's connection rotation reached 0.08 to 0.13 radians. They observed that the tear-out of bolt was a main failure mode for the shear tab connections.

1.3 Finite element modeling of shear tab connections

Ashakul (2004) used software Abaqus to simulate the lab test of Astaneh et al. (1989) and Sarkar (1992). The simulation included two types of shear tabs: single-row and double-row of shear tabs.

Ashakul created 12 finite element models in the research, including 8 models stemmed from Astaneh et al. and Sarkar's lab test, 2 models for showing the effect of the size and length of the test beams, and another two models for investigating the influence of loading type and bolt strength. Table 1.2 shows the summary of the study .

Table 1.2 Summary of the FE simulation results by Ashakul (2004)

Model	Bolts in Simulation	Bolts in Test	Simulation Prediction (kips)	Test Results (kips)	Ratio of Prediction/Exp	Source
1	3-A325X	3-A325N	85.5	84, 94	1.02, 0.91	
2	5-A325X	5-A325N	131.6	137	0.96	
3	7-A325X	7-A325N	189.6	160	1.19	Astaneh et al.
4	3-A490X	3-A490N	84.7	79 (W)	1.07	(1988)
5	5-A490X	5-A490N	158.3	130	1.22	
6	2-A325X	2-A325N	57.7	51.8, 60.8 (W)	1.11, 0.95	
7	4-A325X	4-A325N	109.1	81.6, 84.6	1.34, 1.29	Sarkar
8	6-A325X	6-A325N	128.8	102, 109	1.26, 1.18	(1992)
9	5-A325X	5-A325N	140.3	137	1.02	Astaneh et al.
10	7-A325X	7-A325N	197.0	160	1.23	(1988)
11	4-A325N	4-A325N	83.0	81.6, 84.6	1.02, 0.98	Sarkar
12	6-A325N	6-A325N	104.1	102, 109	1.02, 0.96	(1992)

Note: The failure mode is bolt shear rupture unless indicated otherwise
W = Weld rupture

As shown in Table 1.2, the finite element models had a fair accuracy in predicting the ultimate resistance of the connections, though most of the results were overestimated by the models. Ashakul claimed that the reason why some of the results were 20 percent larger was that the bolt was in the shear plane. Furthermore, Ashakul used 42 finite element models to conduct a parametric study which included 4 variables: “a” distance between the bolt and the welded line, plate thickness, material of the plate, and single or double row shear tabs.

Ashakul’s findings were:

1) “a” distance had no effect on bolt shear rupture resistance;

2) the ductility criteria couldn’t use for connections, and the connections created high horizontal forces in bolts which would reduce the shear resistance of the bolts. Also , there was a moment created by those forces which should be considered in design.

3) in a double row thick plate shear tab connection, the second row (from the support base) resisted most of the stresses, and the first row had very small forces.

4) if the strain hardening performed, the shear stress distribution did not remain unchanged through the cross section of the plate.

Daneshvar and Driver (2011) used software Abaqus to simulate 9 lab tests by Thomson (2009). Figure 1.6 shows the model in the software.

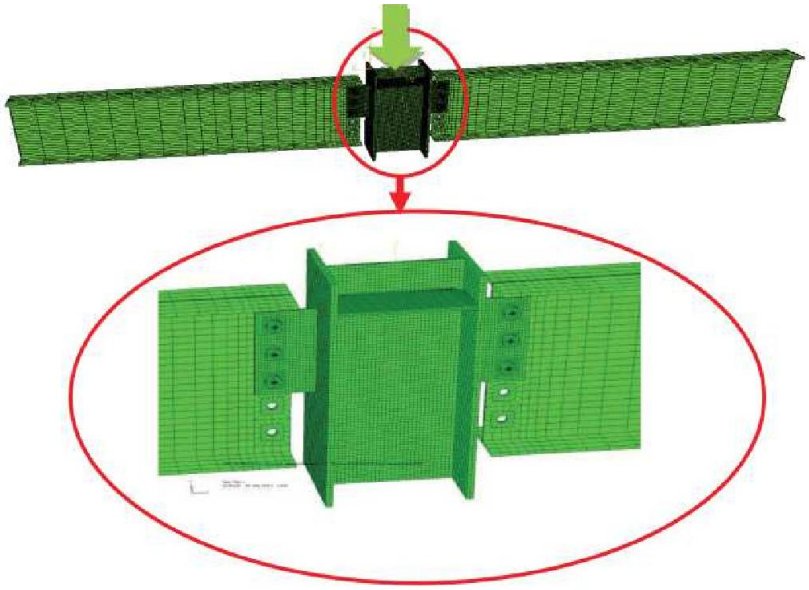

Figure 1.6 Daneshvar and Driver's finite element model

The loading was treated as a displacement assigned to the interior column. Figure 1.7 shows the final deformed shape of the finite element model.

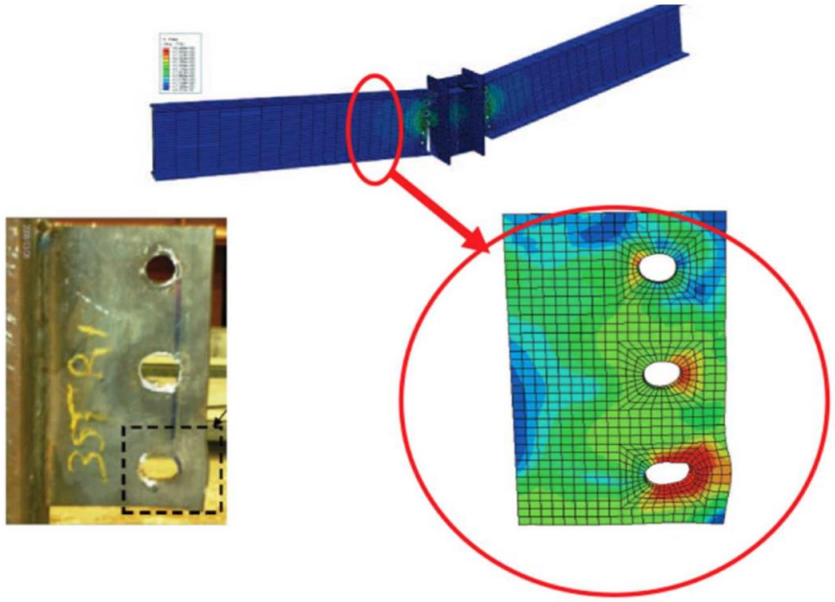

Figure 1.7 Final deformed shape of the finite element model

From the models, one can see that the shear tab connections had a high ductility capability

because of the bearing located around the bolt holes. Daneshvar and Driver concluded that the hardest part of simulation in Abaqus was the nonlinearity definition.

Henning Levanger (2012) used software Abaqus to simulate ductile fracture in steel and compared two models for describing local instability because of ductile fracture. The first model used material's true stress and strain relationship for reducing load-bearing capacity to get the ductile fracture of the material; the other model was based on the assumed energy for forming a crack, and reduced the load-bearing capacity by giving damage to the elements of the model.

Alireza Mirzaei and co-researchers (2014) did a series of full-scale lab tests of shear tab connections and used Abaqus to mimic the performance of these shear tab connections. A series of four full-scale tests were performed on shear tab connections between a W610x140 beam and a W360x196 column, as well as a W310x60 beam and a W360x196 column. The shear tab, which was configured as a double bolt row connection, was subjected to a combined vertical (shear) force and axial tension along with the anticipated rotation of a typical beam-to column joint. A matching specimen was then tested under shear and axial compression. The results from these tests and previous shear tabs tested under gravity load alone were used in the development of a finite element model that was capable of simulating the response of the connection under shear load and predicting the ultimate resistance and the progression of failure. The models presented in the thesis featured special modelling techniques and were able to predict all types of failure modes such as bearing, net area fracture, shear yielding, flexural yielding, and weld tearing of the connections.

Next, the FE models were used to investigate the performance of shear tabs subjected to combined shear and axial force. Shear force–axial force interaction curves were generated for various levels of axial tension and compression force for twelve connections. At last, a design approach was proposed which allowed practicing engineers to include the effect of any axial force level in the design of a shear tab connection.

1.4 Design guideline for shear tab connections

The current design procedure for shear tabs in the CISC Handbook of Steel Construction (2016) is based on the research carried out by Astaneh et al. (1989). Table 3-41 in the Handbook presents the factored resistances of shear tabs with one vertical row of 2 to 7 bolts connected to rigid supports (such as the flange of a W section column) or flexible supports (e.g. the web of a column or a girder) by using E49 fillet welds and diameters ½", ¾", 20 mm and 22 mm A325 bolts. The

methodology behind the values listed in the table is as follows: 1) determine the effective eccentricity for the bolt group based on Astaneh et al's (1989) research; 2) find the single plane shear resistances of the bolts used; 3) determine the thickness of the shear tab plate; and 4) choose the weld size to fully develop the shear tab. The current Canadian approach does not cover the usage of multiple vertical rows of bolts or the use of more than 7 bolts per row. The size and thickness of the shear tab is also limited due to restrictions largely based on the original scope of test specimens. It also does not address the application of an axial force on the connection.

1.5 Thesis outline

Chapter 2 presents laboratory test of 10 shear tab connections under a pure tension load. The test design, setup, procedures and results are discussed in detail.

Chapter 3 describes the finite element modeling of the tested connection specimens using software Abaqus 6.14. The finite element model is calibrated with the experimental results.

Chapter 4 presents a parametric study of the shear tab connections by using the finite element model established in Chapter 3. The design parameters include tab thickness, edge distance, bolt diameter, and the combined effect with shear force.

Chapter 5 proposes a load-deformation curve for the shear tab connections from the elastic stage to the damage stage.

Chapter 6 states the conclusions from this research, and provides some recommendations for future works.

Chapter 2 Experimental test

In this chapter, the details of the lab test of 10 shear tab connections under a pure tension load are presented.

2.1 Test setup and design

The tension test was conducted on a SATEC 500 kips (2225 kN) universal testing machine. Figure 2.1 shows a picture of the setup in lab. Figure 2.2 shows the design of the setup, which consisted of one upper loading arm, one lower loading arm, and a specimen between the loading arms. The design of the shear tab specimen is shown in Figure 2.3. The loading arms were fixed to the loading heads of the universal testing machine by clamping (Figure 2.4 and Figure 2.5). Figure 2.6 shows the measurement of displacement.

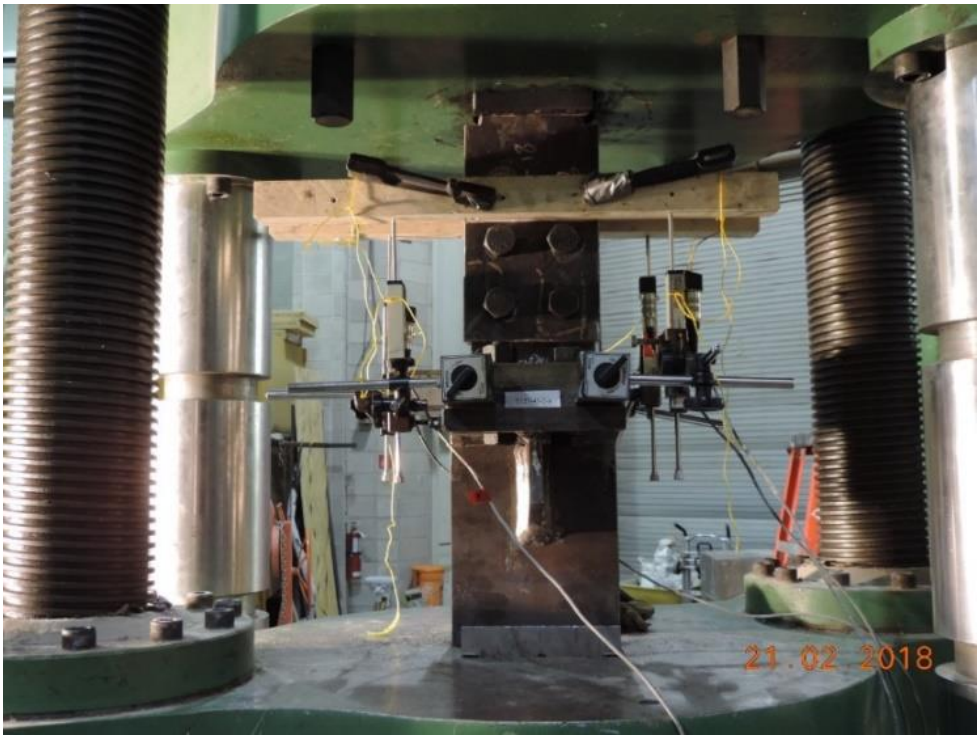

Figure 2.1 The test setup on universal testing machine

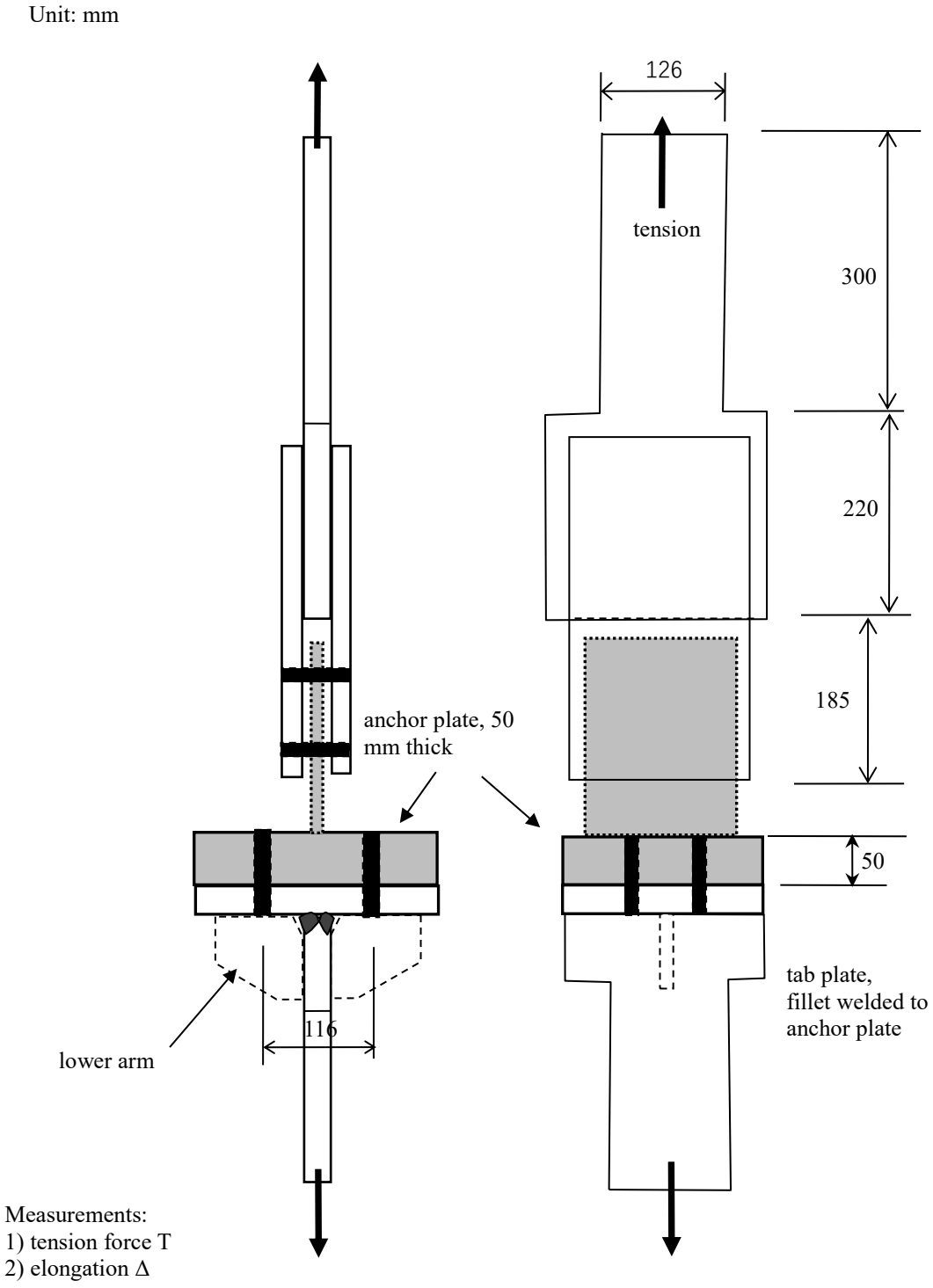

Figure 2.2 Test setup for pure tension

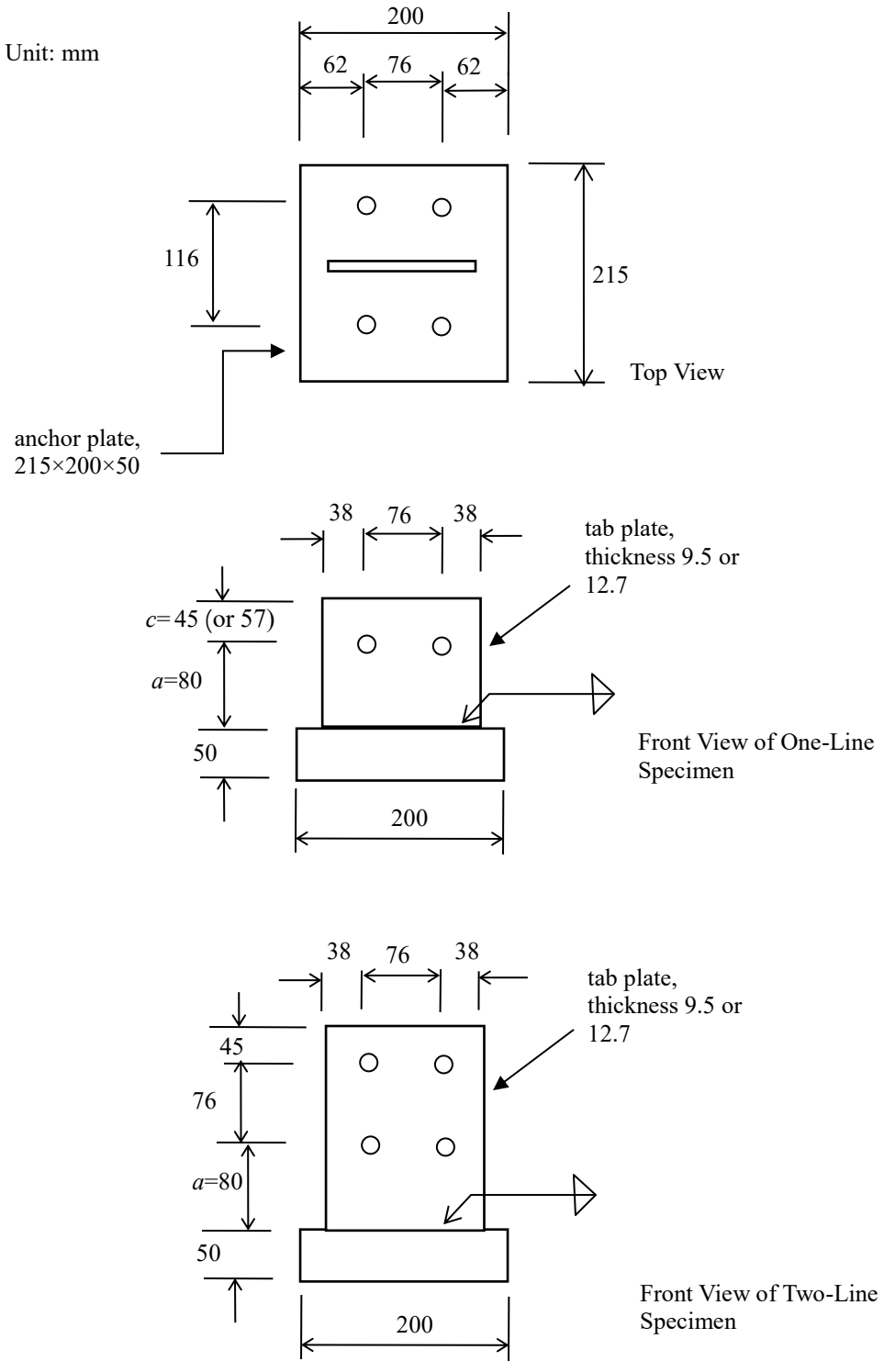

Figure 2.3 Design of shear tab specimens

In this project, we have three kinds of test variables: 1) tab plate thickness t. Use two thicknesses: 9.5 mm and 12.7 mm; 2) tab edge distance c. Use two distances: 45 mm and 57 mm; 3) number of columns of bolts. Use two patterns: one line only, and two lines.

The size of the fillet welds between the shear tab plate and the anchor plate is (5/8)t. Tables 2.1 shows the specimen matrix. Ten specimens were tested in total (Table 2.2).

Table 2.1: Shear tab specimen matrix

	One-line specimen		Two-line specimen, Edge c=45 mm	Bolt length (mm)	
	Edge c=45 mm	Edge c=57 mm		4 tension bolts	2 or 4 shear bolts
Tab thickness t=9.5 mm	2	2	2	108 ($4^1/_4$ in)	108 ($4^1/_4$ in)
Tab thickness t=12.7 mm	2		2		

Table 2.2: Shear tab connection specimens

Shear Tab Specimen ID	Tab thickness t (mm)	Edge distance c (mm)	One- or two-column lines	Note
T95-45-1-a	9.5	45	1	The first
T95-45-1-b	9.5	45	1	The second
T95-57-1-a	9.5	57	1	The first
T95-57-1-b	9.5	57	1	The second
T95-45-2-a	9.5	45	2	The first
T95-45-2-b	9.5	45	2	The second
T127-45-1-a	12.7	45	1	The first
T127-45-1-b	12.7	45	1	The second
T127-45-2-a	12.7	45	2	The first
T127-45-2-b	12.7	45	2	The second

Note: T=shear Tab; followed by thickness, 95=9.5 mm; 127=12.7 mm,; followed by c; followed by number of rows of bolts; and a is the first of the kind, and b is the second of the kind. For example, specimen T95-45-1a had a tab thickness of 9.5 mm, edge distance of 45 mm, one-column of bolts, and the first specimen of the kind. Specimen T127-45-2b had a tab thickness of 12.7 mm, edge distance of 45 mm, two-column of bolts, and the second specimen of the kind.

Unit: mm

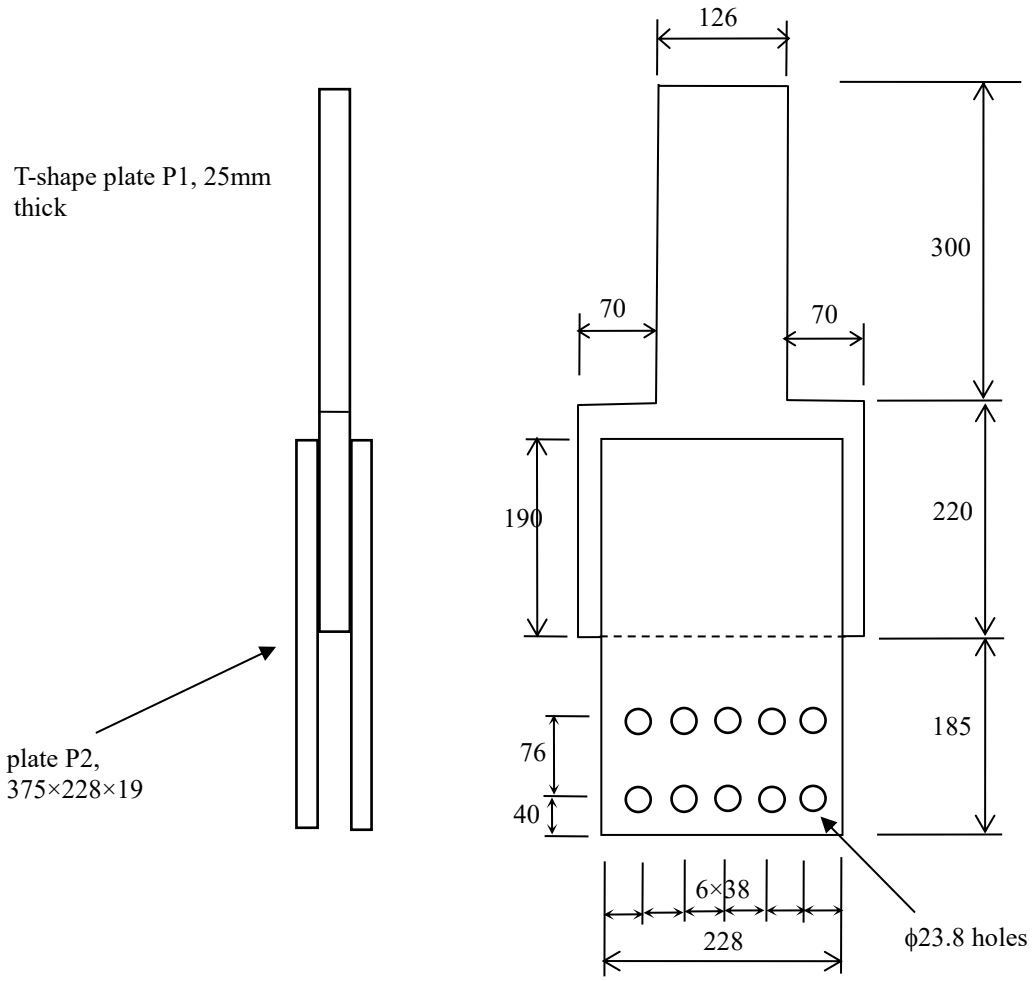

fillet welds between P1 and P2:
12 mm all around

Figure 2.4 Upper arm drawing

Design of lower arm:
(1) lower arm: the g_2 gauge is 45 mm.
(2) PL2 welded to PL3 using complete penetration groove weld
(3) stiffeners welded to PL2 using complete penetration groove weld; and to PL3 using 10 mm fillet welds
(4) PL1, PL2 and PL3 have thickness of 25 mm
(5) Bolt hole diameter 23.8 mm

Unit: mm

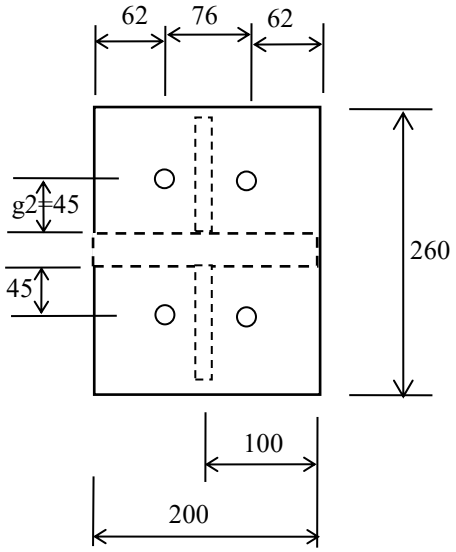

Top View of Lower Arm

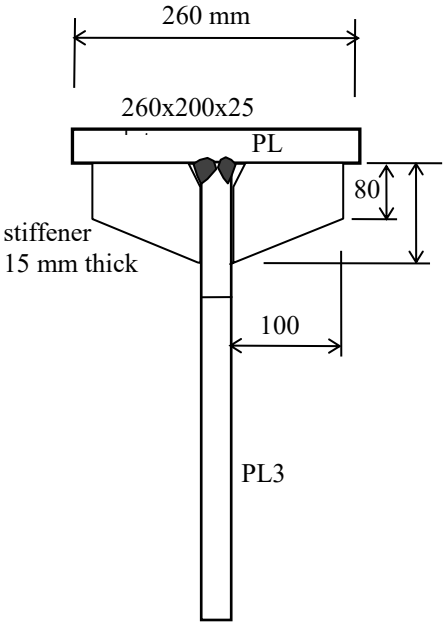

Side View of Lower Arm

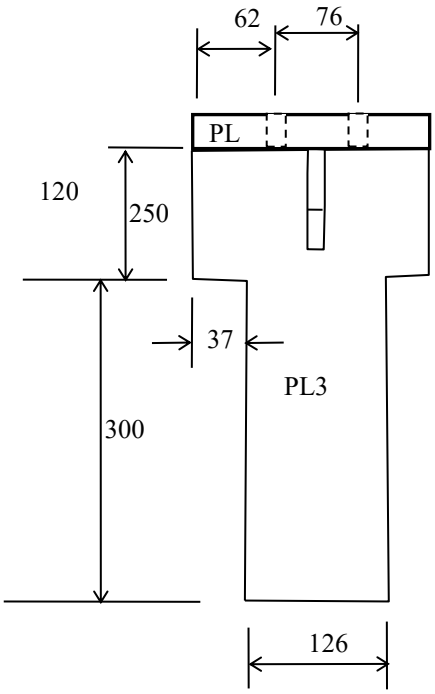

Front View of Lower Arm

Figure 2.5 Lower arm

Four bolts (of ASTM A490, diameter of $^{7}/_{8}$ inch) were used to fasten the specimen to the lower loading arm. Two ASTM A490 high-strength bolts of $^{7}/_{8}$ inch diameter were used to connect the specimen to the upper loading arm. Bolt hole diameter is 23.8mm. The lower and upper arms were re-used throughout the test. Table 2.3 shows the list of bolts and coupons.

Table 2.3: List of bolts and coupons (bolt diameter=$^{7}/_{8}$ in)

Category	Item	Number
Bolts	A490 , length=4 in	
	A490 , length=$4^{1}/_{4}$ in	56 (The tension bolts will be re-used)
Shear tab plate coupons		6 coupons in total; each thickness 3 coupons of 30 mm × 300 mm

The connection design (Figure 2.3) adopted typical North American practice. The tab plate was welded to a 50 mm thick anchoring plate, which was in turn fastened to the lower loading arm during test. The tab materials were CSA/G40.21 300W steel. Their measured strengths were: yield strength F_y=376 MPa and ultimate tensile strength F_u=490 MPa for 9.5 mm thick tab; F_y=387 MPa and F_u=495 MPa for 12.7 mm thick tab (Appendix 2A). The sizes of the welds and bolts were chosen based on a capacity design principle such that rupture failures of the welds and bolts would not occur during the test.

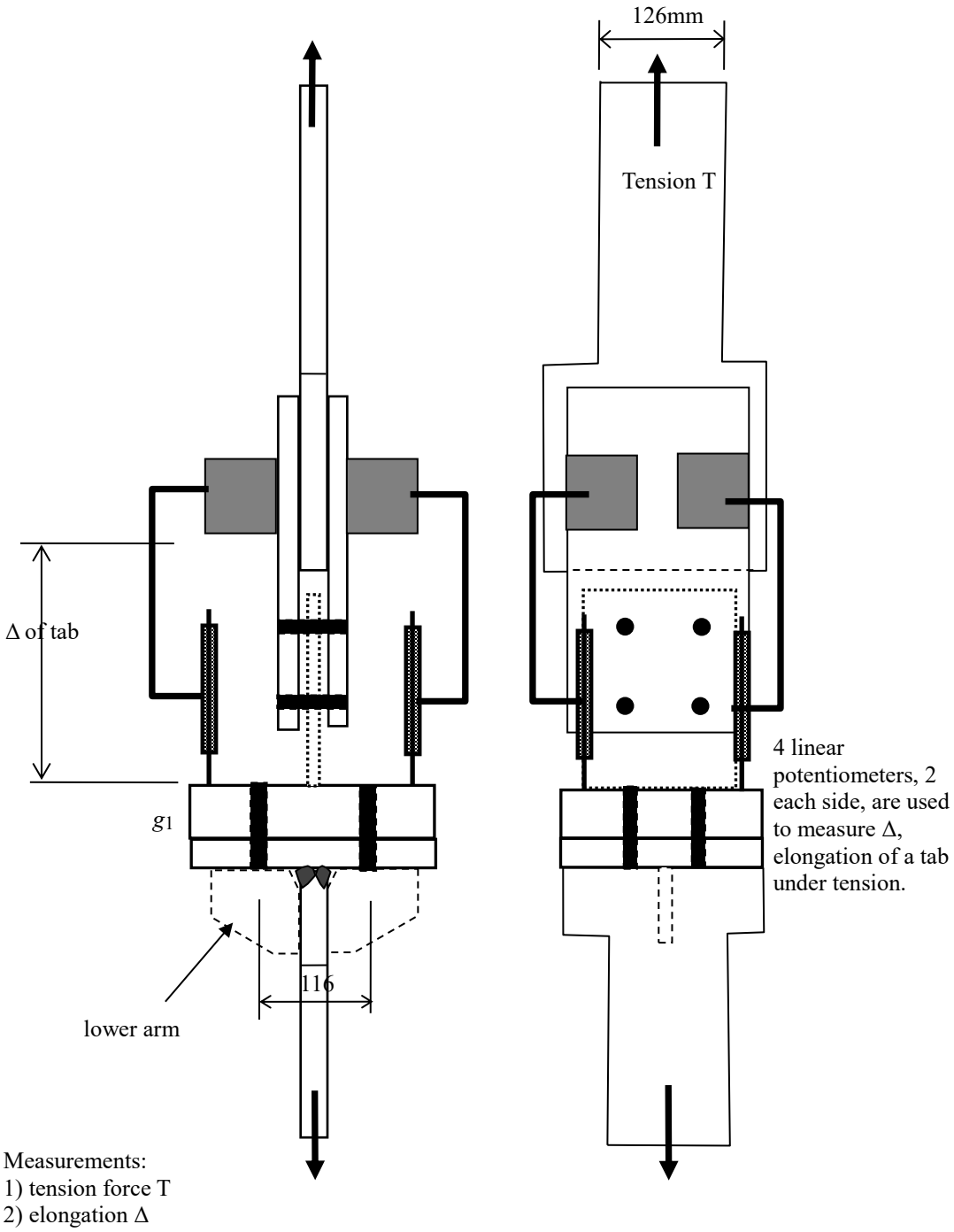

Figure 2.6 Measurement of Δ

2.2 Test procedure

Before starting, measure dimensions of the test arms, check if they match design dimensions. All the shear tab specimens shall be measured and photoed before testing. Photos shall be taken with the tab placed on a clean background (a white color board as background). When taking photos, always include a printed label showing the ID of the connection.

The test procedures are as follows:

1) place the lower arm onto the Universal Testing machine.

2) install shear tab specimen, and snug tighten the tension bolts.

3) place the upper loading arm. Install and snug tighten shear bolts.

4) take photos of the connection, with printed lab of ID.

5) install displacement gauges.

6) check data acquisition system.

7) set up safety screen.

8) start loading while recording data. Load the connection to rupture with displacement-controlled loading.

9) unload.

10) take photos of the connection before taking it off, including printed label ID.

Figure 2.7 shows the photos of two specimens before testing: T95-45-1-a and T95-45-2-b.

Figure 2.7 Photos of specimens T95-45-1-a and T95-45-2-b

2.3 Test results

The yield, ultimate and rupture tensile strengths (T_y, T_u, T_r) of each specimen and its corresponding deformations (Δ_y , Δ_u , Δ_r) are recorded in Table 2.4. The observed failure modes included bearing tear-out and net-section rupture which are presented in Figure 2.8.

Table 2.4 Strength and failure modes of tested specimens

Specimen ID	Tensile strengths T_y, T_u , T_r (kN)	Failure mode
T95-45-1a,b	385, 430, 200	Bearing tear-out
T95-57-1a,b	376, 488, 270	Net-section rupture
T127-45-1a,b	510, 535, 380	Bearing tear-out
T95-45-2a,b	440, 480, 105	Net-section rupture
T127-45-2a,b	592, 640, 95	Net-section rupture

T95-45-1-a: bearing tear-out

T95-45-1-b: bearing tear-out

T95-57-1-a: net-section rupture

T95-57-1-b: net-section rupture

T127-45-1-a: bearing tear-out

T127-45-1-b: bearing tear-out

T95-45-2-a: net-section rupture

T95-45-2-b: net-section rupture

T127-45-2-a: net-section rupture

T127-45-2-b: net-section rupture

Figure 2.8 Failure modes

There were four plastic deformation patterns at failure: bearing of hole, bending of hole edge, shear tearing of hole, and tensile necking. Figure 2.9 shows the measurement of these permanent deformations. Table 2.5 records the results after measuring the deformations.

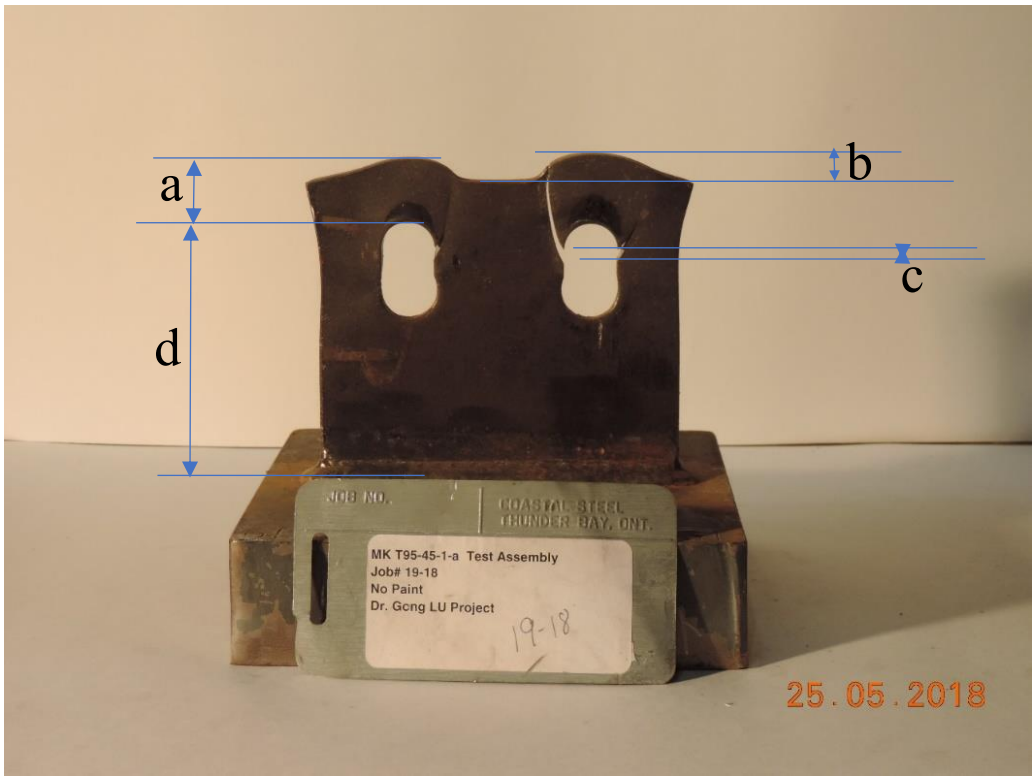

Figure 2.9 Deformation sources

The permanent plastic deformations were measured as follows:

1) bearing deformation of a hole = (dimension a before test) – (dimension a after test)

2) bending deformation of a hole edge = dimension *b*

3) Shear tearing deformation of a hole = dimension *c*

4) Tensile necking deformation = (total deformation) – (hole bearing deformation) – *b* – *c*

5) Total plastic deformation = (dimension d after test) – (dimension d before test)

Table 2.5 Results of deformations

Specimen ID	Hole bearing deformation (mm)	Hole bending deformation (mm)	Shear tearing deformation (mm)	Necking (mm)	Total plastic deformation (mm)
T95-45-1a,b	4.0	10.0	4.0	0.0	18.0
T95-57-1a,b	7.0	1.0	0.0	9.0	17.0
T127-45-1a,b	3.0	10.0	3.0	0.0	16.0
T95-45-2a,b	4.0	1.0	0.0	5.0	10.0
T127-45-2a,b	4.0	1.0	0.0	5.0	10.0

The tensile load T versus deformation Δ curves of the ten specimens are illustrated as following (Figures 2.10 to 19). Typically, the T-Δ curves had a bolt slippage in the beginning, followed by a linear elastic stage, then a gradual decrease of stiffness, followed by another linear stage until a rupture was initiated. Note that the tensile load indicated in the curves is a quarter of the real tensile load (i.e, ¼ of T) for the convenience of comparing with the finite element models in Chapter 3.

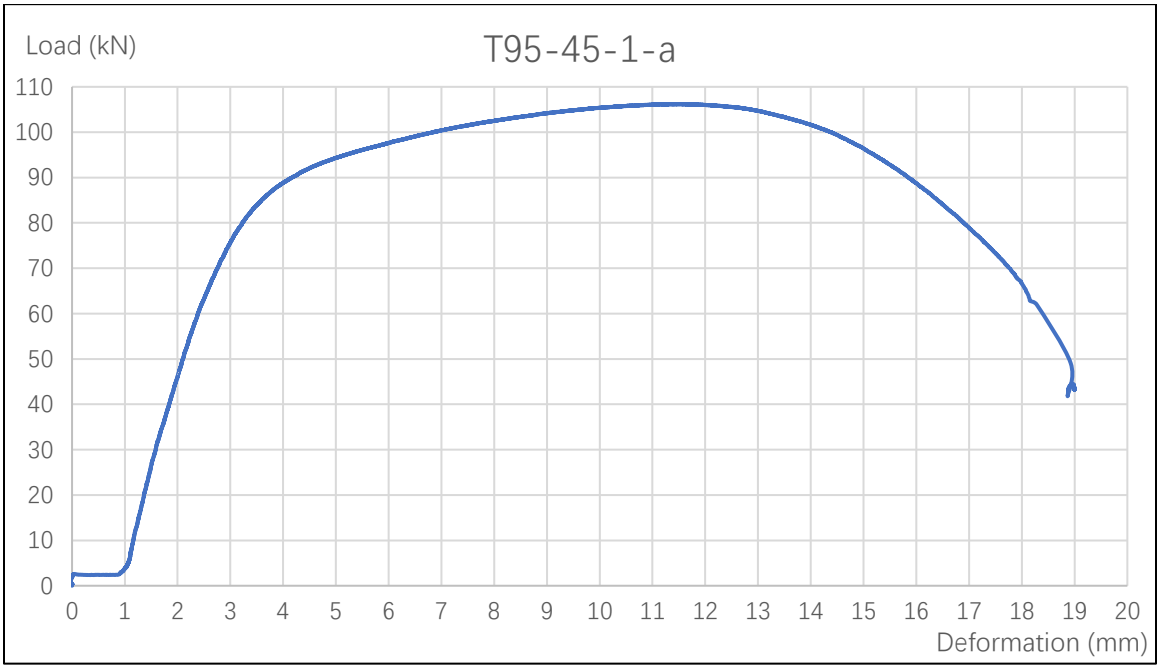

Figure 2.10 Load-deformation curve of T95-45-1-a

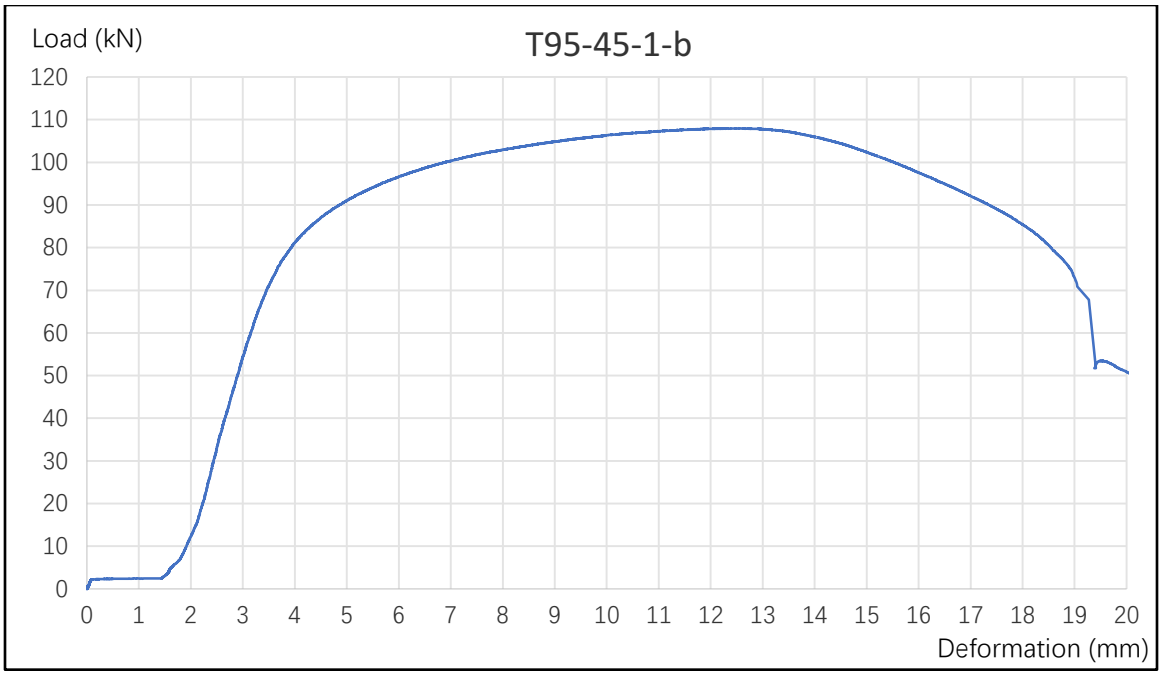

Figure 2.11 Load-deformation curve of T95-45-1-b

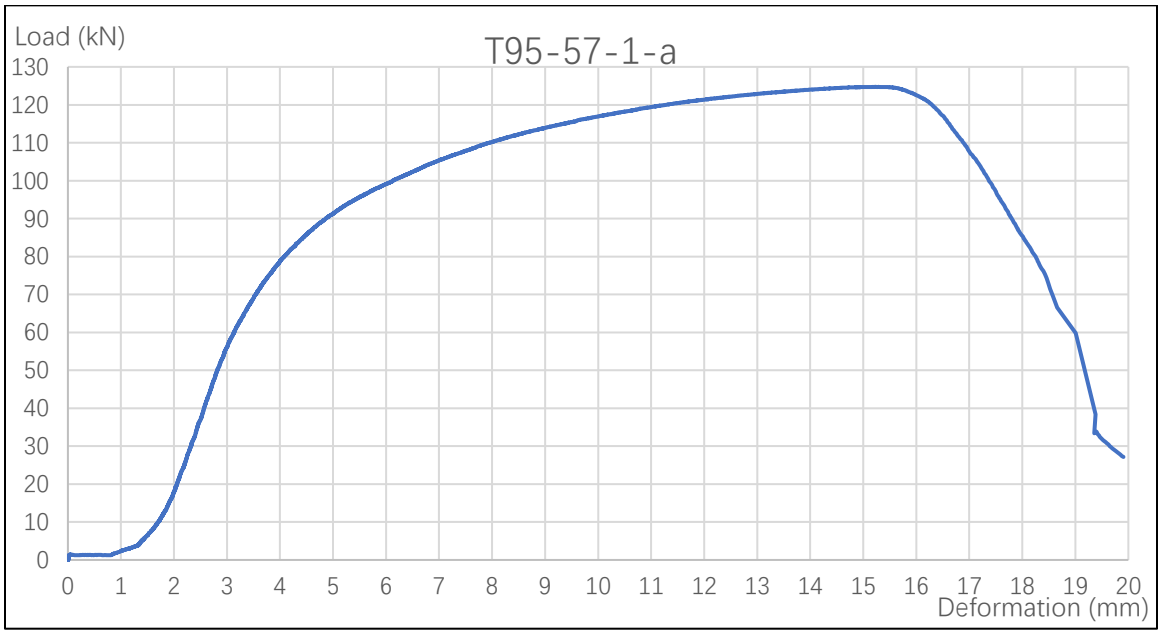

Figure 2.12 Load-deformation curve of T95-57-1-a

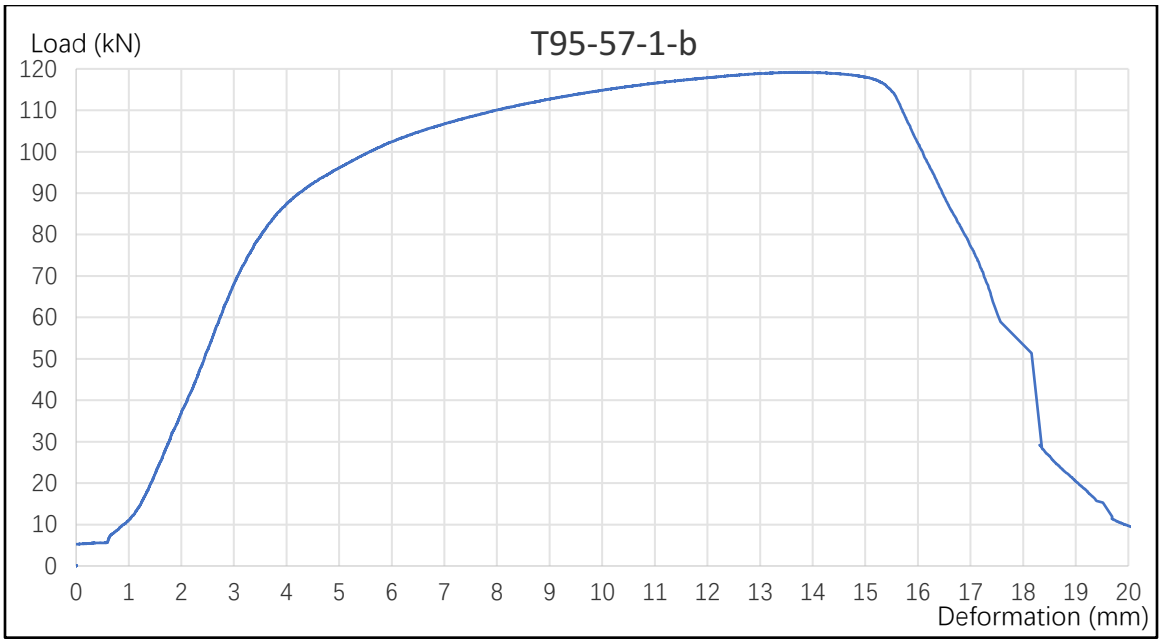

Figure 2.13 Load-deformation curve of T95-57-1-b

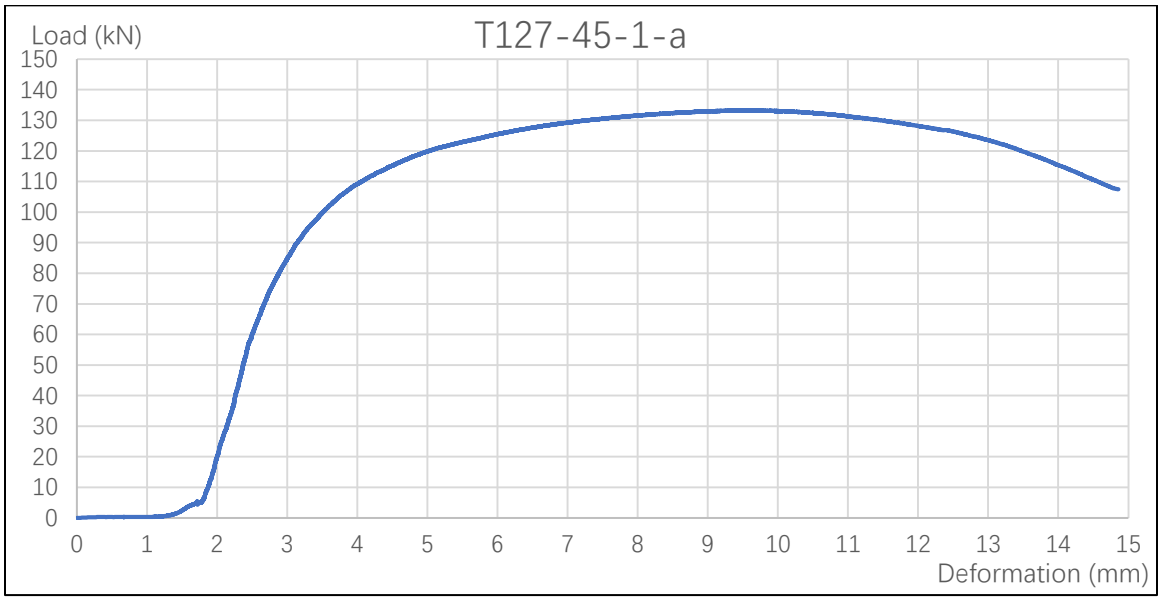

Figure 2.14 Load-deformation curve of T127-45-1-a

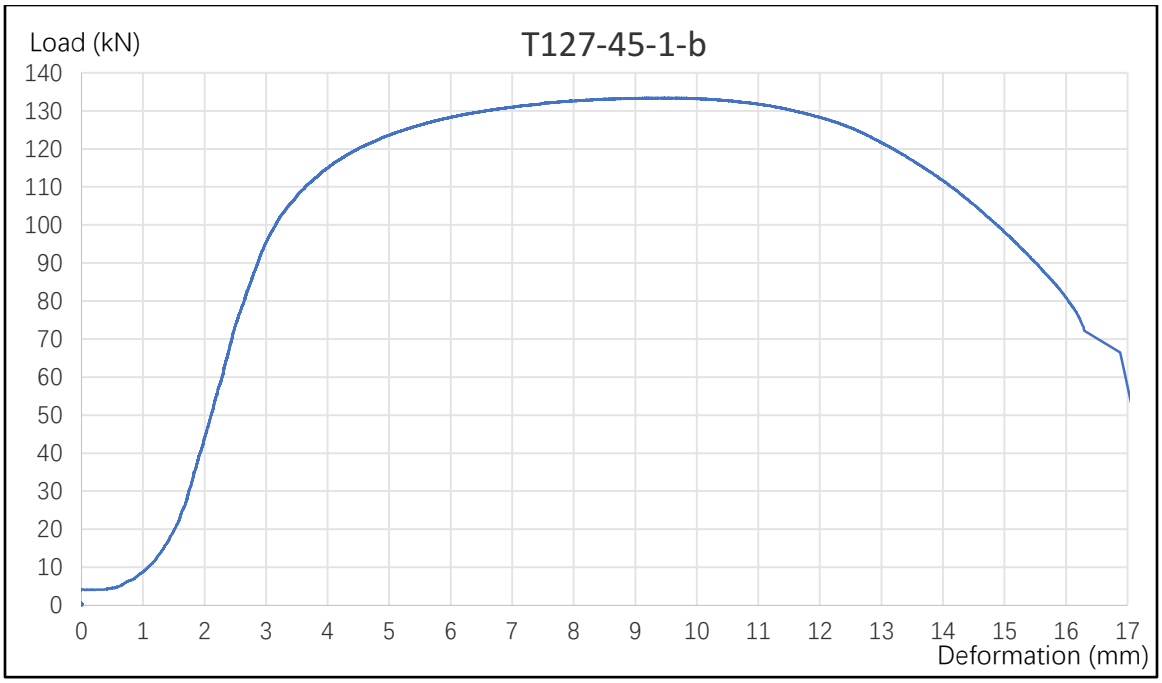

Figure 2.15 Load-deformation curve of T127-45-1-b

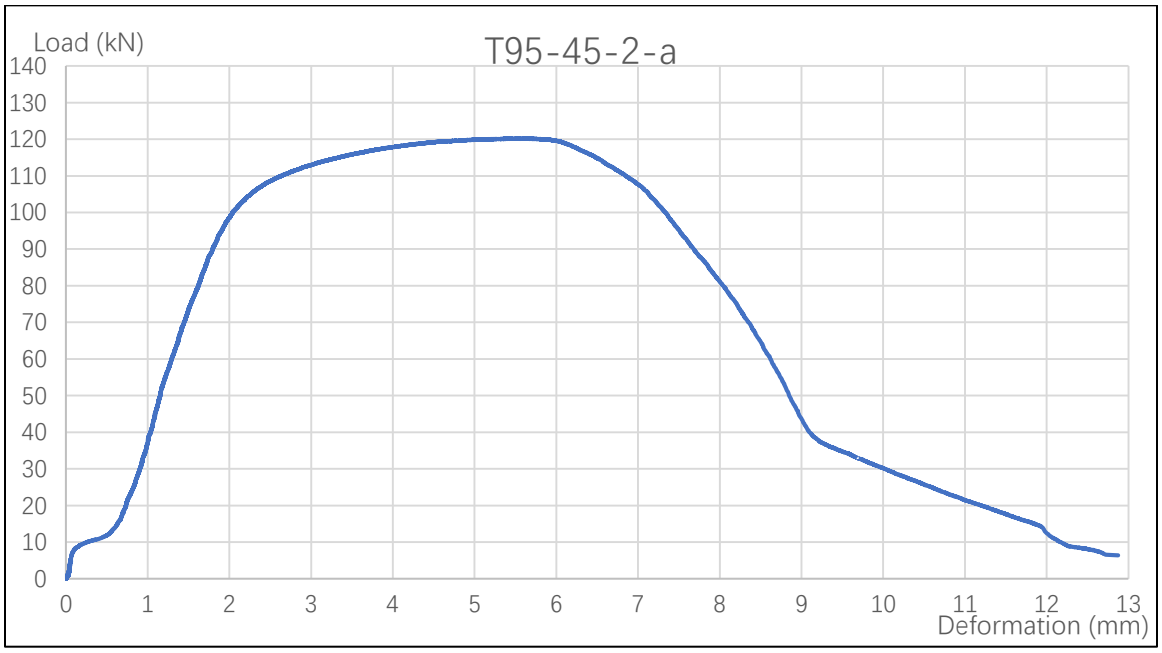

Figure 2.16 Load-deformation curve of T95-45-2-a

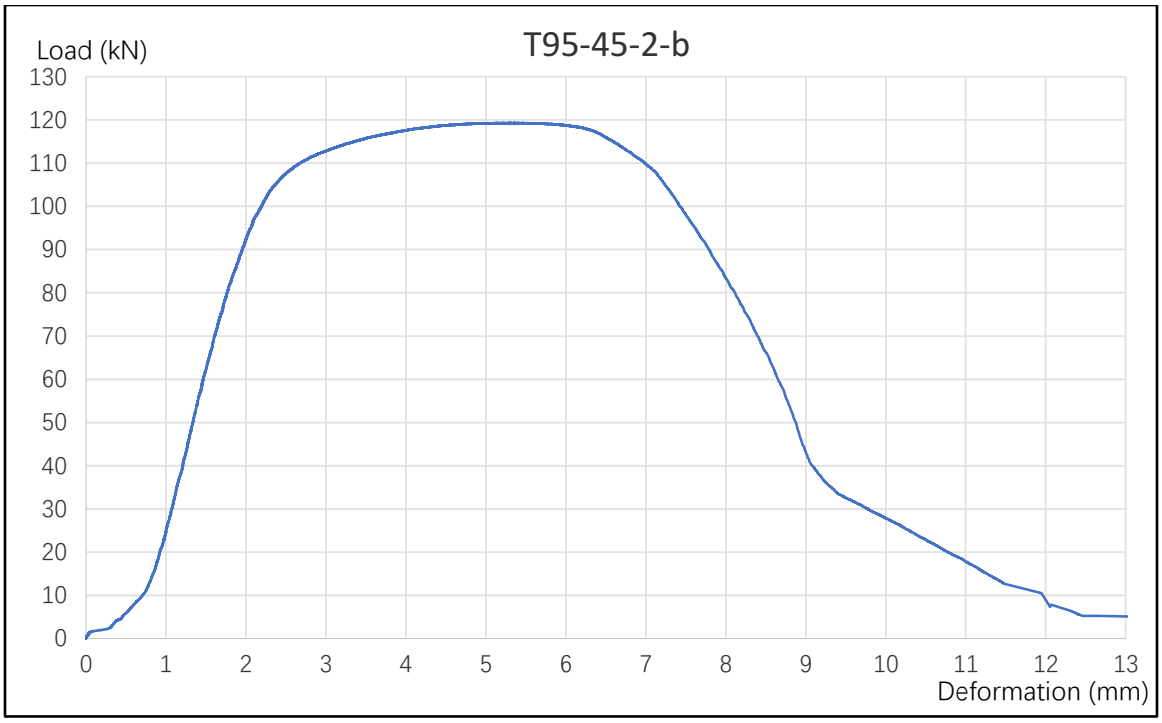

Figure 2.17 Load-deformation curve of T95-45-2-b

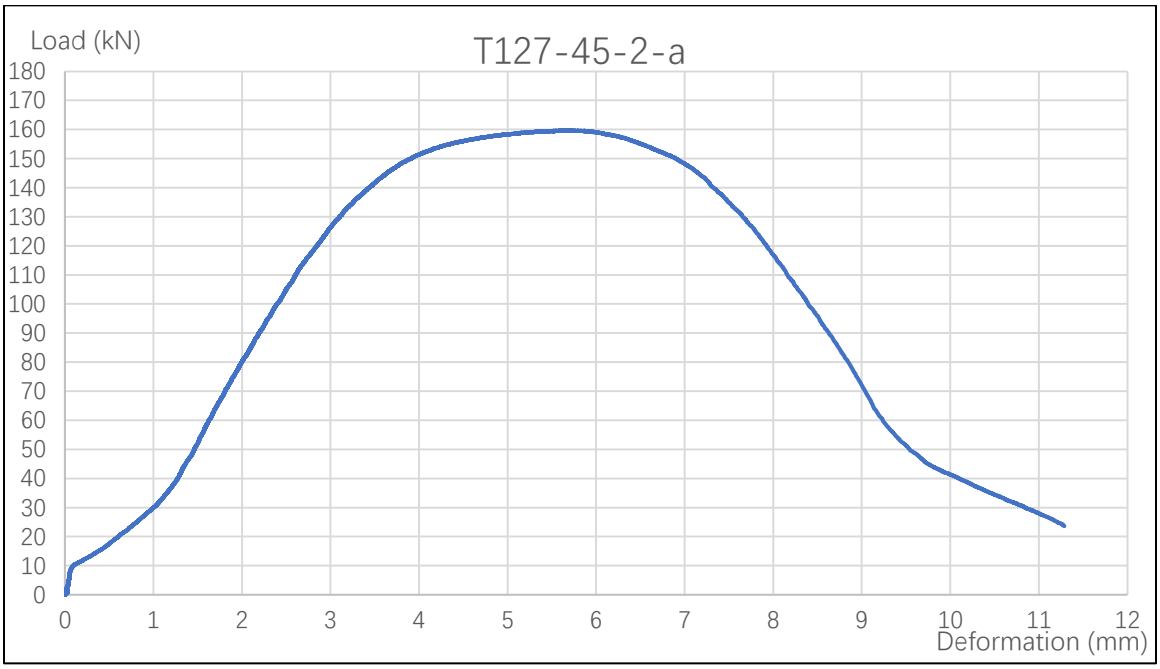

Figure 2.18 Load-deformation curve of T127-45-2-a

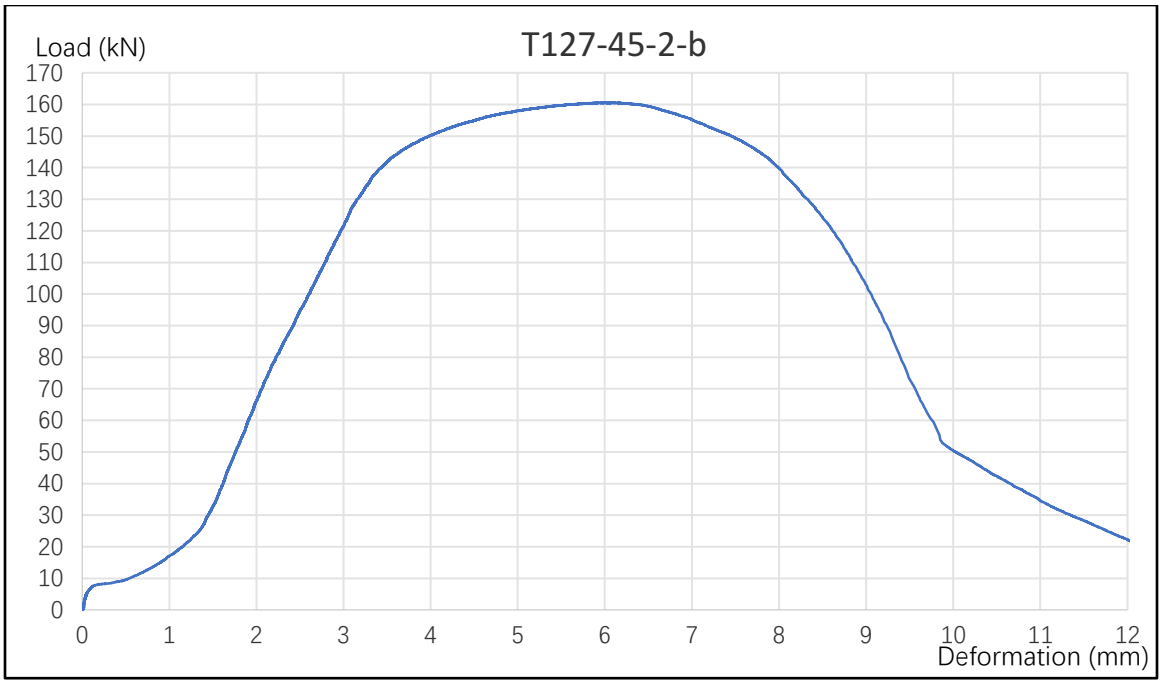

Figure 2.19 Load-deformation curve of T127-45-2-b

2A Appendix Coupon test

Tensile coupon tests were used to determine the material's yield strength, ultimate strength, and fracture strain. In this study, tensile coupon tests were carried out using Tinius Olsen universal testing machine.

The coupons (300mm × 30mm) were cut from the shear tab plates. The specified material for shear tab plates was G40.21 300W steel.

Three coupons were cut for 9.5mm thickness tab and 12.7mm thickness tab, respectively. Figure 2.20 shows the dimensions of the coupons.

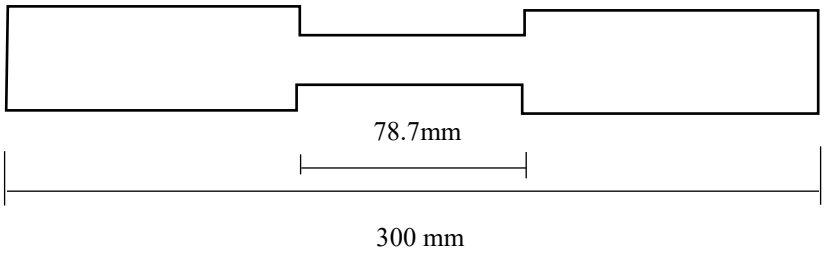

Figure 2.20 Coupon size

Test Procedure:

1) measure the length and thickness of the coupons
2) install the coupons to Tinius Olsen universal testing machine
3) install the gauges on the coupon
4) input the essential parameters to the computer
5) start recording data
6) start loading to rupture
7) unload
8) measure the length and thickness of the coupons

Figure 2.21 shows the testing machine with a coupon on it and the coupons after test.



Figure 2.21 Coupon setup and photos after test

The thickness, middle length before and after testing of each coupon were recorded in Table 2.6.

Table 2.6 Measurement of each coupon

Coupon ID	Thickness (mm)	Middle length (mm)	Middle length after test (mm)	elongation
Coupon 1	12.31	7.87	9.87	0.25
Coupon 3	12.29	7.87	9.74	0.24
Coupon 4	9.32	7.87	9.88	0.25
Coupon 5	9.34	7.87	9.81	0.25
Coupon 6	9.42	7.87	9.88	0.26

The load versus position curves of each coupon are given as Figures 2.22 to 26 (unit: lbf, in). The yielding strength and ultimate strength of each coupon can be obtained from the load vs. position curves (Table 2.7).

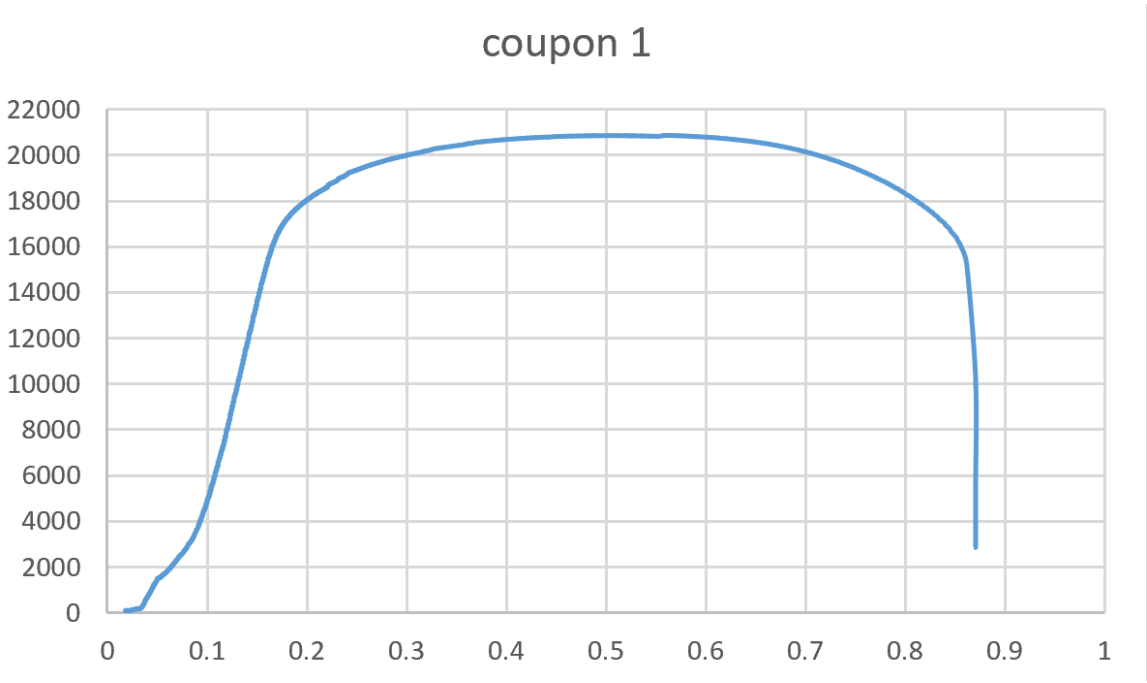

Figure 2.22 Load-position curve of coupon 1

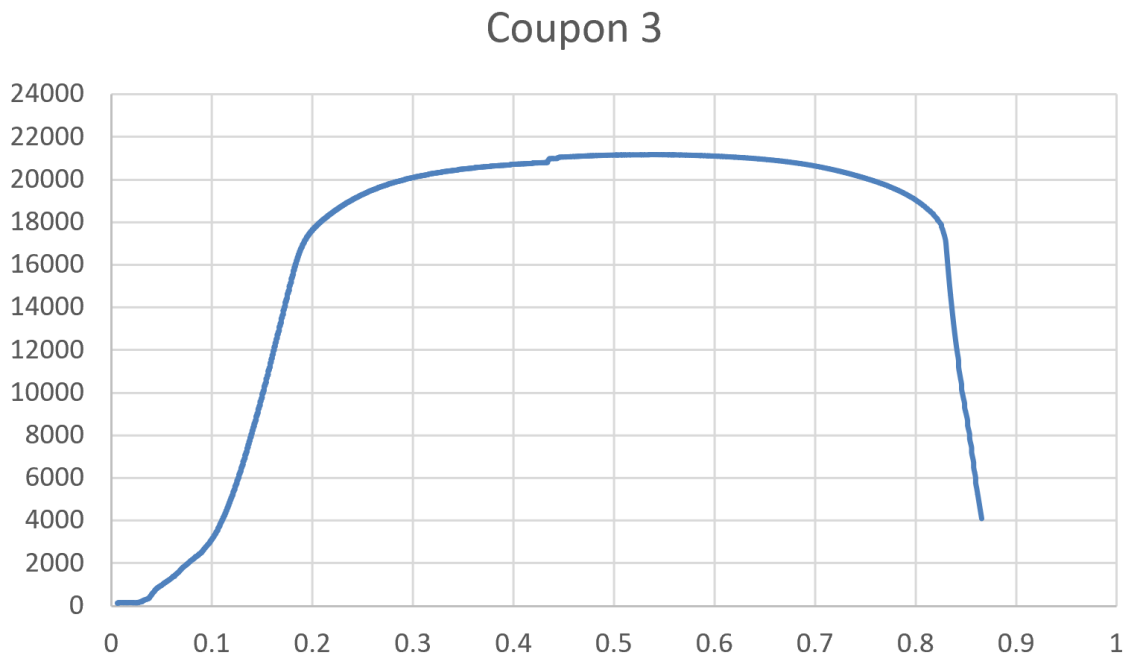

Figure 2.23 Load-position curve of coupon 3

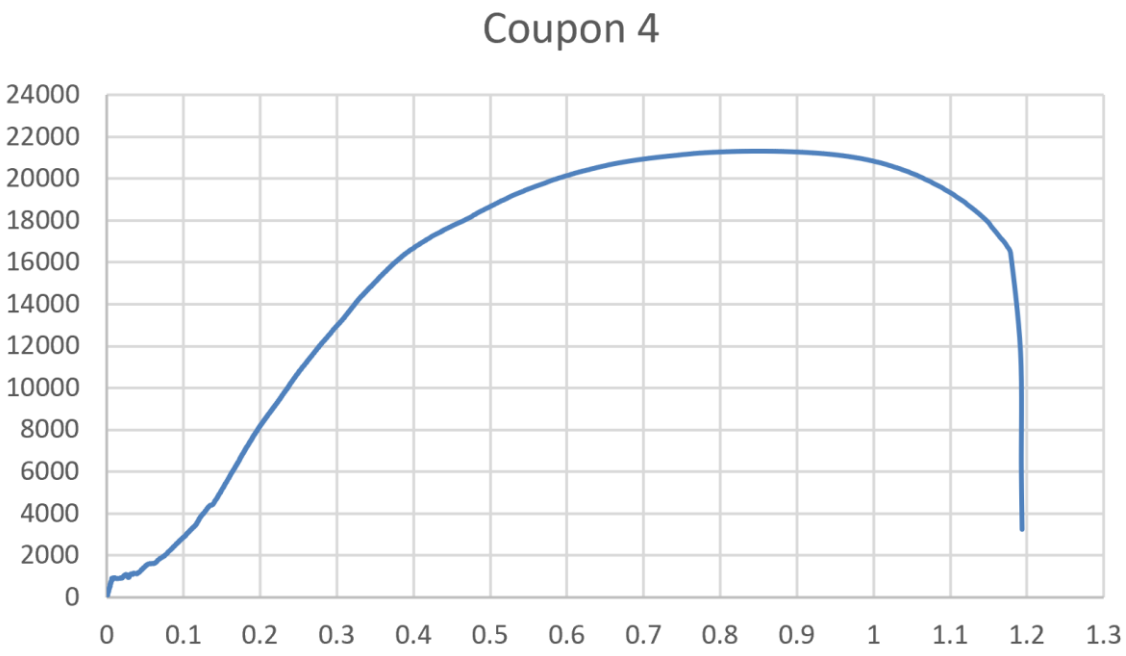

Figure 2.24 Load-position curve of coupon 4

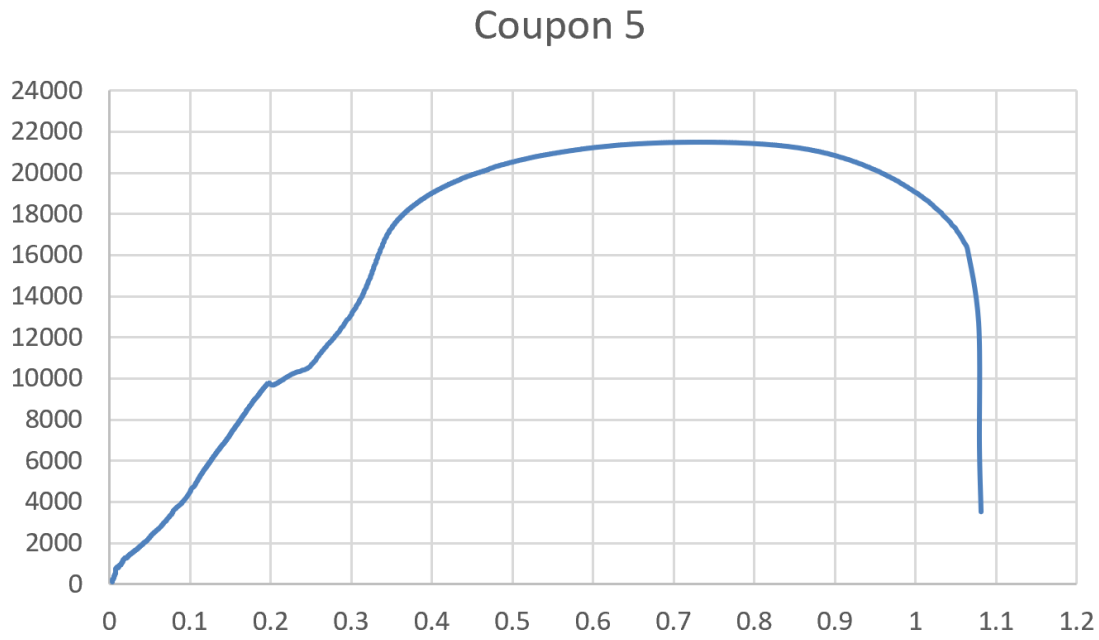

Figure 2.25 Load-position curve of coupon 5

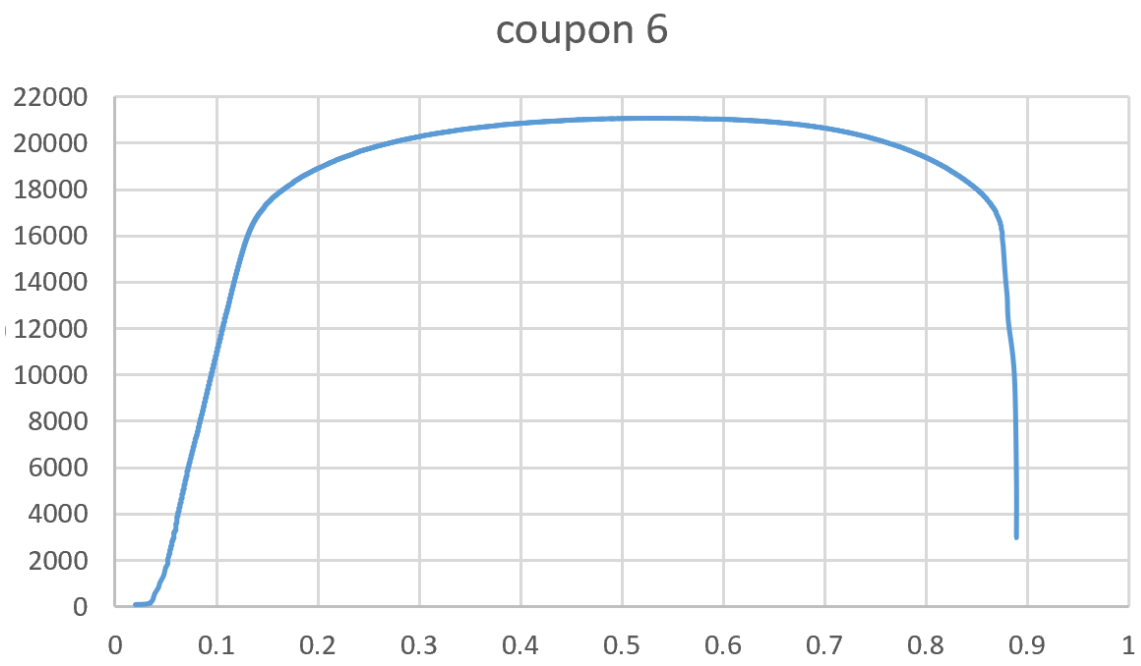

Figure 2.26 Load-position curve of coupon 6

Table 2.7 Yield strength and ultimate strength of coupons

Coupon ID	Yield strength (MPa)	Ultimate strength (MPa)	Average of yield strength (MPa)	Average of ultimate strength (MPa)
Coupon 1	380	495	387	495
Coupon 3	394	496		
Coupon 4	365	493	376	491
Coupon 5	399	499		
Coupon 6	365	481		

Chapter 3 Finite element modeling

This chapter describes the finite element modeling of the tested specimens, using software Abaqus 6.14. In a finite element analysis, a shear tab is discretized into many small elements, and the displacements at each node and the stresses within every element are obtained under the applied load.

3.1 Modeling process

In Abaqus, the modeling process includes 9 main parts: geometry modeling, material property, assembly, analysis step, interaction, loading, meshing, job and visualization. The relationships among these parts are shown in Figure 3.1.

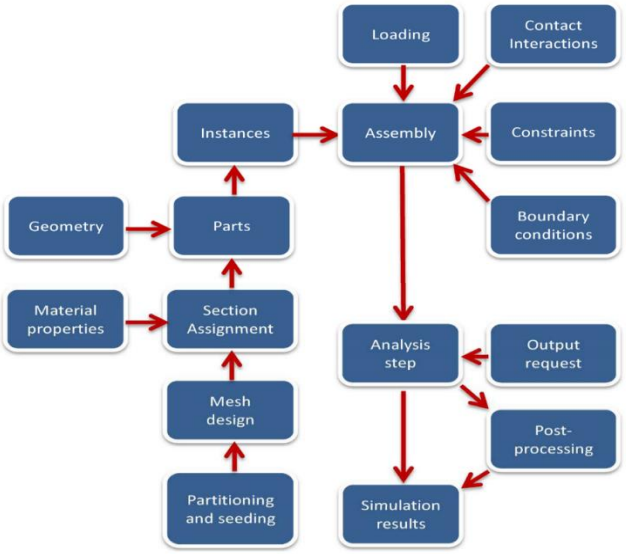

Figure 3.1 Modeling process in Abaqus

The following presents each part of the modeling process and the details of the finite element modeling of a shear tab.

3.1.1 Generate the geometry

In geometry modeling part, Abaqus provides some ways and tools to build every part of the whole model. Also, it allows to input the geometry parts from a third-party graphic software.

In order to reduce computer time, a quarter of the whole specimen is simulated because the specimen is a bi-symmetry geometry. Figure 3.2 shows the formation of a quarter model.

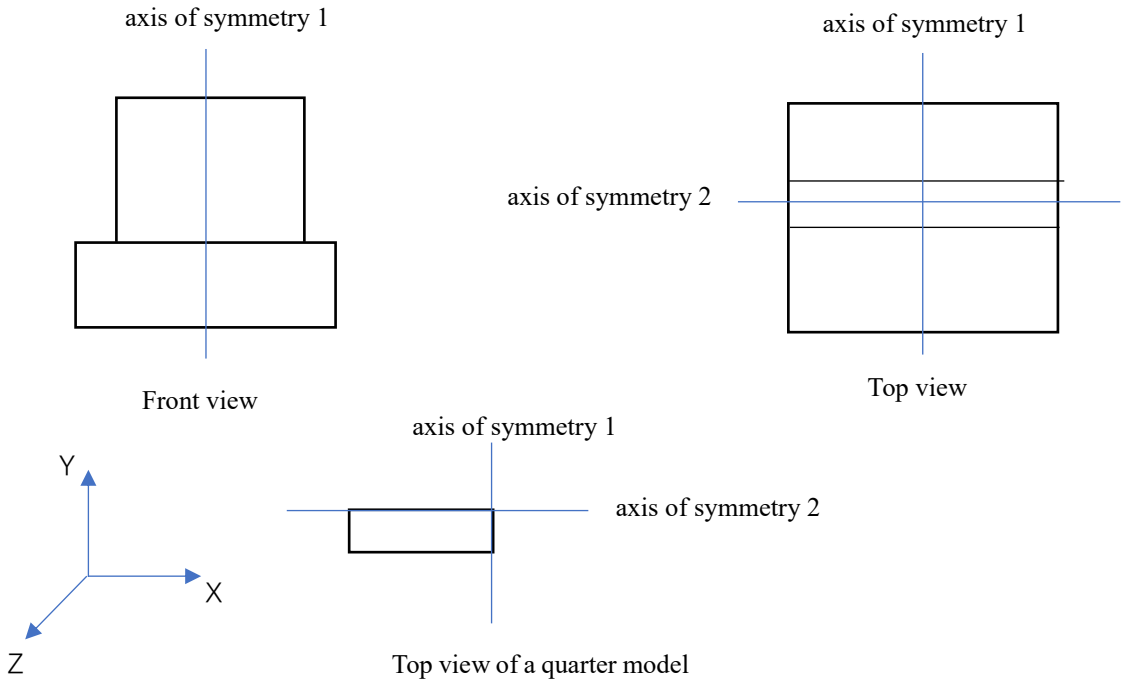

Figure 3.2 The quarter model

In Figure 3.2, there are two axes of symmetry in the shear plate. For axis of symmetry 1, the cut section is just allowed movement in Y-Z plane, and forbid movement in X direction. For axis of symmetry 2, the cut plane is prohibited movement in Z direction, and can has movement in X-Y plane. Also, the anchor plate is treated as a fix support and thus omitted in the modeling, and three geometrical configurations are used to model the weld connection between the shear plate and the anchor plate.

In total, there are 5 parts which are needed to create a quarter of the whole lab test specimen. Figure 3.3 shows the 5 parts in Abaqus.

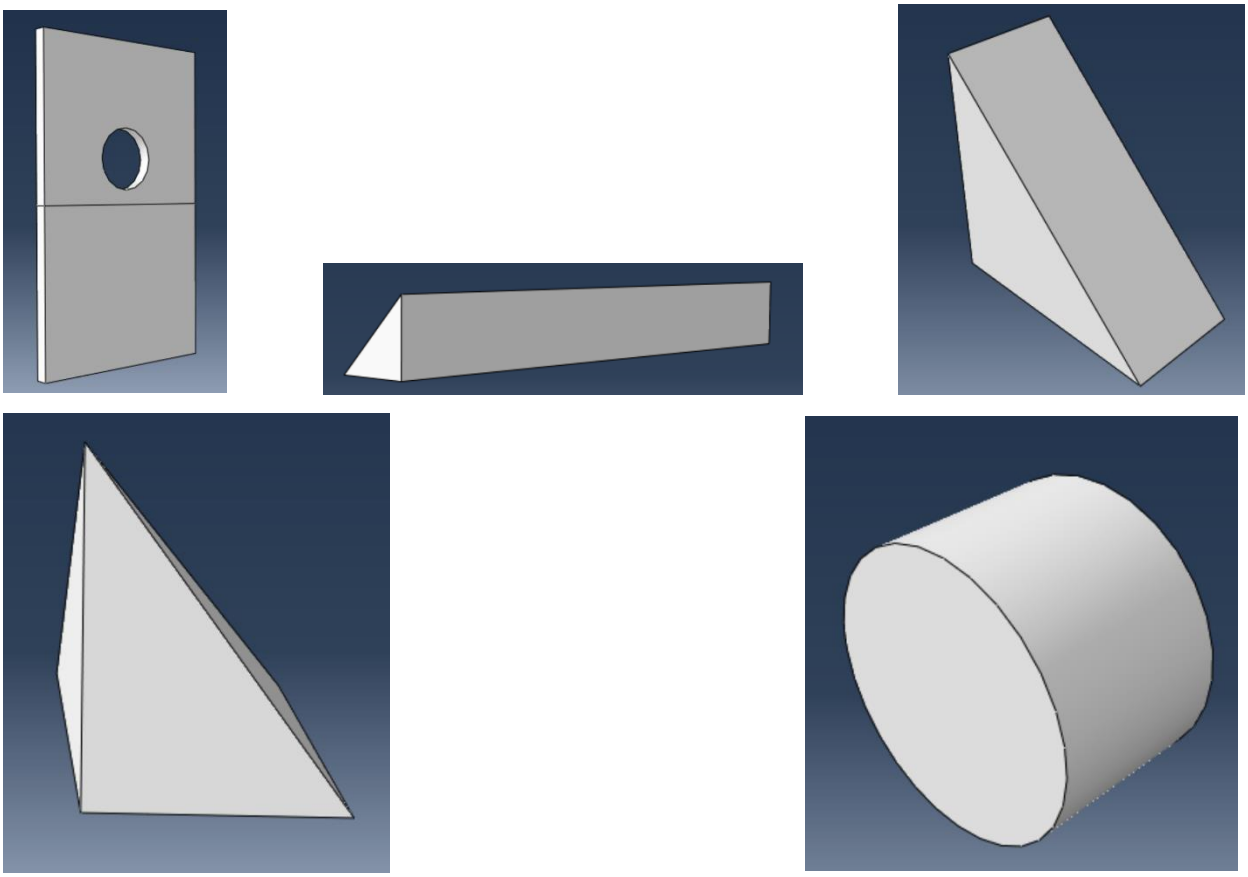

Figure 3.3 Five parts of finite element modeling

The first one is a quarter of the whole shear tab; the last one is used to simulate the bolt; the other three parts are combined together into the welding line between the shear tab and the anchor plate. Table 3.1 shows the sizes of these 5 parts for specimen T95-45-1.

Table 3.1 The dimensions of 5 parts of specimen T95-45-1 in Abaqus

Part ID	Dimensions (mm)
Part 1	76 × 125 × 4.75
Part 2	9.5 × 9.5 × 76
Part 3	9.5 × 9.5 × 4.75
Part 4	9.5 × 9.5 × 9.5
Part 5	22.2 × 14.525

Note: the size of the hole on the shear plate is 23.8mm × 9.5mm.

3.1.2 Input material property

The material properties of three stages were needed: elastic, plastic and damage. The yield and ultimate strengths of steel materials in terms of engineering stress were obtained by coupon tests

(see 2A appendix for details).

In elastic stage, 200 GPa and 0.3 for Young's Modulus and Poisson's ratio were used. In plastic stage, the stress and strain are required to be expressed as the true stress and strain instead of engineering stress and strain. The relationships between true strain, stress and engineering strain, stress are as follows:

$$\sigma = \sigma_E (1 + \varepsilon_E) \tag{3.1}$$

and

$$\varepsilon = ln(1 + \varepsilon_E) \tag{3.2}$$

where ε and σ are true strain and stress, respectively; ε_E and σ_E are engineering strain and stress, respectively.

Table 3.2 and Figure 3.4 show the engineering stress, strain and true stress, plastic strain for T95 models.

Table 3.2 True stress, strain and engineering stress, strain (T95 models)

Engineering stress (MPa)	Engineering strain	True stress (MPa)	Plastic strain
376	0.00188	377	0.000
377	0.02900	388	0.027
378	0.03200	390	0.030
425	0.04600	445	0.043
448	0.05900	474	0.055
477	0.08900	519	0.083
486	0.11500	542	0.106
491	0.14500	562	0.133
463	0.25000	579	0.220

Note: in the software Abaqus, the first data of plastic strain is equal to 0, corresponding to the initial yield stress of the material.

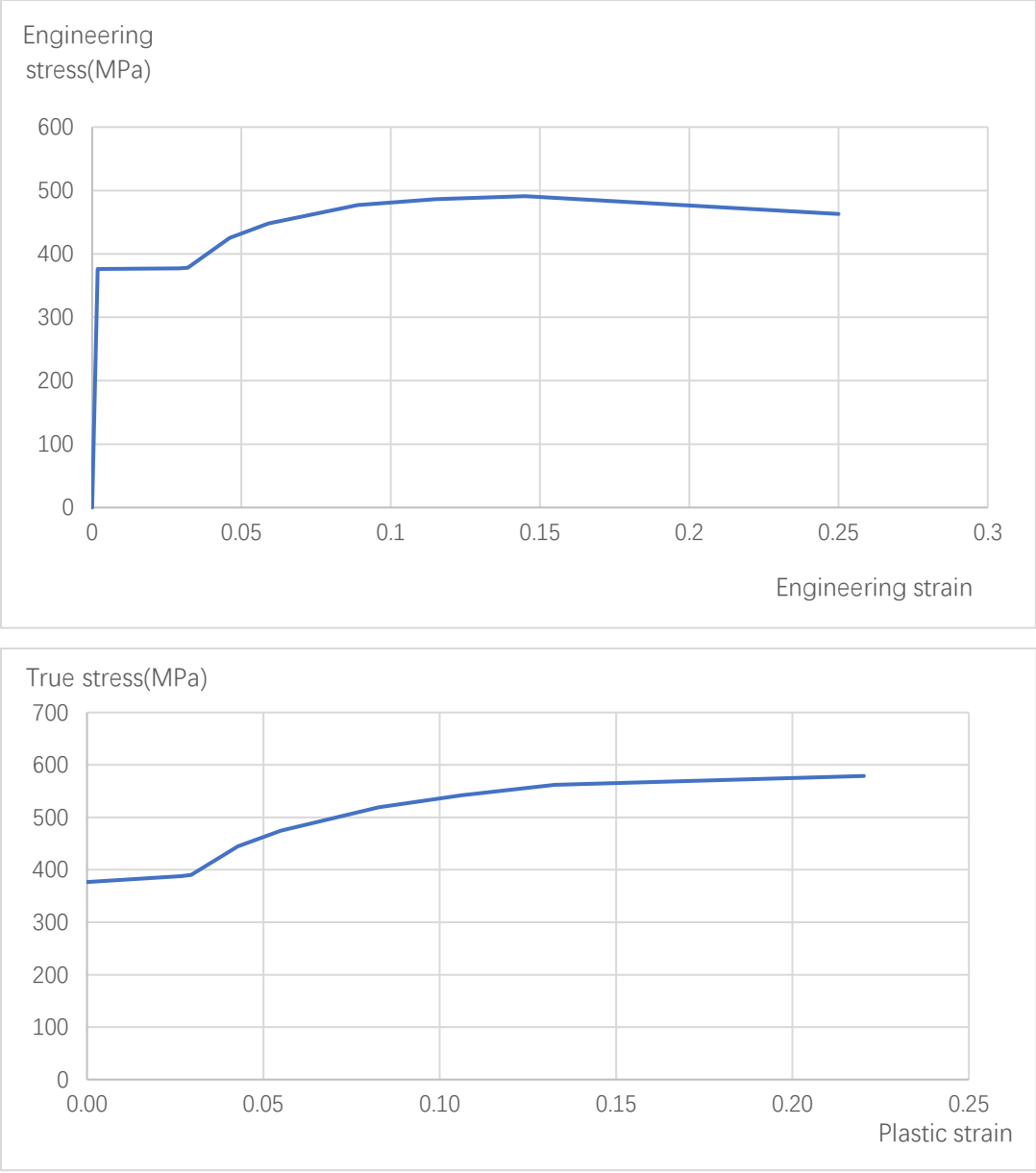

Figure 3.4 Engineering stress, strain and true stress, strain for T95 models

For T127 models, similar to T95 models, Table 3.3 and Figure 3.5 show the details of stress and strain relationships.

Table 3.3 True stress, strain and engineering stress, strain (T127 models)

Engineering stress (MPa)	Engineering strain	True stress (MPa)	Plastic strain
387	0.00194	388	0.000
389	0.03200	401	0.030
391	0.03400	404	0.031
446	0.05300	470	0.050
469	0.06900	501	0.064
481	0.09300	526	0.084
489	0.11800	547	0.109
495	0.15400	572	0.140
474	0.25000	593	0.220

Note: in the software Abaqus, the first data of plastic strain is equal to 0, corresponding to the initial yield stress of the material.

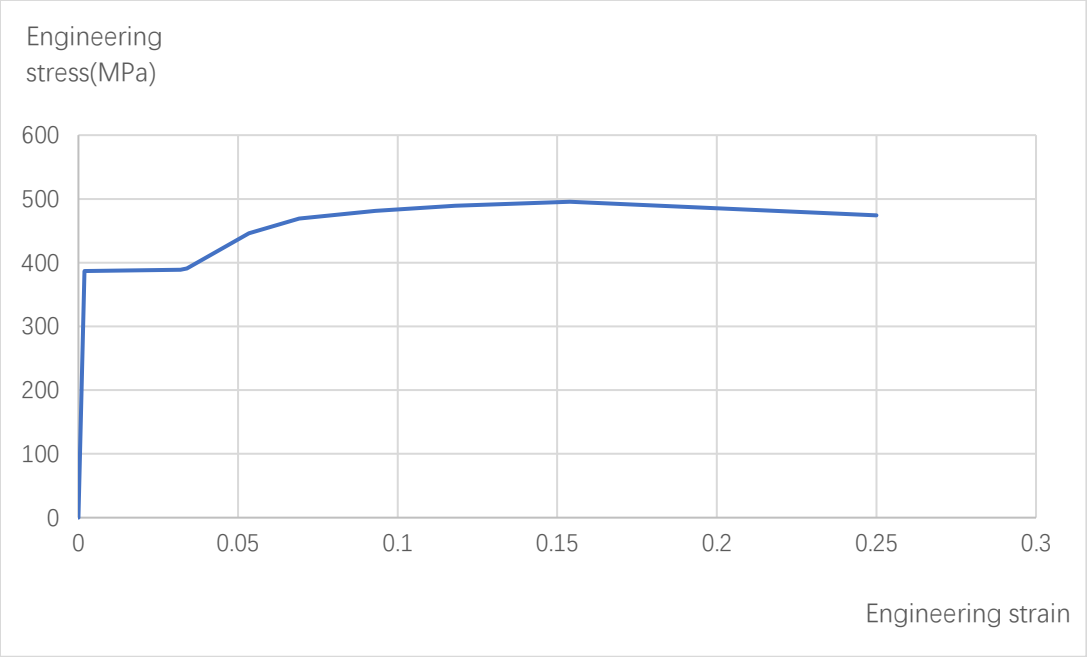

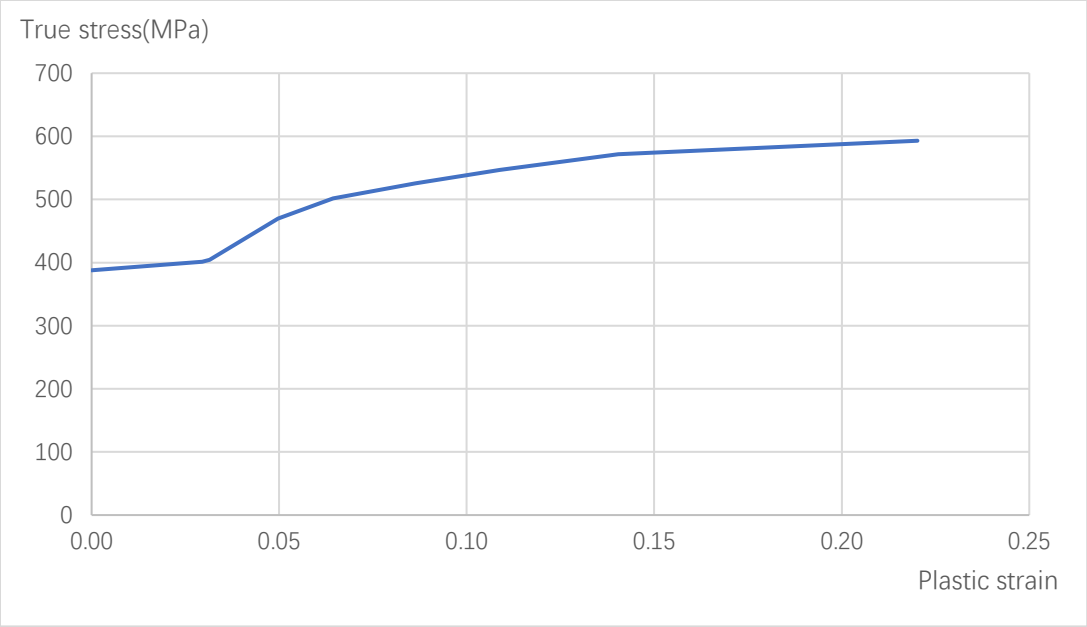

Figure 3.5 Engineering stress, strain and true stress, strain for T127 models

In damage stage, there are two sections which are required to simulate: ductile damage initial and damage evolution. For ductile damage initial, the ductile criterion is a phenomenological model for predicting the onset of damage due to nucleation, growth, and coalescence of voids. The model assumes that the equivalent plastic strain (fracture strain) at the onset of damage is a function of stress triaxiality and strain rate. The stress triaxiality (Ravi Kiran and Kapil Khandelwal, 2014) is defined as the ratio of hydrostatic stress and the Mises stress as follows:

$$T_\sigma = \sigma_H / \sigma_M \tag{3.3}$$

$$\sigma_H = (\sigma_1+\sigma_2+\sigma_3) / 3 \tag{3.4}$$

$$\sigma_M = [\sigma_1^2+\sigma_2^2+\sigma_3^2 - (\sigma_1\sigma_2 +\sigma_2\sigma_3 +\sigma_1\sigma_3)]^{0.5} \tag{3.5}$$

where: T_σ=stress triaxiality; σ_H=hydrostatic stress; σ_M=Mises stress; σ_1, σ_2 and σ_3 are principal stresses.

According to Ravi Kiran and Kapil Khandelwal (2014), the stress triaxiality is a key factor to cause dominant damage of microvoid elongation and dilation, and the stress triaxiality above which the softening caused by the microvoid dilation exceeds the strengthening caused by the matrix hardening is taken as the triaxiality limit where the damage mechanism shifts from microvoid elongation to dilation. This triaxiality limit is referred to as the transition triaxiality limit, which is taken as 0.75 in this thesis. In order to develop a computational fracture locus, it is

assumed that microvoid elongation and dilation are the only mechanisms of damage at low (less than the transition triaxiality limit) and high triaxiality (larger than the transition triaxiality limit), respectively.

For the low triaxiality regime (T_σ ranges from zero to the transition limit), it is assumed that the void elongation ratio reaches a critical value before the ligament between two neighboring elongated microvoid fails (causing a local material to fracture). The critical value of void elongation ratio is taken as 4 in this thesis.

For the high stress triaxiality regime, a rapid microvoid growth is observed at a certain macroscopic effective plastic strain value. At this strain, the softening due to rapid microvoid dilation dominates the matrix hardening leading to strain localization in the intervoid ligaments resulting in overall softening behavior and finally leading to local material fracture.

In other words, for the fracture locus, in the low triaxiality regime the fracture strain increases with the increase in triaxiality because the tendency of microvoids to elongate decreases with the increase of the stress triaxiality. For high regime, the fracture strain decreases rapidly with the increase of the stress triaxiality due to the fact that microvoids dilate rapidly at the high stress triaxiality.

Figure 3.6 and 3.7 shows the evolution of stress triaxiality in the critical finite elements of the shear tab (T95-45-1 and T95-45-2). The finite elements at which the failure initiated are referred to as critical finite elements. Tables 3.4 and 3.5, Figures 3.8 and 3.9 show the calibration results for T95 and T127 models.

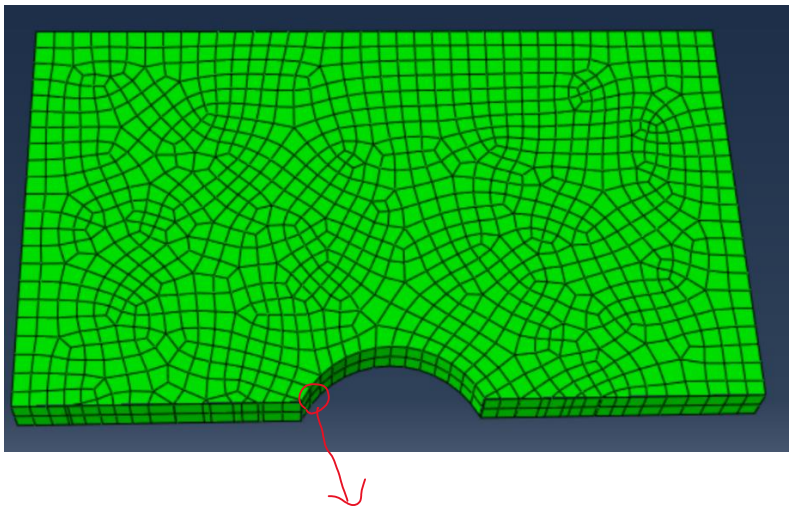

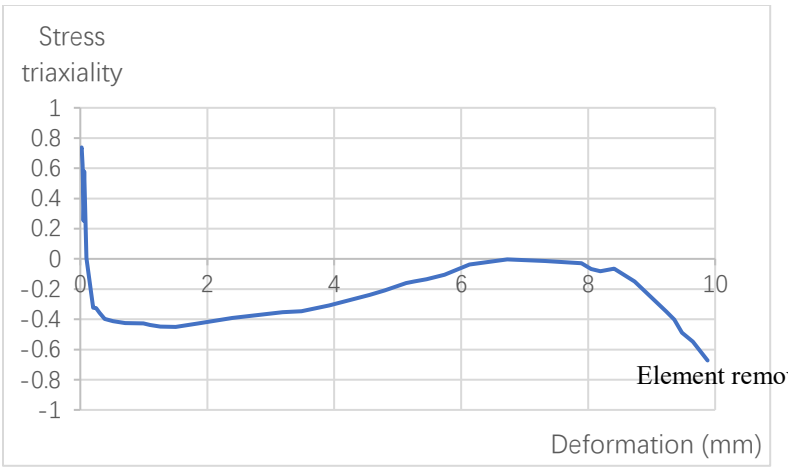

Figure 3.6 Evolution of stress triaxiality in the critical finite element (bearing tear-out)

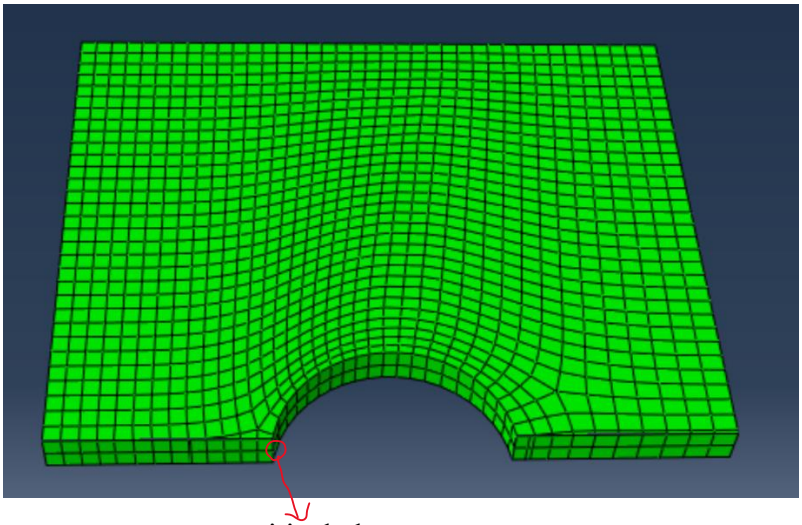

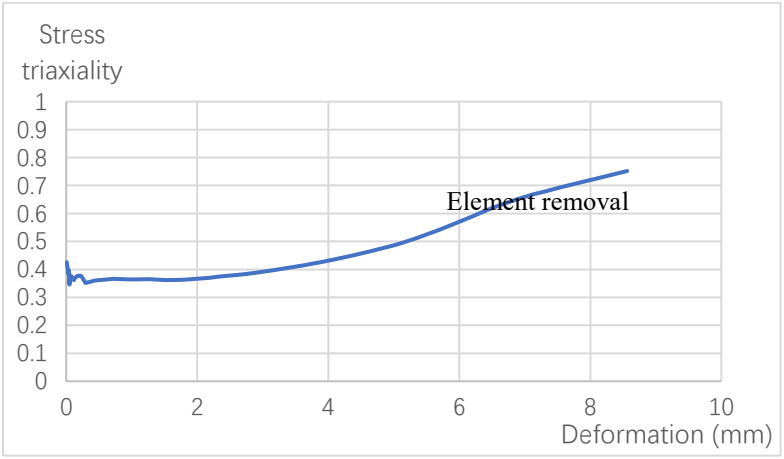

Figure 3.7 Evolution of stress triaxiality in the critical finite element (net-section rupture)

Table 3.4 Calibration results of the fracture initiation for T95 models

Fracture strain	Stress triaxiality	Strain rate
33.800	-0.333	0.010
27.780	-0.330	0.010
21.160	-0.325	0.010
13.780	-0.320	0.010
7.780	-0.312	0.010
2.240	-0.306	0.010
1.308	-0.297	0.010
0.824	-0.270	0.010
0.616	-0.235	0.010
0.500	-0.198	0.010
0.360	-0.166	0.010
0.320	-0.138	0.010
0.300	-0.118	0.010
0.280	-0.086	0.010
0.260	-0.050	0.010
0.220	0.000	0.010
0.226	0.105	0.010
0.254	0.265	0.010
0.260	0.290	0.010
0.266	0.333	0.010
0.300	0.480	0.010
0.340	0.610	0.010
0.400	0.750	0.010
0.300	1.000	0.010
0.200	1.400	0.010
0.130	2.000	0.010
0.100	3.000	0.010
0.080	4.000	0.010

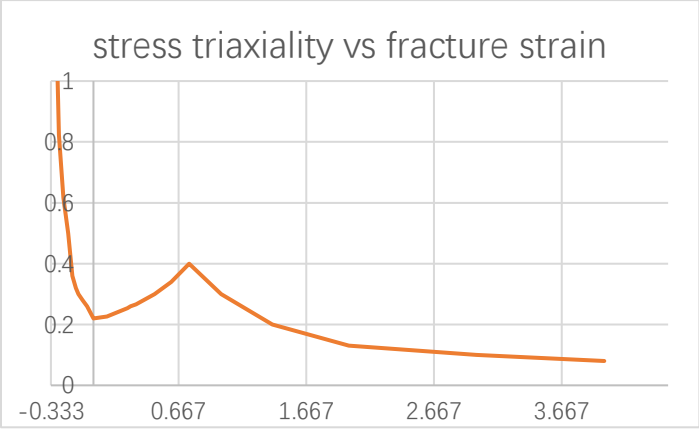

Figure 3.8 Stress triaxiality vs. fracture strain for T95 models

Table 3.5 Calibration results of the fracture initiation for T127 models

Fracture strain	Stress triaxiality	Strain rate
16.900	-0.333	0.010
13.890	-0.330	0.010
10.580	-0.325	0.010
6.890	-0.320	0.010
3.890	-0.312	0.010
1.120	-0.306	0.010
0.654	-0.297	0.010
0.412	-0.270	0.010
0.308	-0.235	0.010
0.265	-0.198	0.010
0.245	-0.166	0.010
0.234	-0.138	0.010
0.220	-0.118	0.010
0.210	-0.086	0.010
0.205	-0.049	0.010
0.200	0.000	0.010
0.205	0.105	0.010
0.225	0.265	0.010
0.240	0.333	0.010
0.310	0.480	0.010
0.460	0.666	0.010
0.595	0.780	0.010
0.380	1.000	0.010
0.150	1.500	0.010
0.110	2.000	0.010
0.090	3.000	0.010
0.080	4.000	0.010

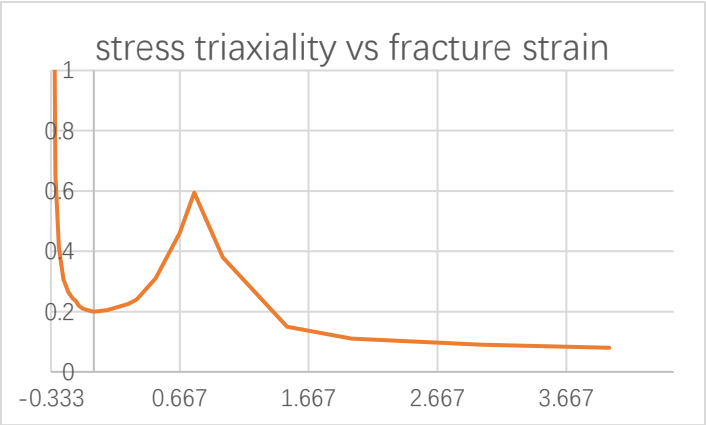

Figure 3.9 Stress triaxiality vs. fracture strain for T127 models

For damage evolution, in the context of an elastic-plastic material with isotropic hardening, the damage manifests itself in two forms: softening of the yield stress and degradation of the elasticity. The solid curve in Figure 3.10 represents the damaged stress-strain response, while the dashed curve is the response in the absence of damage.

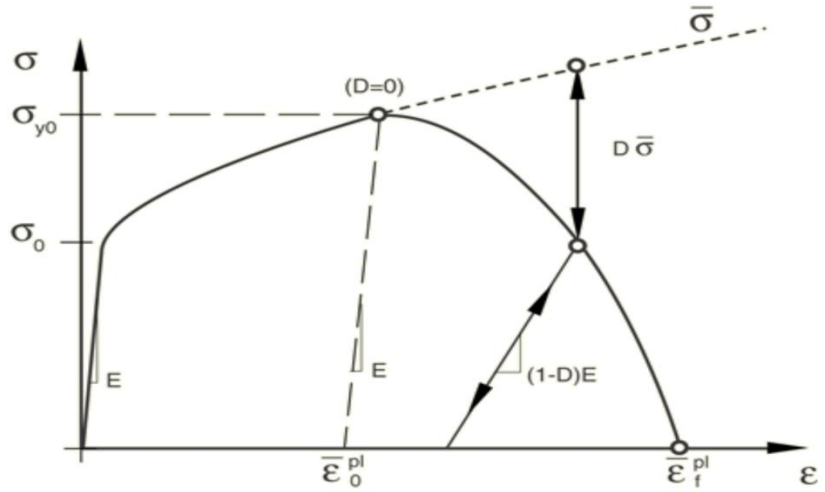

Figure 3.10 Stress-strain curve with progressive damage degradation

In Figure 3.10, σ_{y0} and $\bar{\varepsilon}_0^{pl}$ are the yield stress and the equivalent plastic strain at the onset of damage, and $\bar{\varepsilon}_f^{pl}$ is the equivalent plastic strain at failure, at which the overall damage variable D reaches the value of 1. The overall damage variable, D, captures the combined effect of all active mechanisms and is computed in terms of individual damage variables, d_i, for each mechanism.

The damage evolution is based on the effective plastic deformation (displacement at failure) which is taken as 0.5mm herein, and once the damage initiation criterion has been reached, the effective plastic displacement, $\bar{u}^{pl}$, is defined with the evolution equation $\bar{u}^{pl}=L\varepsilon^{pl}$, where L is the characteristic length of the element.

The evolution of the damage variable with the relative plastic displacement was specified in linear form herein (Figure 3.11).

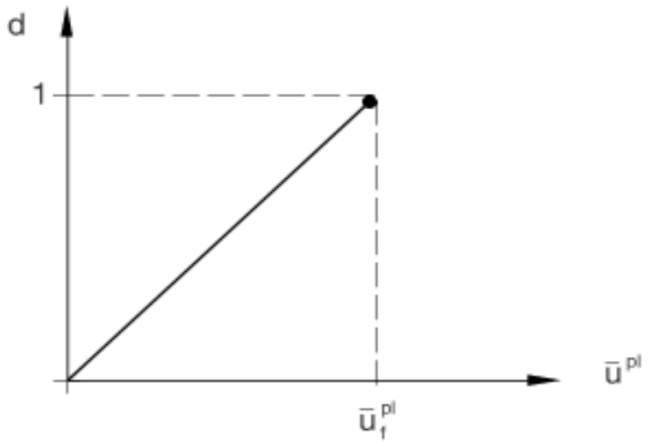

Figure 3.11 Definitions of damage evolution based on plastic displacement (linear)

The bolt and welded were regarded as elastic material with 200 GPa and 0.3 for Young's Modulus and Poisson's ratio for the whole analysis

3.1.3 Assembly

In this step, all the parts which were created in the first step were moved into one coordinate system, and then were combined into one model. Figures 3.12 shows the T95-45-1 model after assembling. The bolt was put in the central of the hole (Figure 3.13), so it has a 0.8mm bolt slippage in the all simulations.

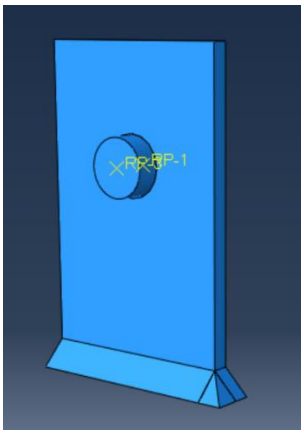

Figure 3.12 The analysis model in Abaqus

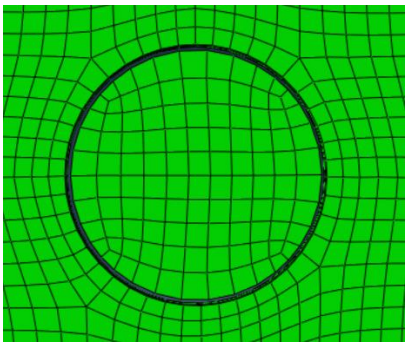

Figure 3.13 The position of bolt

3.1.4 Setting analysis step

Abaqus provides the “step” for users to set analysis process. Each step can output any relative variables by user’s setting. In this research, two general steps are employed: step 1 for elastic analysis, and step 2 for plastic analysis. In each step, the software further employs many incremental steps in the analysis automatically, and the maximum incremental step and incremental size in each one can be set by users. Herein, 1000 and 1E-009 to 0.1 were used for maximum incremental steps and the incremental size.

3.1.5 Applying interaction

In this part, the interaction properties and constraints can be applied for the model. The Abaqus provides many contact interactions: general contact, surface-to-surface contact, self-contact, fluid cavity, fluid exchange and so on. In this research, all the contact interactions were created as the surface-to-surface contact. This type of contact uses finite sliding formulation which is based on a master-slave contact pair algorithm. This algorithm can prohibit the nodes on the slave surface from getting into the master surface, but allows the nodes on the master surface to get into the slave surface. Therefore, it is important to select the proper surface type in the simulation. According to Simulia (2011b), there are two rules for surface type selection: first, the slave surface should be a surface with a finer mesh; second, the surface with softer material should be set as slave surface if two surfaces’ mesh are similar.

For the interaction properties, friction was used in the modeling. The normal behavior was used in the interaction properties, and the hard contact was chosen for pressure-overclosure which created a contact constraint to surfaces and transferred the contact pressure between the two surfaces if the clearance becomes zero. “Allow separation after contact” was used, and when the

contact pressure becomes zero or negative, this hard contact constraint was removed. The tangential behavior was used with penalty friction formulation. This friction type controls the shear stress transformation between the two surfaces. The tangential behavior occurred when the shear stress reached a certain value and the slip appears between the two surfaces. Herein, the friction coefficient was taken as 0.3.

The following three contacts with friction were used in the model:

1) the contact between the bolt surface and hole surface

2) the contact between the shear tab plate and the weld parts

3) the contact between the weld parts

For the constraint, “tie” and “coupling” were used in the modeling: the “tie” constraints were for the surfaces of weld parts and shear plate, and the “coupling” was for the central point of the circle surface of the bolt.

3.1.6 Applying load

In this part, boundary conditions and load were created. Four boundary conditions were built in this model as follows:

1) the bottom surface of the model: U1= U2 = U3 = UR1 = UR2 = UR3 = 0

2) the cut surface of the shear plate (surface 1): U1 = UR2 = UR3 = 0

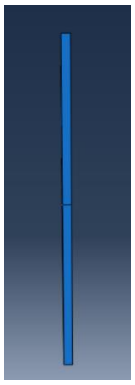

Figure 3.14 Surface 1

3) the cut surface of the shear plate (surface 2): U3 = UR1 = UR2 = 0

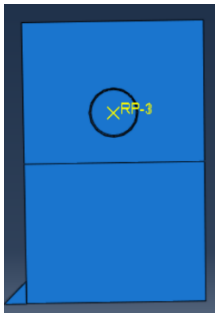

Figure 3.15 Surface 2

4) the cut surface of the bolt: U3 = UR1 = UR2 = 0

For the load, a displacement load was applied to the central point of the circle surface of the bolt and acted on the coupling point which was created in the interaction part.

3.1.7 Mesh design

Mesh design is critical in the modelling, because it has major influence on the analysis results.

The first step of meshing was to partition each individual part, because the Abaqus could not fix the complex geometry models. Then applying the seeds was used to determine the element size. Next, choose the proper element type for each part. Last, choose the mesh type for meshing. Table 3.6 shows the details of meshing in each part.

Table 3.6 Mesh design of each part

Part ID	Element code	Shape	Order	Nodes	Size (mm)
Part 1	C3D8R	Hexahedral	Linear	8	2
Part 2	C3D8R	Hexahedral	Linear	8	2
Part 3	C3D8R	Hexahedral	Linear	8	2
Part 4	C3D4H	Tetrahedron	Linear	4	2
Part 5	C3D8R	Hexahedral	Linear	8	2

Note that for the element size, 4 mm was used at first to do the modeling, but the analysis results could not converge. Then, a smaller element size of 2 mm was used for modeling, and it gave a better result (computational time between 15-20 mins). For comparison, 1 mm element size was also used for modeling, and it had the same failure mode and similar load-deformation curve as the 2 mm element size model (but computational time was more than one hour). Therefore, 2 mm element size was chosen as the final element size for modeling.

3.1.8 Job

After all the defining parts, use “job” part to do the analysis, and it provides real time monitoring during the analyzing.

3.1.9 Visualization

This part provides the display of the model and analysis results. Also, any variables and other result information which are needed can be outputted in this section.

3.2 Simulation results

The following Figure 3.17 to Figure 3.26 show the load-deformation curves and deformation shapes of the five simulations. Note that the deformation shapes shown by the figures are corresponding to the red dots in the load-deformation curves.

The different colors on the final shape of simulations in this research represent the different levels of stress at this moment, and the stress decreases with Figure 3.16 from left (red) to right (blue). Note that all the Figures of deformations shape from Abaqus were used to check the failure mode in this research, and the stresses were not concerned here.

Figure 3.16 Spectrum of stresses

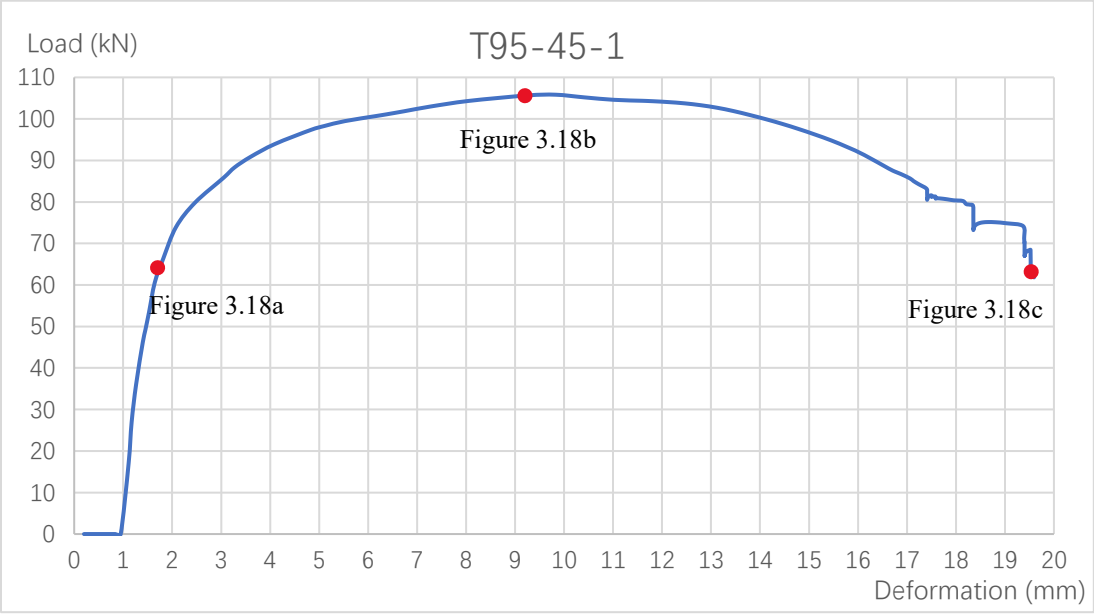

Figure 3.17 Load-deformation curve of T95-45-1

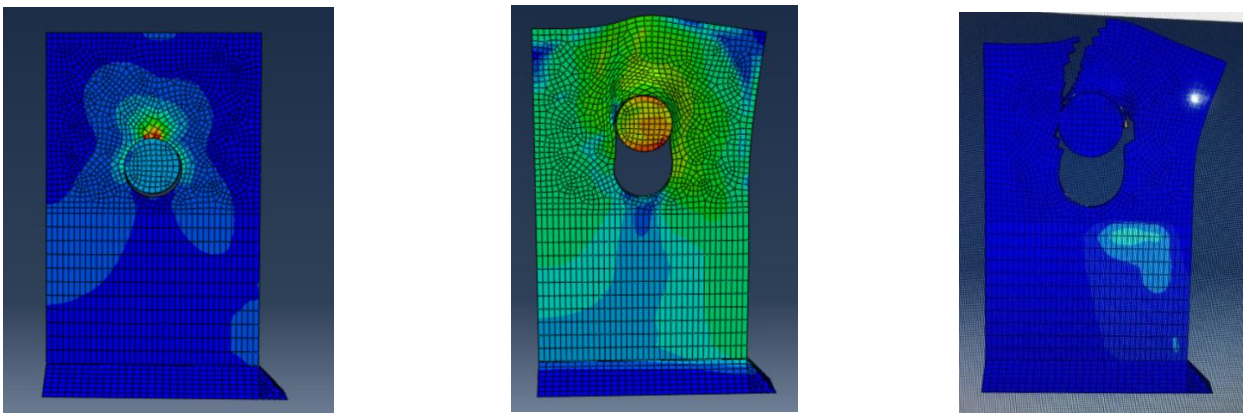

(a) (b) First fracture (c)

Figure 3.18 Deformation shapes of T95-45-1

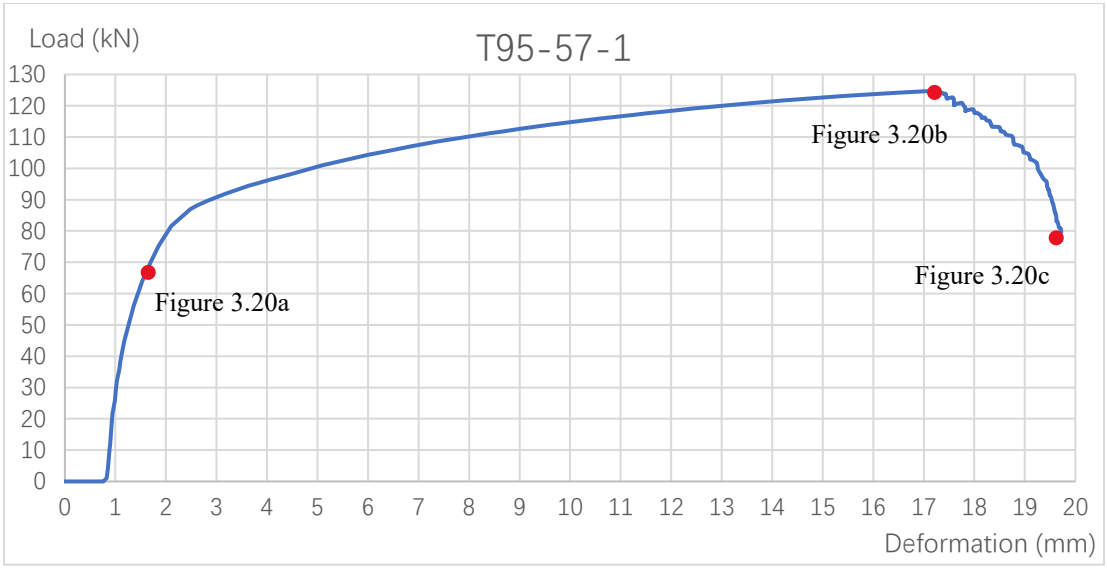

Figure 3.19 Load-deformation curve of T95-57-1

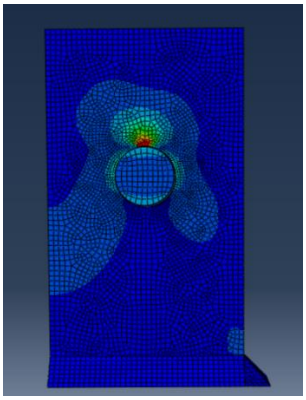

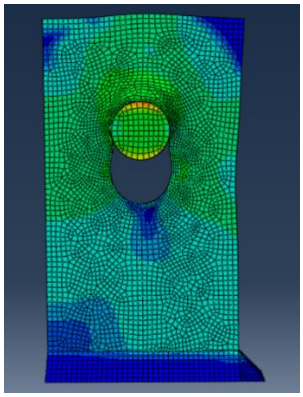

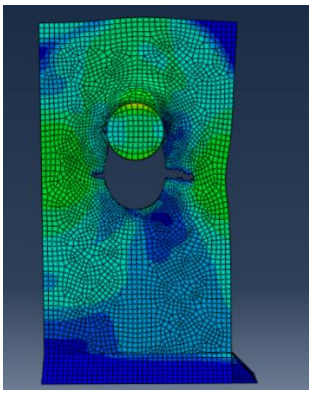

(a) (b) First fracture c

Figure 3.20 Deformation shape of T95-57-1

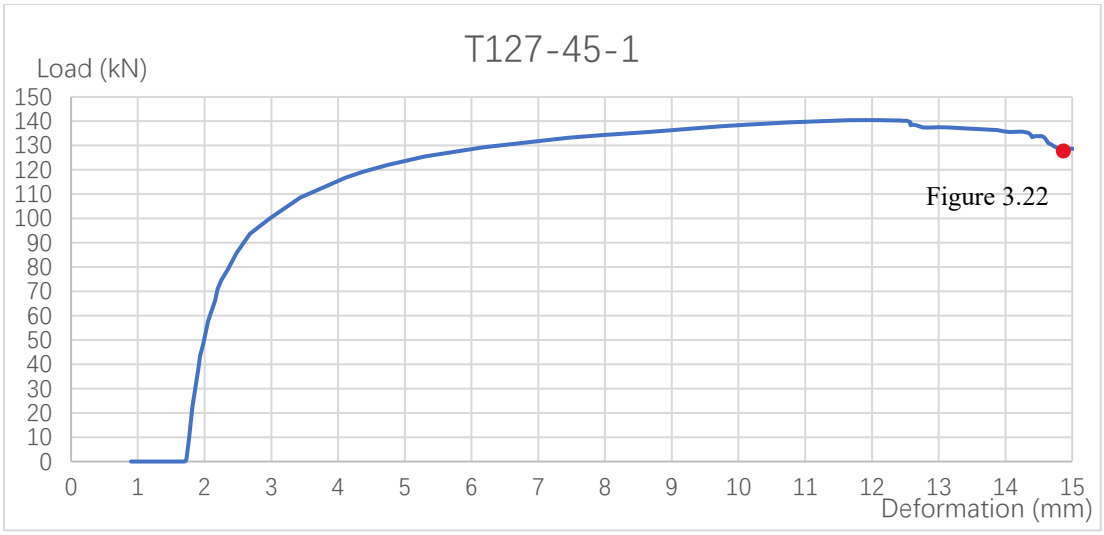

Figure 3.21 Load-deformation curve of T127-45-1

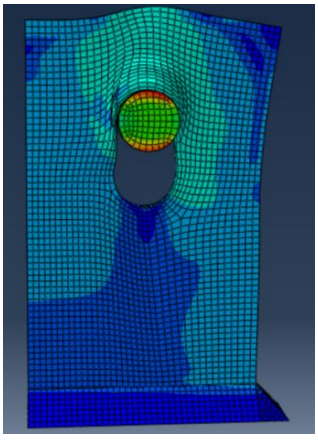

Figure 3.22 Deformation shape of T127-45-1

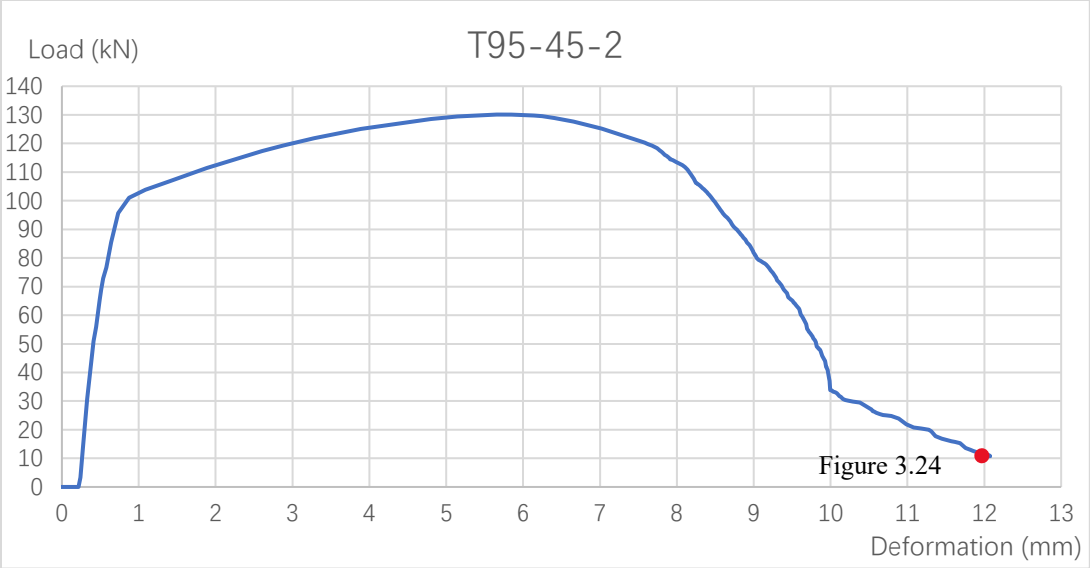

Figure 3.23 Load-deformation curve of T95-45-2

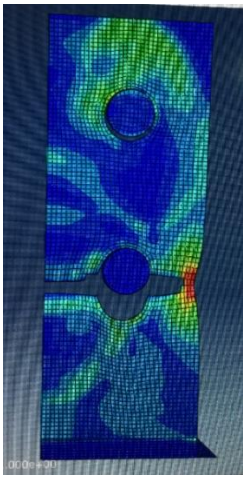

Figure 3.24 Deformation shape of T95-45-2

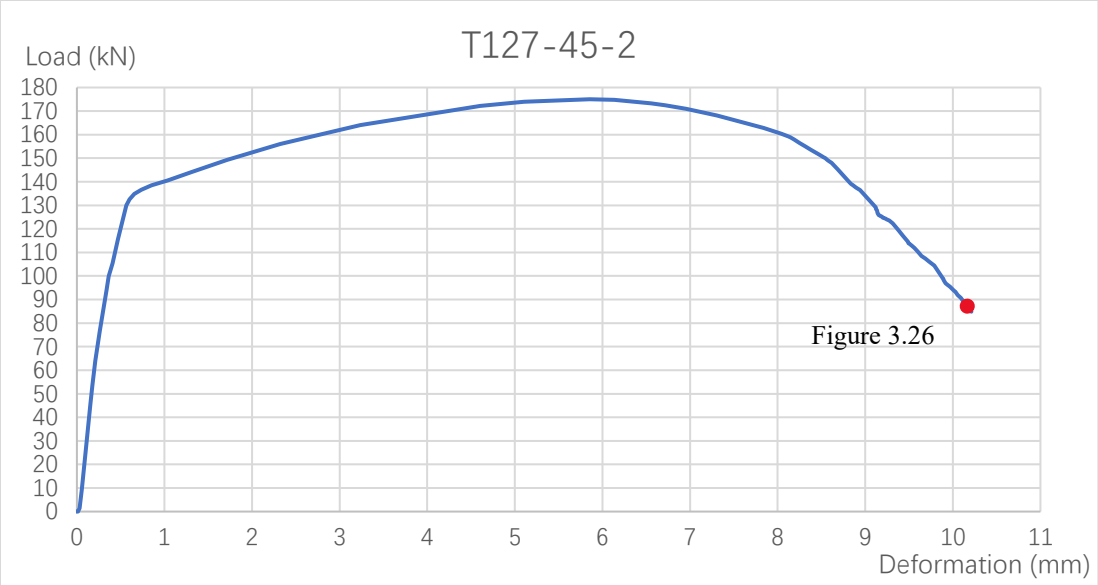

Figure 3.25 Load-deformation curve of T127-45-2

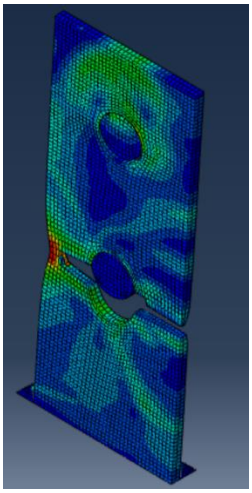

Figure 3.26 Deformation shape of T127-45-2

Table 3.7 Simulation results of lab tests

Simulation ID	T_y (kN)	Rupture deformation (mm)	Failure mode
T95-45-1	368	19.1	Bearing tear-out
T95-57-1	372	18.8	Net-section rupture
T127-45-1	476	14.5	Bearing tear-out
T95-45-2	444	10.5	Net-section rupture
T127-45-2	604	10.6	Net-section rupture

Note: T_y definition is given in Chapter 5.

3.3 Comparison

Figure 3.27 to Figure 3.31 show the comparison of software and lab test curves of each specimen.

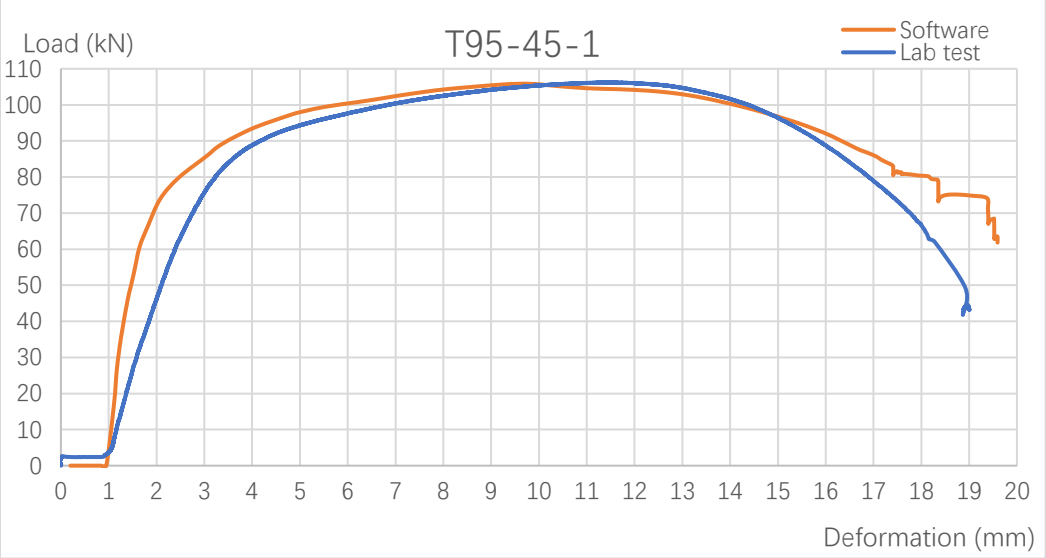

Figure 3.27 Specimen T95-45-1

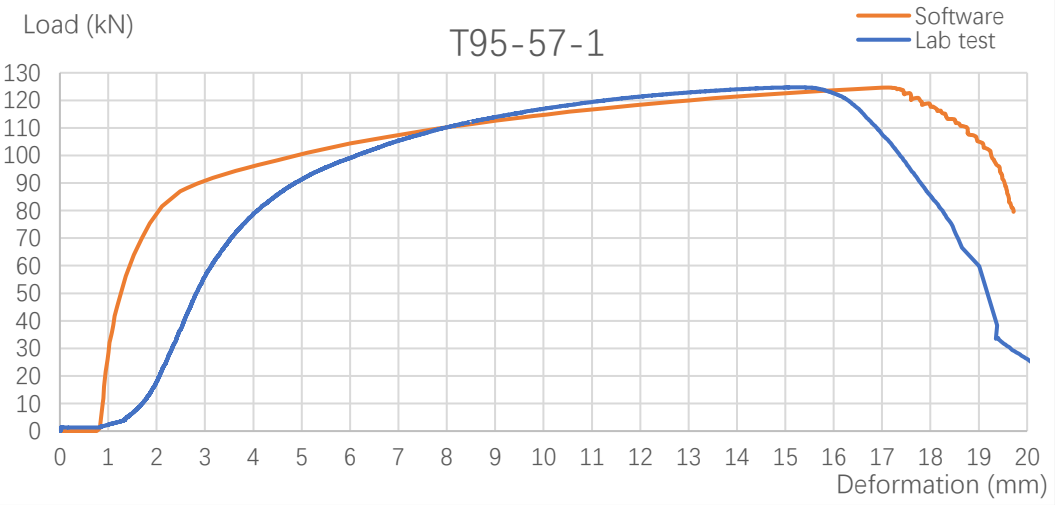

Figure 3.28 Specimen T95-57-1

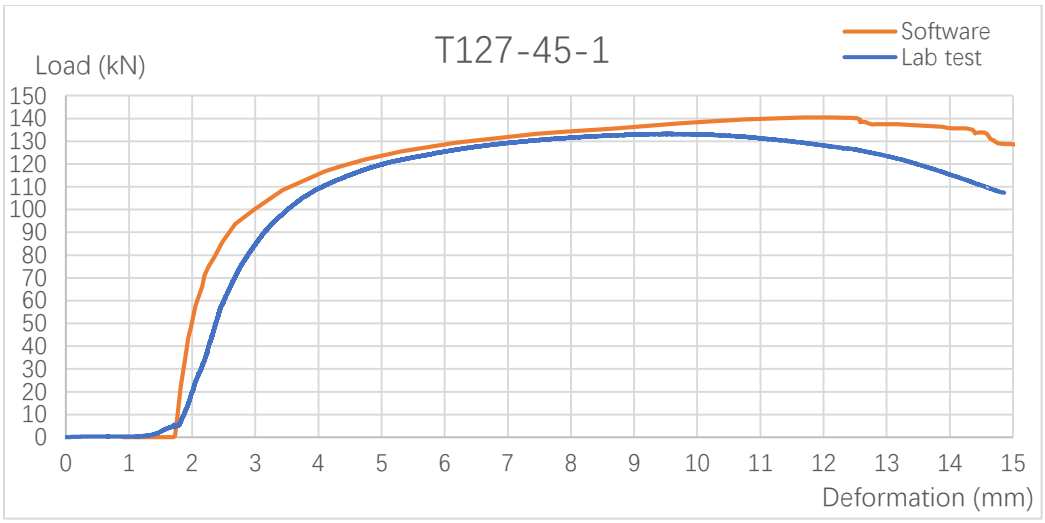

Figure 3.29 Specimen T127-45-1

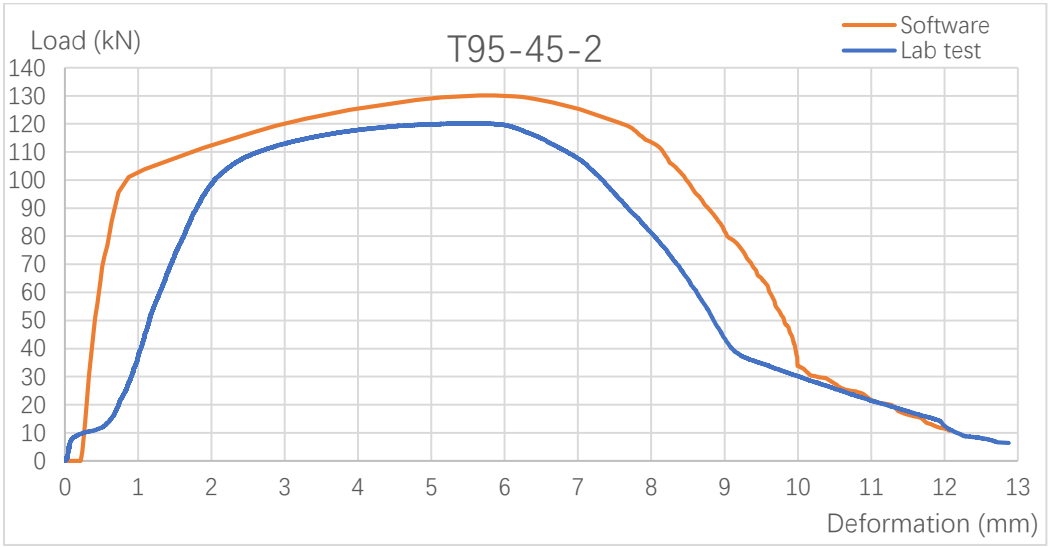

Figure 3.30 Specimen T95-45-2

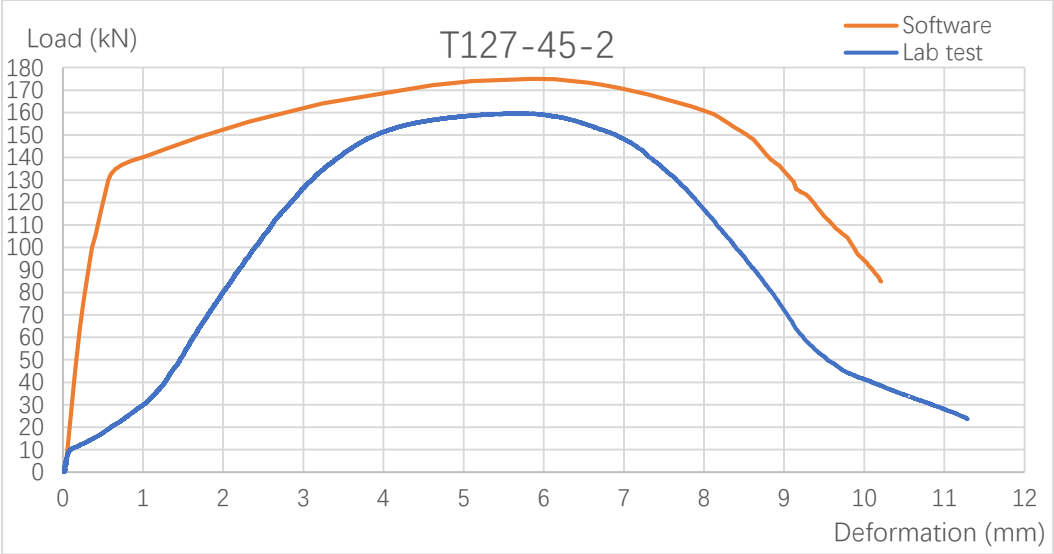

Figure 3.31 Specimen T127-45-2

3.4 Summary

Finite element models of lab test specimens were created through Abaqus to replicate the pure tension tests. Table 3.8 shows the summary of the simulation results in comparison with the predicted and test results.

By implementing the FE simulations strategy equipped with the ductile damage for metal model and appropriate material properties, all the models succeeded in duplicating the failure modes of bearing tear-out and net-section rupture of the tested shear tab connections.

Furthermore, the finite element models developed in this chapter can satisfactorily duplicate the load-deformation curve of the specimens with one-column bolts only. However, more works need to be done to improve the accuracy of the models corresponding to the two-column bolt specimens.

The work done in this chapter provides confidence for the author to conduct a parametric study on the shear tab connections having one column bolts only in next chapter.

Table 3.8 Summary of the simulation results in comparison with the predicted and test results

Specimen ID	Predicted resistance (kN)	Test resistance (kN)	FE simulation resistance (kN)
T95-45-1	110.75	104.75	106.00
T95-57-1	121.25	122.75	125.00
T127-45-1	144.50	130.75	140.00
T95-45-2	121.25	118.50	130.00
T127-45-2	160.75	157.00	175.00

Chapter 4 Parametric study

In this chapter, the finite element models established in the previous chapter were used to conduct a parametric study for the shear tabs having one column of bolts.

4.1 Parameters

The parameters of the shear tab connections are plate thickness, edge distance, bolt diameter and shear load.

Three different plate thicknesses were considered: 6.4 mm, 9.5 mm and 12.7 mm; three different bolt sizes were considered: diameter 19 mm, diameter 22.2 mm and diameter 25.4 mm; two different edge distances were considered: 2.0d and 2.5d. For example, 45 mm and 57 mm for bolt size of diameter 22.2 mm. In this way, 38 mm and 48 mm for bolt diameter 19 mm models, and 51mm and 64mm for bolt diameter 25.4 mm models; three different accompanied shear loads were considered: V=0.15T, 0.30T, and 0.45T (d is bolt diameter, V is shear force, T is tension force). Figure 4.1 shows how the shear load is applied.

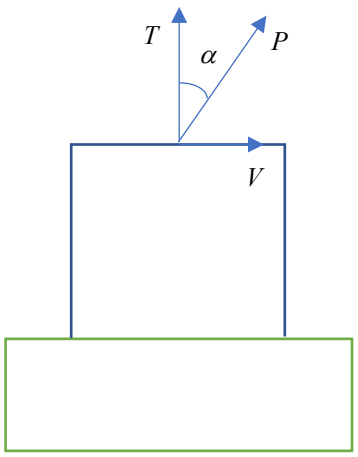

α is load orientation.
when $\alpha = 0^0$, it is zero shear force or pure tension force;
when $\alpha = 90^0$, it is pure shear force;
when $0^0 < \alpha < 90^0$, it is combined tension and shear, $T = P \times cos\alpha$, $V = P \times sin\alpha$;

Figure 4.1 Combined tension and shear force

4.2 Simulation results of 19mm bolt diameter

Figures 4.2 to 4.13 show load-deformation curves and the final deformed shapes of the six simulations. Note that the material properties of the T64 models were taken the same as those of the T95 models (see Chapter 3 for details).

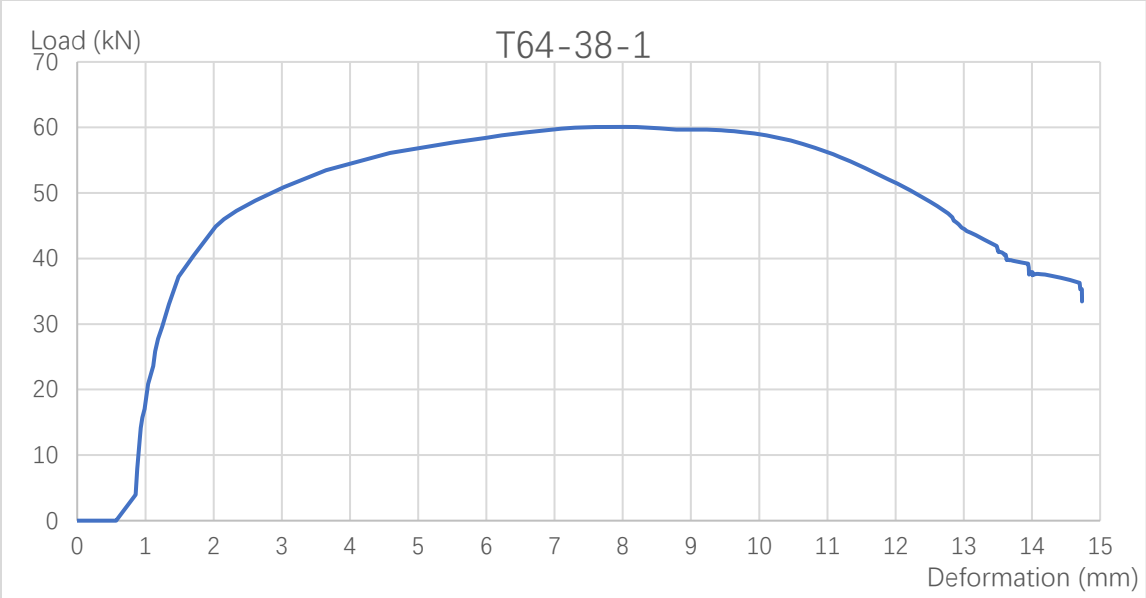

Figure 4.2 Load-deformation curve of T64-38-1

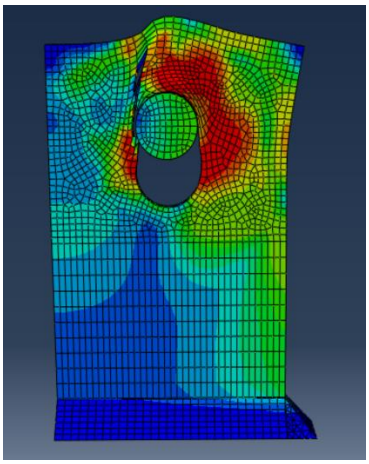

Figure 4.3 Final deformed shape of T64-38-1

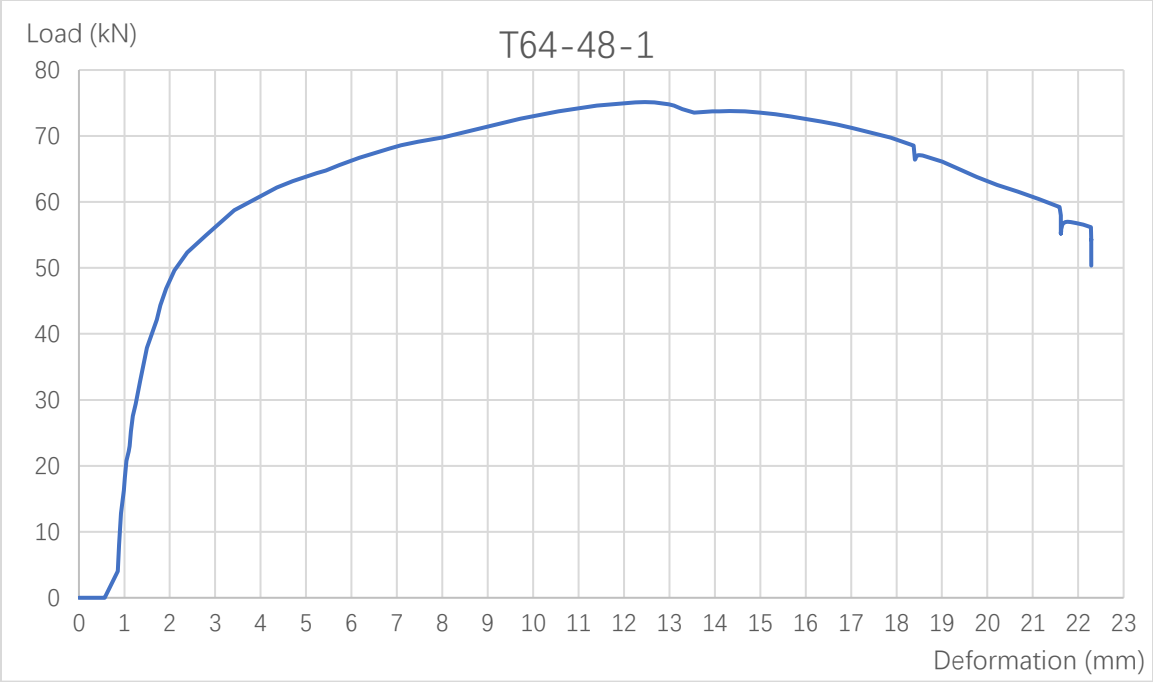

Figure 4.4 Load-deformation curve of T64-48-1

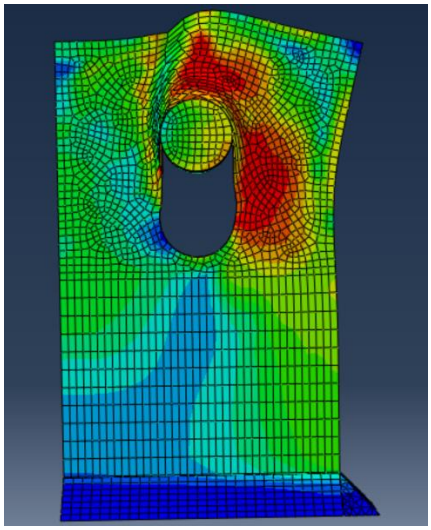

Figure 4.5 Final deformed shape of T64-48-1

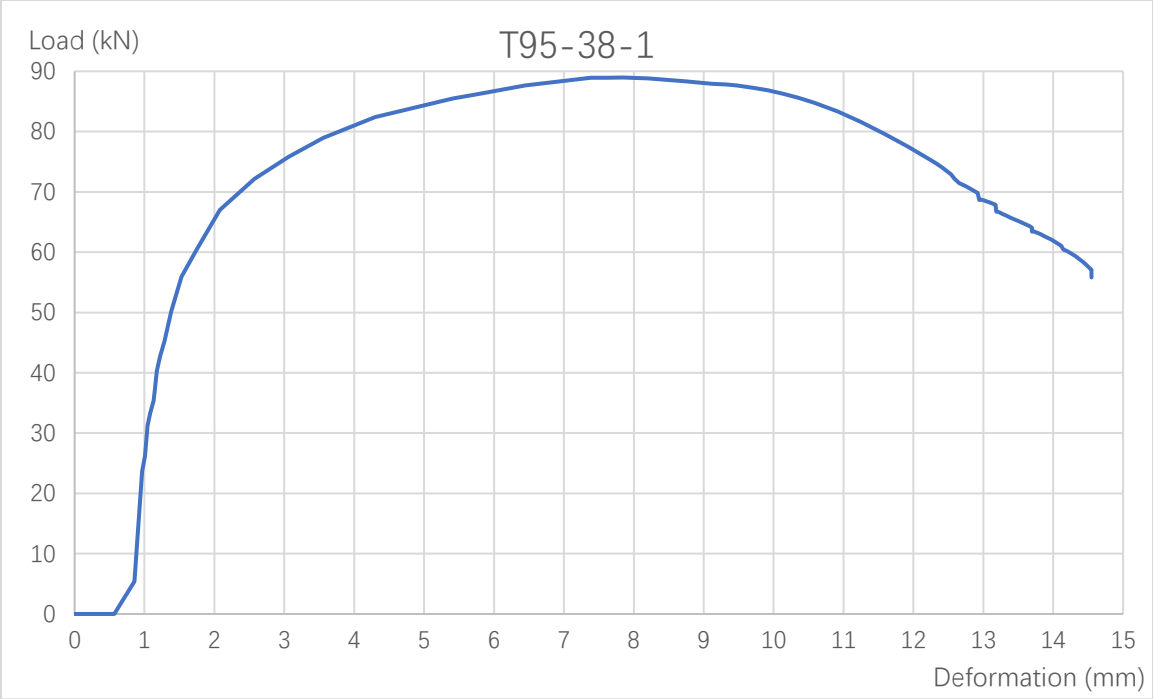

Figure 4.6 Load-deformation curve of T95-38-1

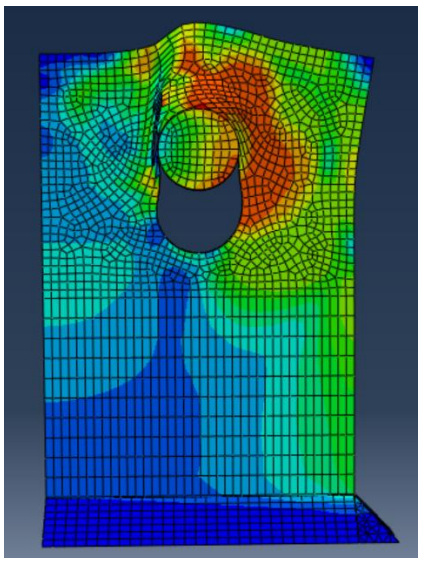

Figure 4.7 Final deformed shape of T95-38-1

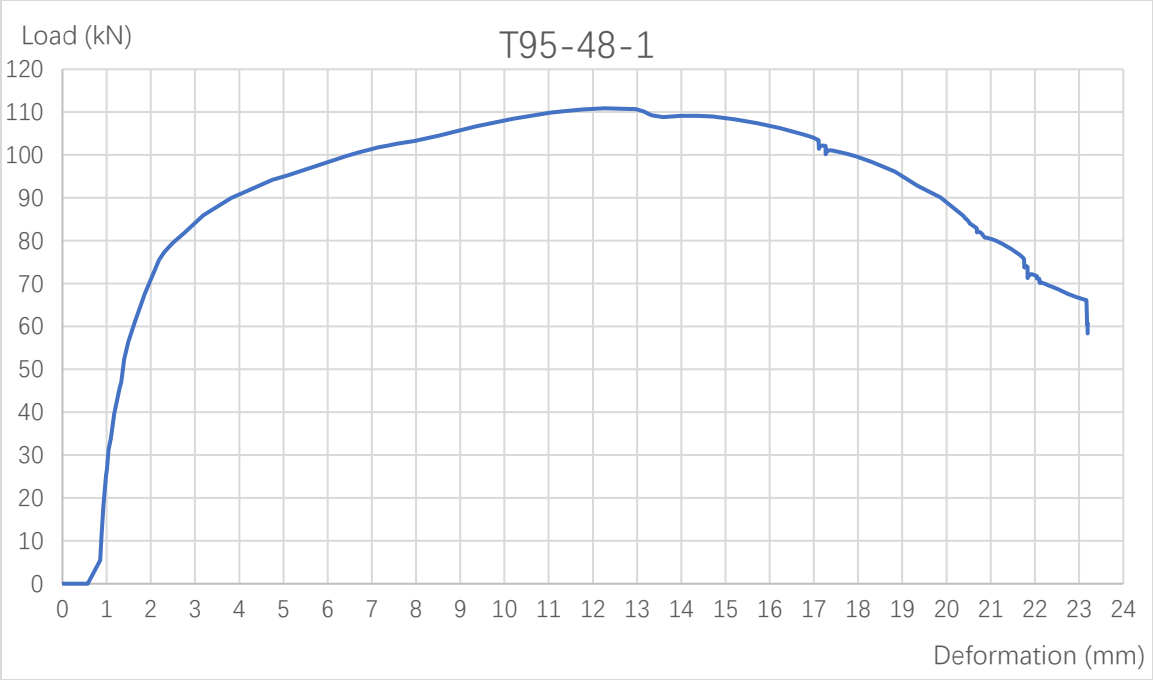

Figure 4.8 Load-deformation curve of T95-48-1

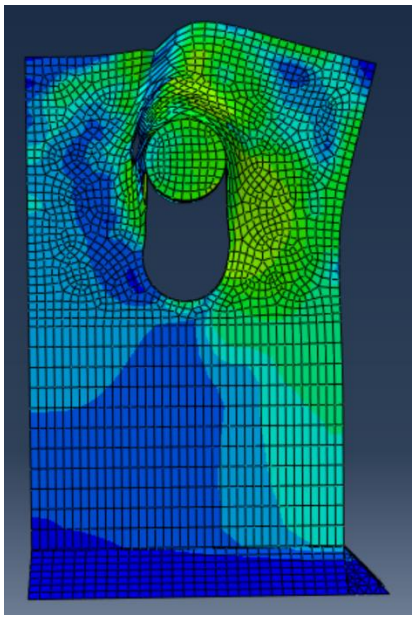

Figure 4.9 Final deformed shape of T95-48-1

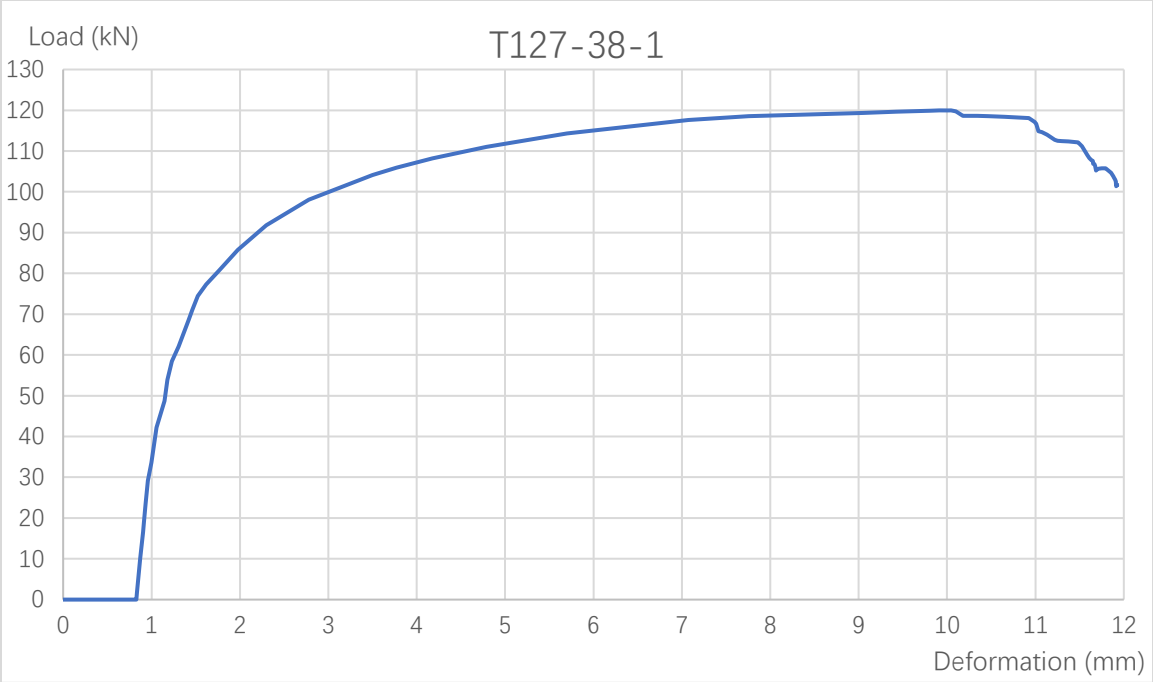

Figure 4.10 Load-deformation curve of T127-38-1

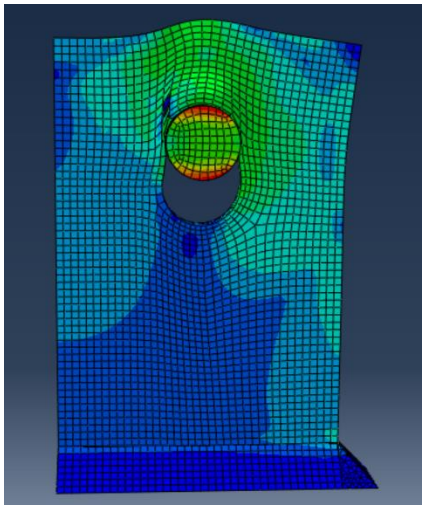

Figure 4.11 Final deformed shape of T127-38-1

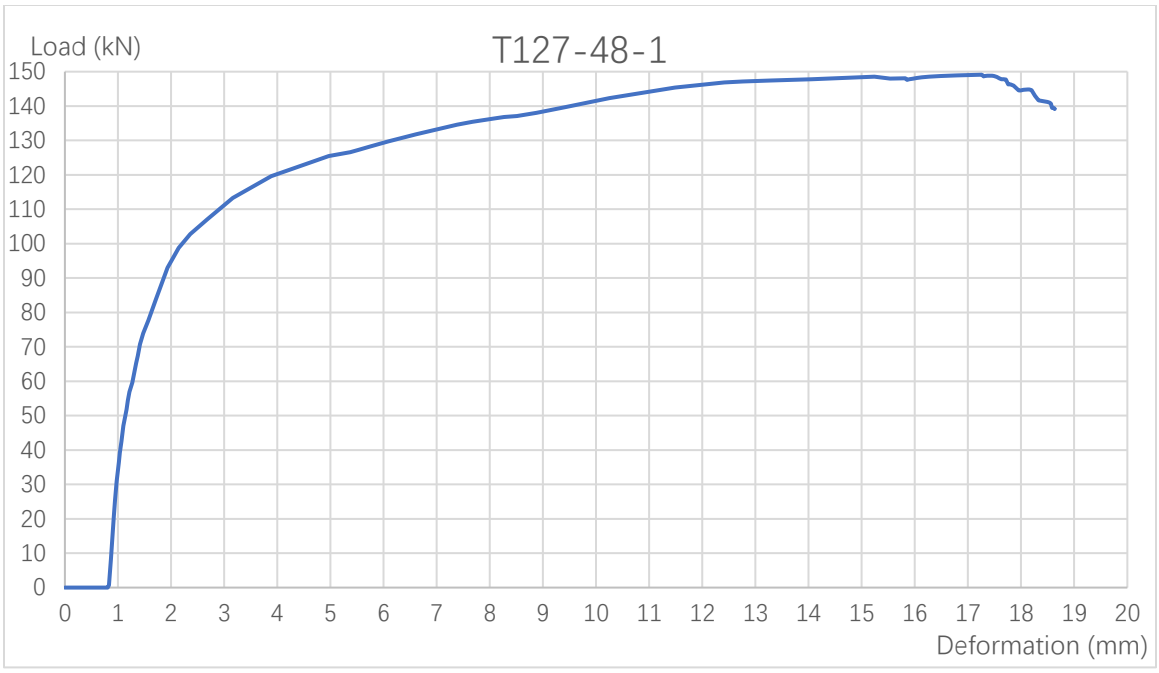

Figure 4.12 Load-deformation curve of T127-48-1

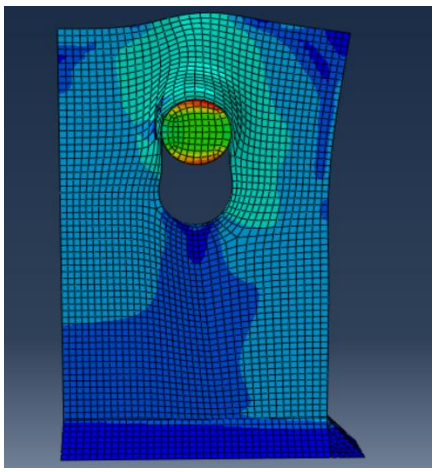

Figure 4.13 Final deformed shape of T127-48-1

4.3 Simulation results of 22.2mm bolt diameter

Figures 4.14 to 4.19 show load-deformation curves and the final deformed shapes of the three simulations.

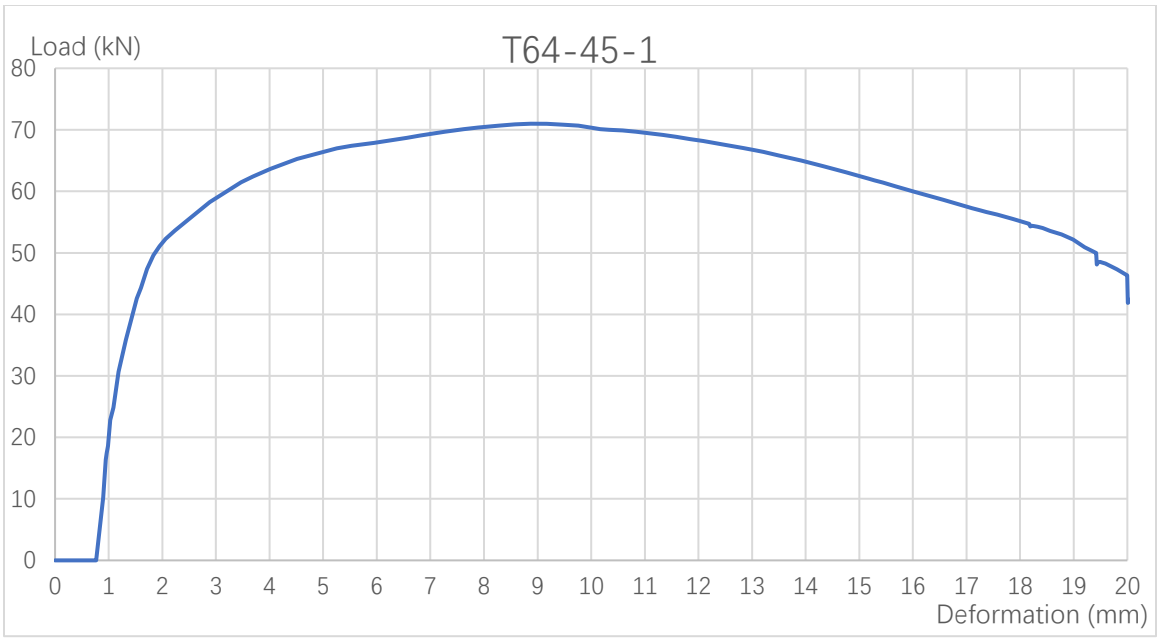

Figure 4.14 Load-deformation curve of T64-45-1

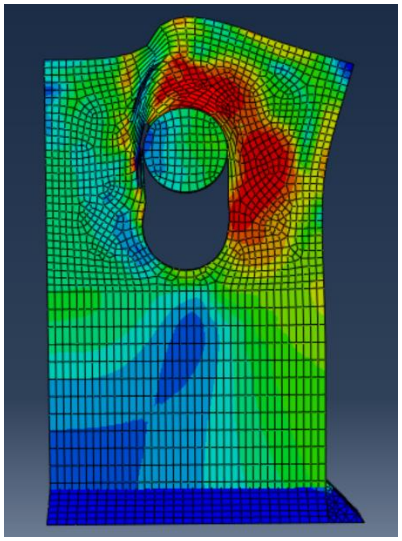

Figure 4.15 Final deformed shape of T64-45-1

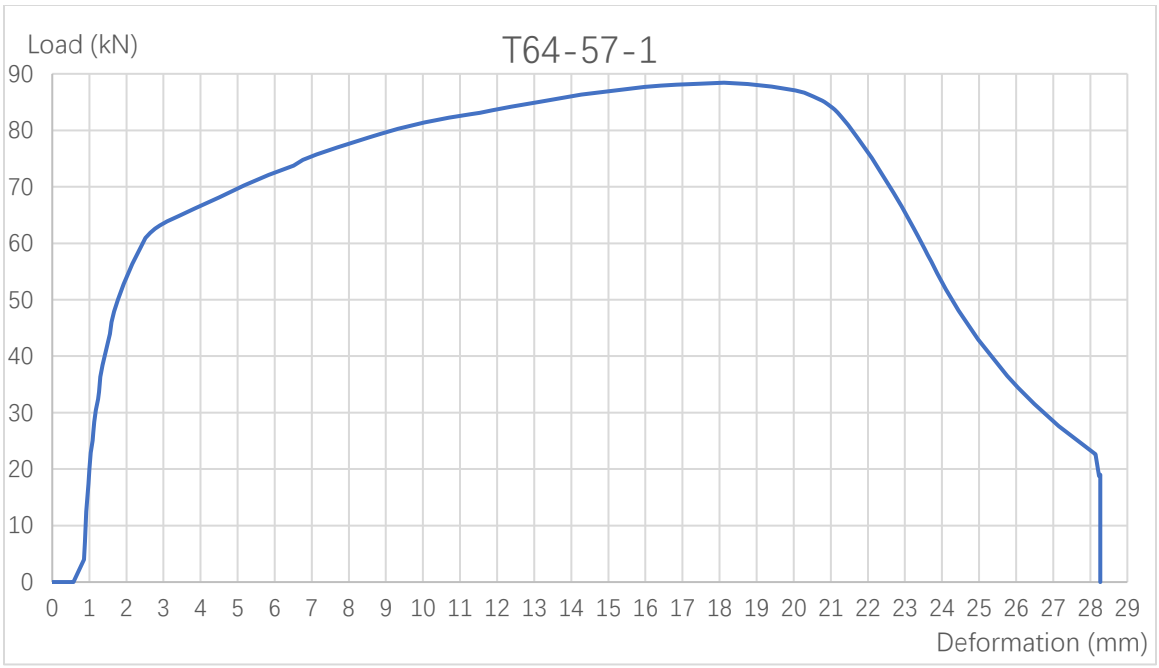

Figure 4.16 Load-deformation curve of T64-57-1

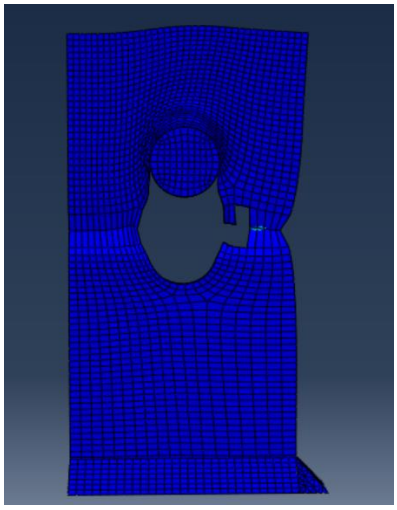

Figure 4.17 Final deformed shape of T64-57-1

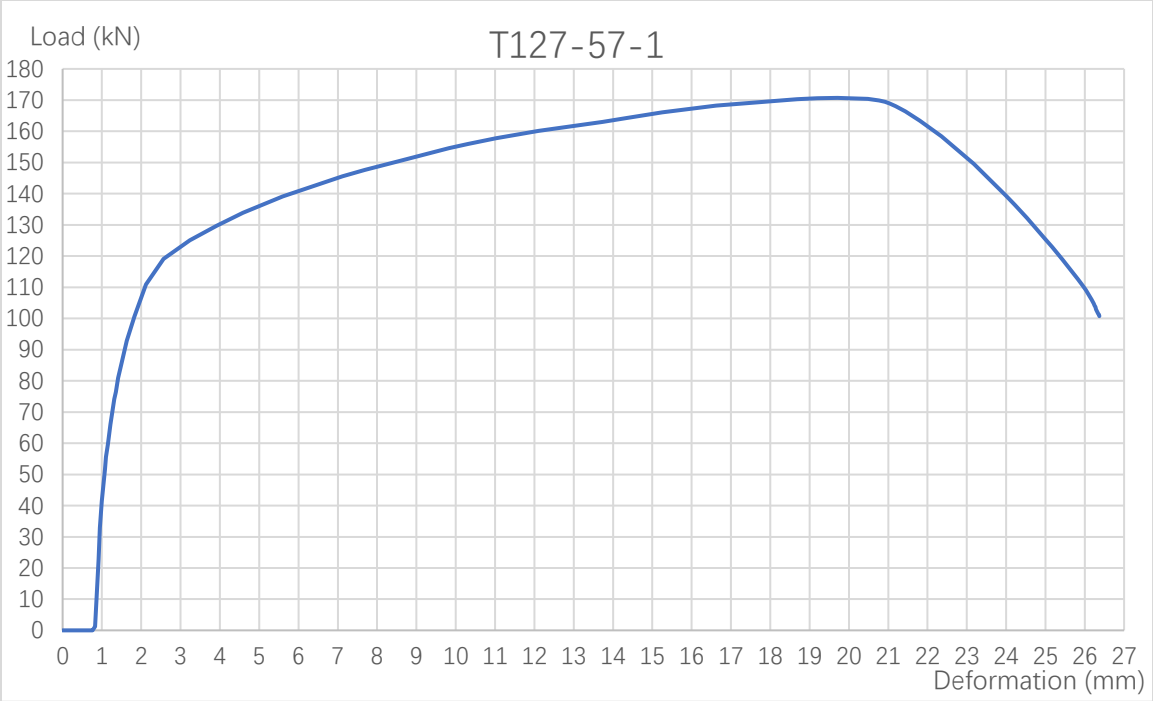

Figure 4.18 Load-deformation curve of T127-57-1

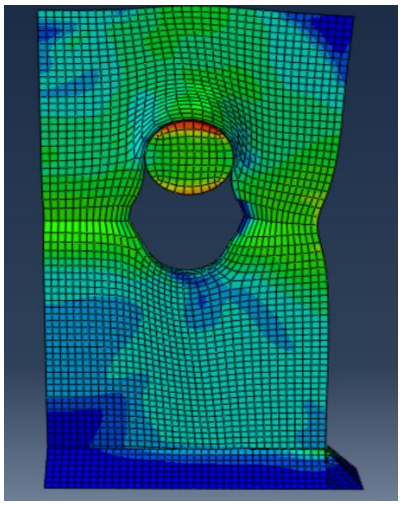

Figure 4.19 Final deformed shape of T127-57-1

4.4 Simulation results of 23.8mm bolt diameter

Figures 4.20 to 4.31 show load-deformation curves and the final deformed shapes of the six simulations.

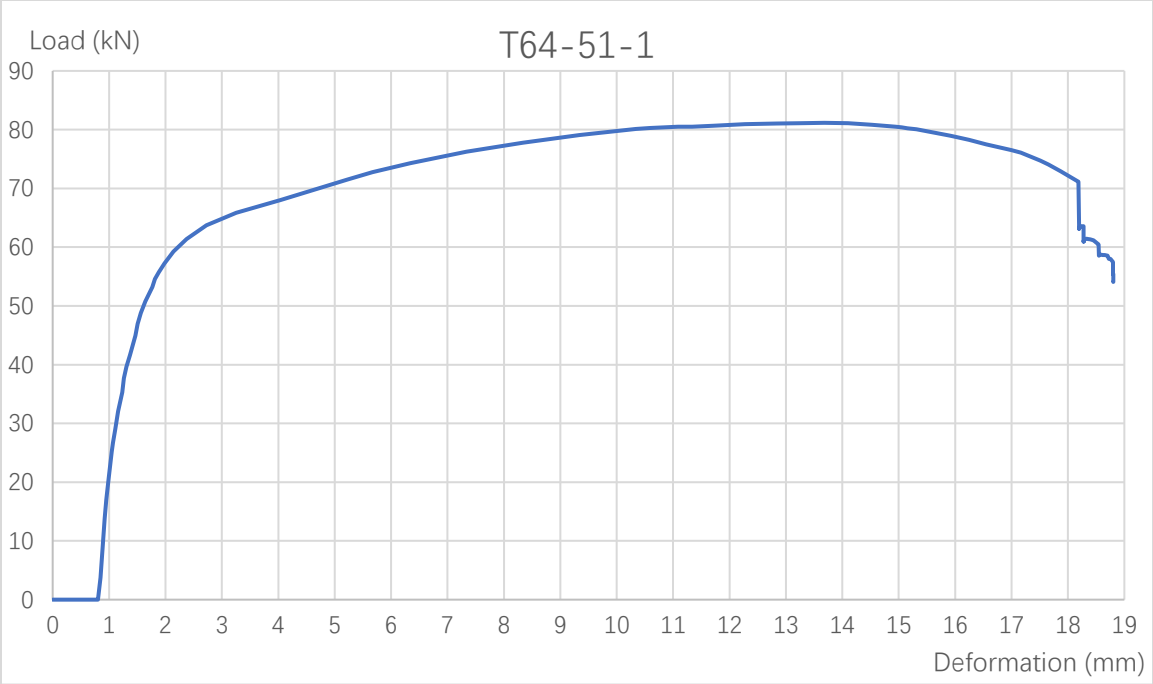

Figure 4.20 Load-deformation curve of T64-51-1

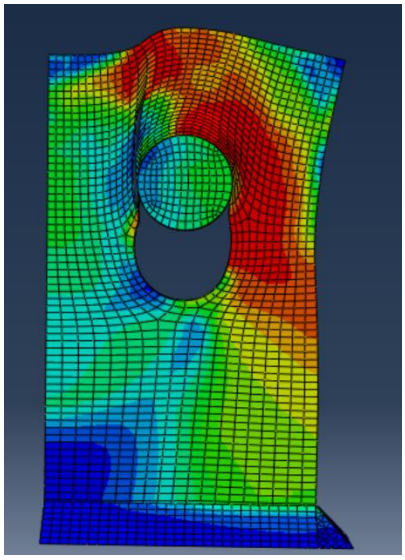

Figure 4.21 Final deformed shape of T64-51-1

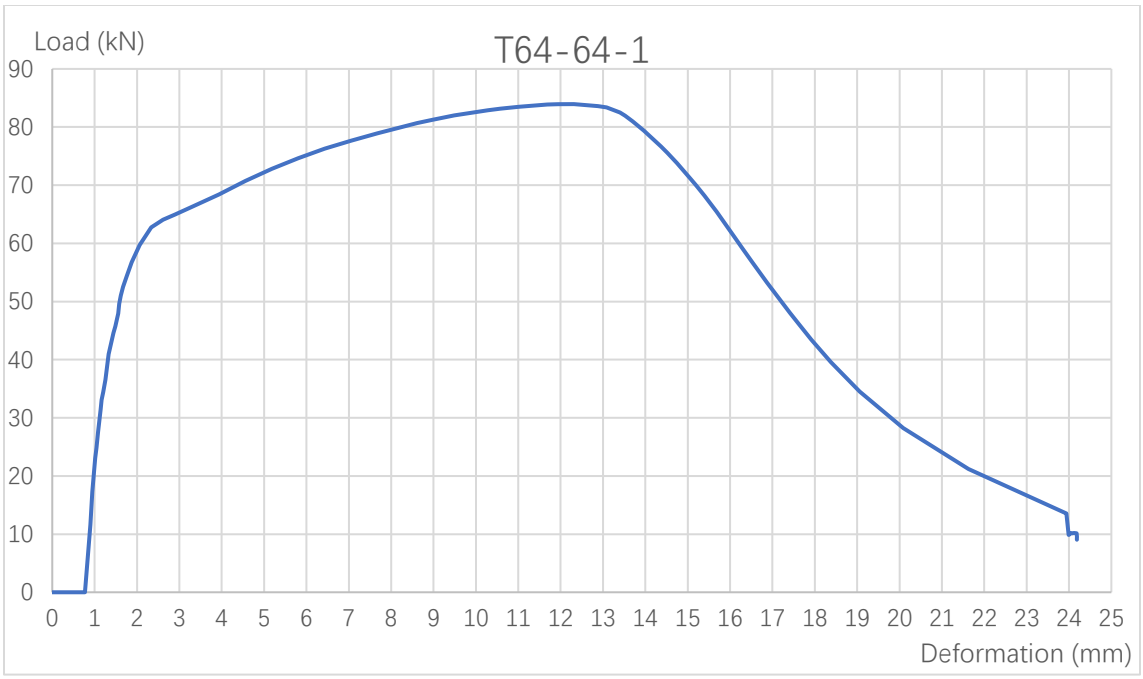

Figure 4.22 Load-deformation curve of T64-64-1

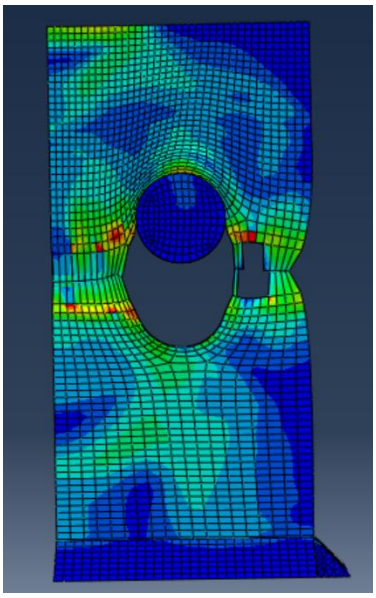

Figure 4.23 Final deformed shape of T64-64-1

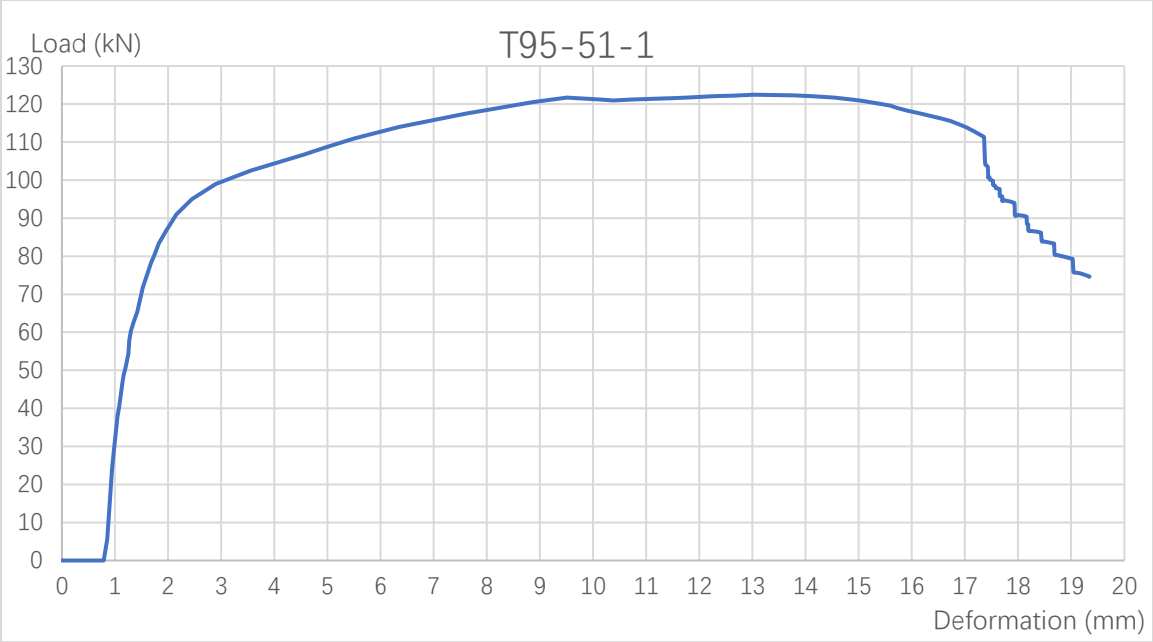

Figure 4.24 Load-deformation curve of T95-51-1

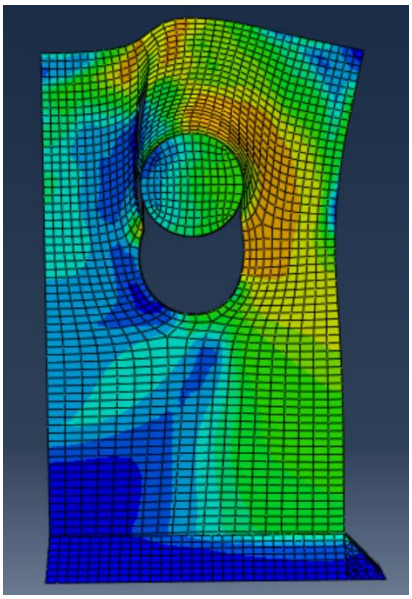

Figure 4.25 Final deformed shape of T95-51-1

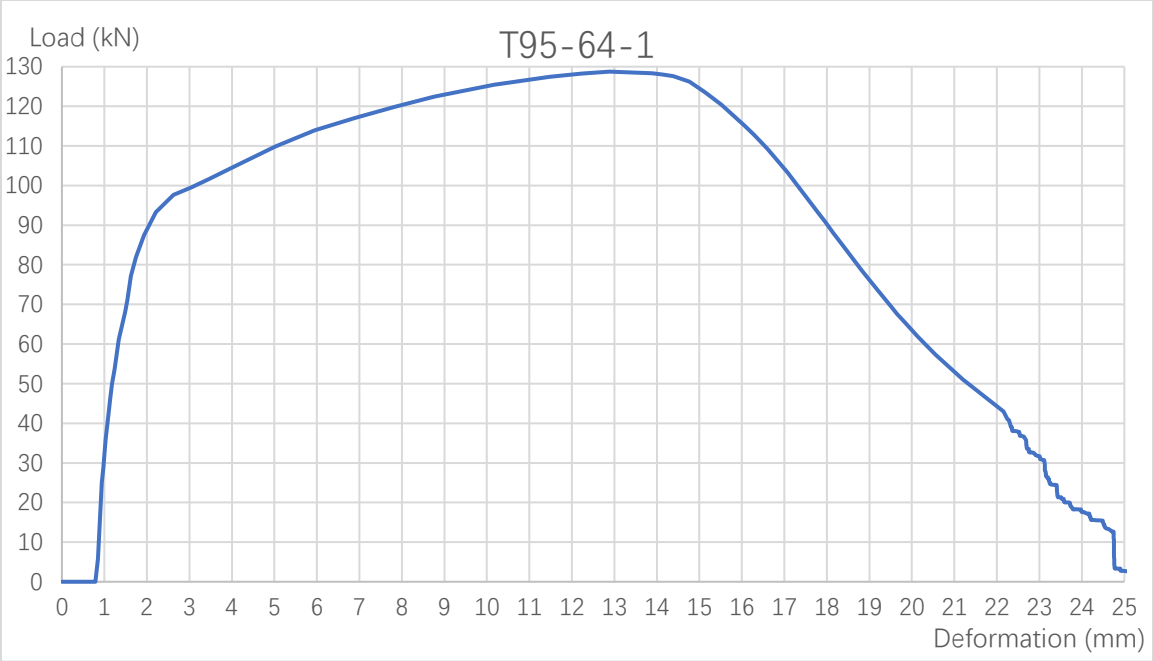

Figure 4.26 Load-deformation curve of T95-64-1

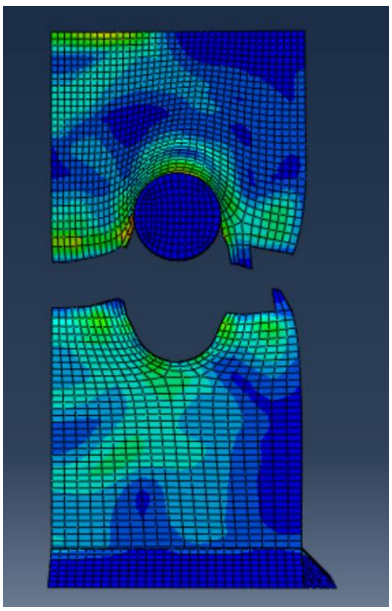

Figure 4.27 Final deformed shape of T95-64-1

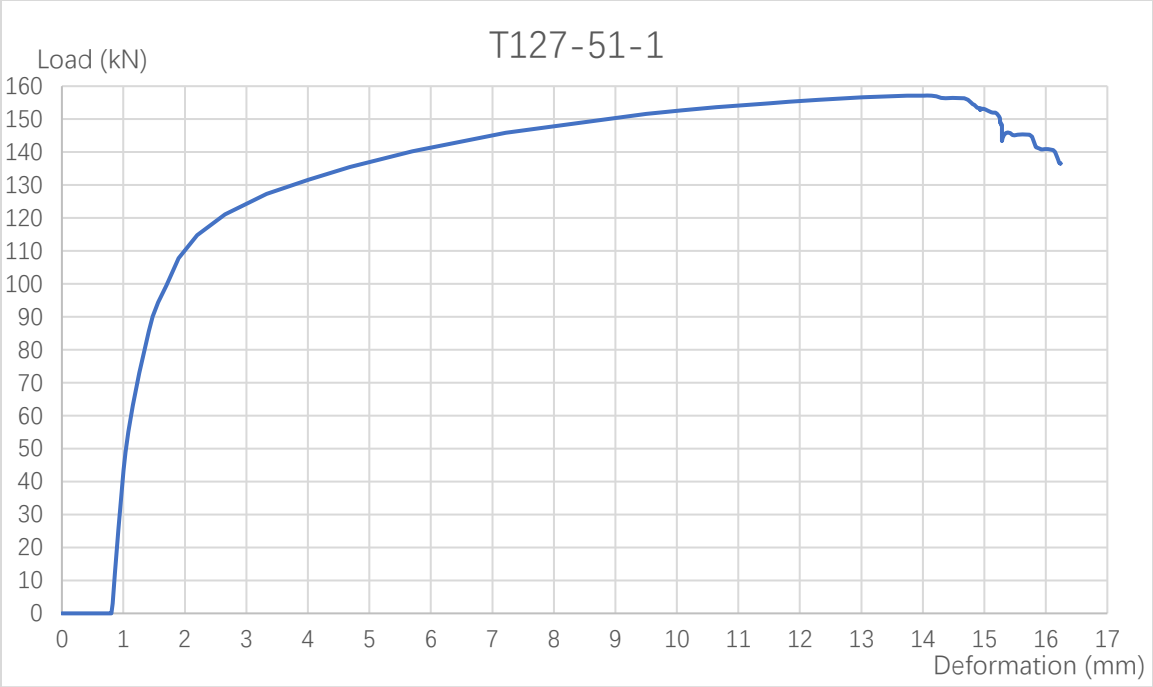

Figure 4.28 Load-deformation curve of T127-51-1

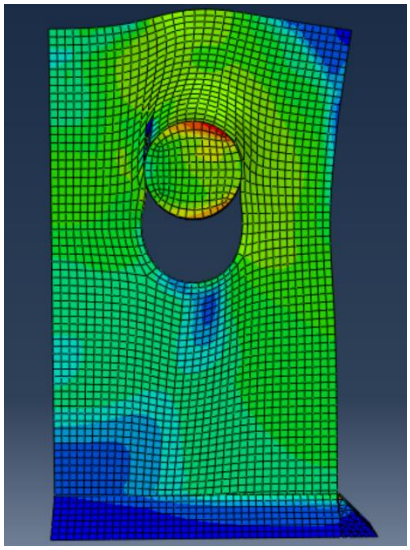

Figure 4.29 Final deformed shape of T127-51-1

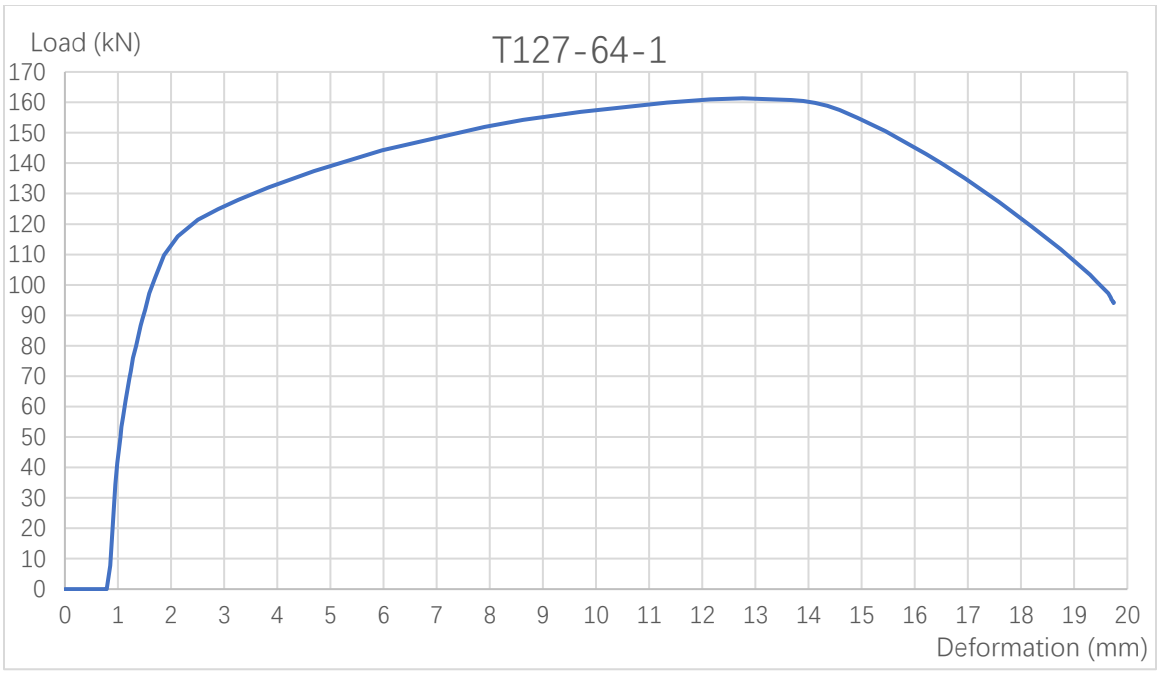

Figure 4.30 Load-deformation curve of T127-64-1

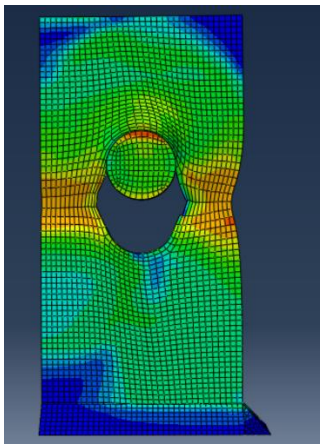

Figure 4.31 Final deformed shape of T127-64-1

4.5 Simulation results of combined tension and shear

Model T95-45-1 was used to do the simulation of combined tension and shear force. Due to the existence of the shear load, the symmetry about axis 1 (Figure 3.2) is no longer valid. In order to use the same one-quarter model, the constraints on the axis 1 surface were removed (Figures 4.33c, 4.33d and 4.33e) when V was not equal to zero, which allowed the plate to undergo deformation in V direction. Figure 4.32 shows the load-deformation curves. Figure 4.33 shows the failure

modes of the 5 cases.

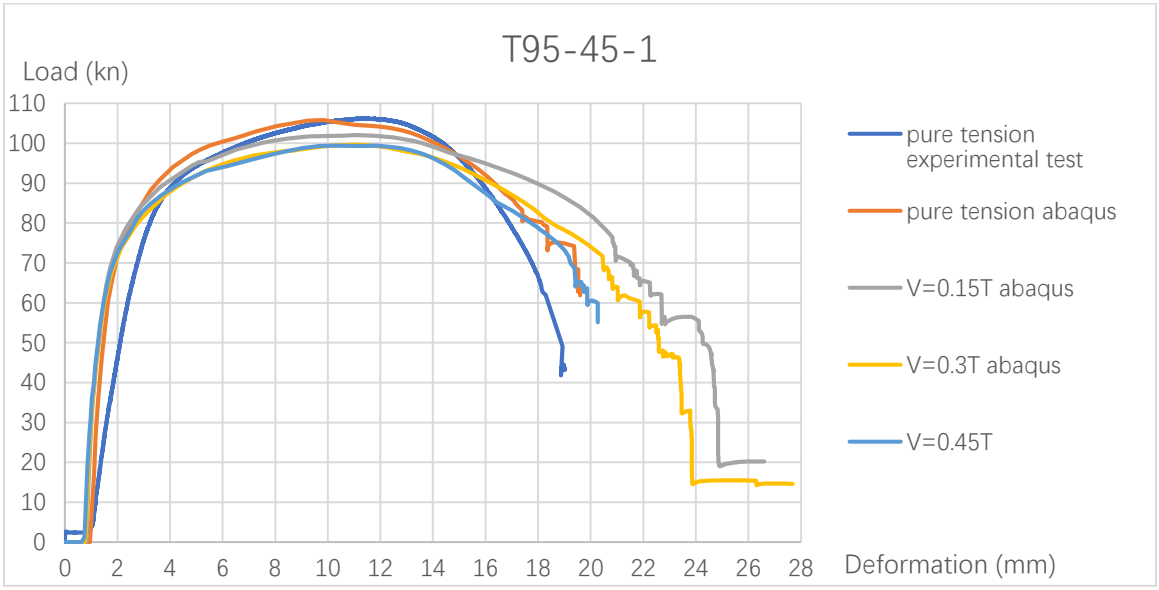

Figure 4.32 Load vs. deformation of T95-45-1 under combined tension and shear

(a) pure tension (experimental test)

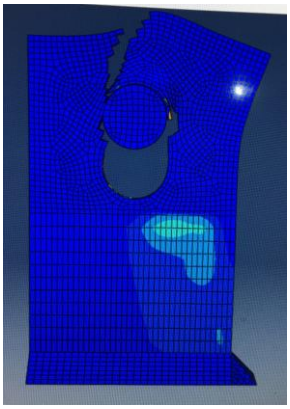

(b) pure tension (Abaqus)

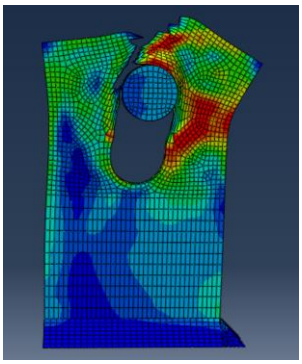

(c) V=0.15T (Abaqus)

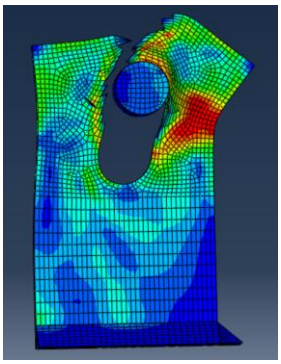

(d) V=0.3T (Abaqus)

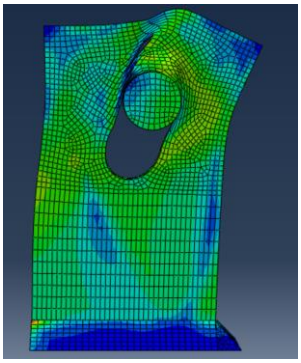

(e) V=0.45T (Abaqus)

Figure 4.33 Failure modes of T95-45-1 under combined tension and shear

4.6 Observations

For the connections having 19 mm bolts, bearing tear-out was the only failure mode. For the other connections, the failure mode mainly depended on the edge distance. When the edge distance was 2.5d, it had net-section rupture, and when the edge distance was 2d, it experienced a bearing tear-out failure (Table 4.1).

When the shear load V was less than 0.45T, it had negligible influence on the results of the shear tab connections, including the failure mode and the ultimate tensile strength.

Table 4.1 The summary of failure modes of the 18 simulations

Thickness (mm)	Bolt diameter (mm)	Simulation ID	Failure mode
6.4	19	T64-38-1	Bearing tear-out
		T64-48-1	Bearing tear-out
	22.2	T64-45-1	Bearing tear-out
		T64-57-1	Net-section rupture
	23.8	T64-51-1	Bearing tear-out
		T64-64-1	Net-section rupture
9.5	19	T95-38-1	Bearing tear-out
		T95-48-1	Bearing tear-out
	22	T95-45-1	Bearing tear-out
		T95-57-1	Net-section rupture
	23.8	T95-51-1	Bearing tear-out
		T95-64-1	Net-section rupture
12.7	19	T127-38-1	Bearing tear-out
		T127-48-1	Bearing tear-out
	22	T127-45-1	Bearing tear-out
		T127-57-1	Net-section rupture
	23.8	T127-51-1	Bearing tear-out
		T127-64-1	Net-section rupture

Chapter 5 Analysis of the load versus deformation curve

In this chapter, a tri-linear load-deformation curve based on a three-stages of loading is developed.

5.1 The method of a tri-linear curve

The load-deformation curve of specimen T95-45-1 is used as an example for the explanation of the proposed method hereafter.

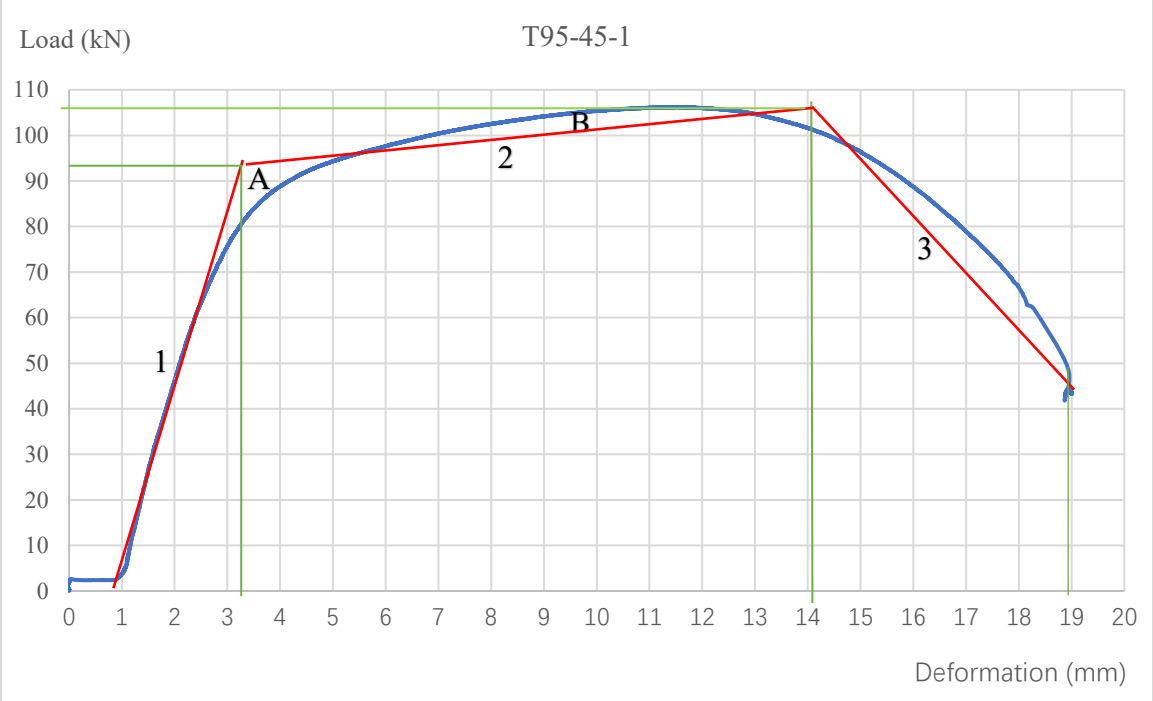

Figure 5.1 Tri-linear curve of T95-45-1

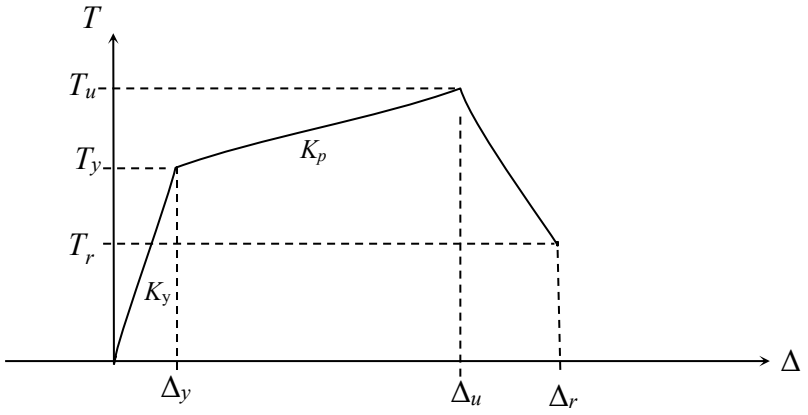

Figure 5.2 Load versus deformation of a nonlinear spring

In Figure 5.1, a tri-linear curve, which is highlighted in red, is generated to replace the original curve. This trilinear curve, representing the elastic, plastic and damage stages of the specimen, is characterized by three critical points (Figure 5.2): effective yield tensile strength T_y and its corresponding deformation Δ_y, ultimate tensile strength T_u and its corresponding deformation Δ_u, residual strength T_r and its corresponding deformation Δ_r. Note that in this idealized tri-linear curve bolt slippage is excluded. Thus, $\Delta_y = \frac{T_y}{K_y}$, where K_y is the stiffness of the elastic stage. Three rules are employed to generate the tri-linear curve: first, the area A above the actual curve should be approximately equal to the area B below the actual curve; secondly, the effective elastic stiffness K_y shall be taken as the secant stiffness calculated at a force equal to 60 percent of the effective yield strength of the connection T_y; thirdly, the ultimate strength at the end of the plastic stage should be between $0.95T_u$ to T_u (T_u is the ultimate strength of the original curve).

5.2 Determination of T_y and Δ_y

Six lab tests and fifteen simulations are used for the analysis. Table 5.1 records the deformation values of Δ_y—Δ_b, Δ_u—Δ_b, and Δ_r—Δ_b, in which the bolt slippage deformation Δ_b is excluded from the deformation data, corresponding to the Δ_y, Δ_u, and Δ_r in Figure 5.2. The effective yield strength T_y and the effective elastic stiffness K_y, measured based on the procedure described in Section 5.1, are also recorded in Table 5.1.

Table 5.1 Summary of 6 lab tests and 15 simulations

Specimen ID	Δ_b (mm)	$\Delta_y - \Delta_b$ (mm)	$\Delta_u - \Delta_b$ (mm)	$\Delta_r - \Delta_b$ (mm)	T_y for 2 bolts (N)	n	t (mm)	d (mm)
T95-45-1-a	0.9	2.3	13.2	17.3	384925	2	9.5	22.2
T95-45-1-b	1.7	2.3	12.9	17.6	382700	2	9.5	22.2
T95-57-1-a	1.5	2.7	14.9	17.	387150	2	9.5	22.2
T95-57-1-b	0.8	2.6	14.6	16.3	384925	2	9.5	22.2
T127-45-1-a	2.5	2.2	9.6	13.3	516200	2	12.7	22.2
T127-45-1-b	1.3	2.1	10.3	13.9	511750	2	12.7	22.2
T95-38-1	0.8	1.0	9.6	13.4	330000	2	9.5	19.0
T95-48-1	0.8	1.0	15.6	21.7	334000	2	9.5	19.0
T95-51-1	0.8	1.0	15.7	18.2	434000	2	9.5	23.8
T95-64-1	0.8	1.0	15.1	18.6	440000	2	9.5	23.8
T64-45-1	0.8	0.9	10.5	18.3	238000	2	6.4	22.2
T64-57-1	0.8	0.9	20.3	23.1	245000	2	6.4	22.2
T64-38-1	0.8	0.9	10.1	13.3	210000	2	6.4	19.0
T64-48-1	0.8	0.9	13.3	20.8	215000	2	6.4	19.0
T64-51-1	0.8	0.9	15.1	17.4	276000	2	6.4	23.8
T64-64-1	0.8	0.9	13.4	15.5	276500	2	6.4	23.8
T127-38-1	0.8	0.9	9.9	10.7	410000	2	12.7	19.0
T127-48-1	0.8	0.9	17.1	17.7	415500	2	12.7	19.0
T127-51-1	0.8	0.9	14.3	15.4	545000	2	12.7	23.8
T127-64-1	0.8	0.9	14.3	18.3	550000	2	12.7	23.8
T127-57-1	0.8	1.0	21.0	24.9	520000	2	12.7	22.2

F_u (MPa)	F_y (MPa)	$nt\,dF_u$	$nt\,dF_y$	$\frac{T_y}{nt\,dF_u}$	$\frac{T_y}{nt\,dF_y}$	Measured $K_y = \frac{T_y}{\Delta_y - \Delta_b}$ for 2 bolts (N/mm)	$\frac{K_y}{tF_y(d/25.4)}$
491	376	207103	158596	1.9	2.4	167358	53.6
491	376	207103	158596	1.8	2.4	166391	53.3
491	376	207103	158596	1.9	2.4	143388	45.9
491	376	207103	158596	1.9	2.4	148048	47.4
495	387	279402	218221	1.8	2.4	234636	54.6
495	387	279402	218221	1.8	2.3	243690	56.7
491	376	177251	135736	1.9	2.4	330000	123.5
491	376	177251	135736	1.9	2.5	334000	125.0
491	376	222030	170027	1.8	2.4	434000	121.5
491	376	222030	170027	1.9	2.4	440000	123.2
491	376	139522	106844	1.7	2.2	264444	125.7
491	376	139522	106844	1.8	2.3	272222	129.4
491	376	119411	91443	1.8	2.3	233333	129.6
491	376	119411	91443	1.8	2.4	238888	132.7
491	376	149578	114544	1.7	2.3	306666	127.4
491	376	149578	114544	1.7	2.3	307222	127.7
495	387	239128	186766	1.7	2.2	455555	124.0
495	387	239128	186766	1.7	2.2	461666	125.6
495	387	299539	233949	1.7	2.2	605555	123.0
495	387	299539	233949	1.7	2.2	611111	124.0
495	387	279402	218221	1.9	2.4	520000	121.0

Note: Δ_b is the bolt slippage; n is the number of bolts; t is the thickness of tab plate; d is bolt diameter.

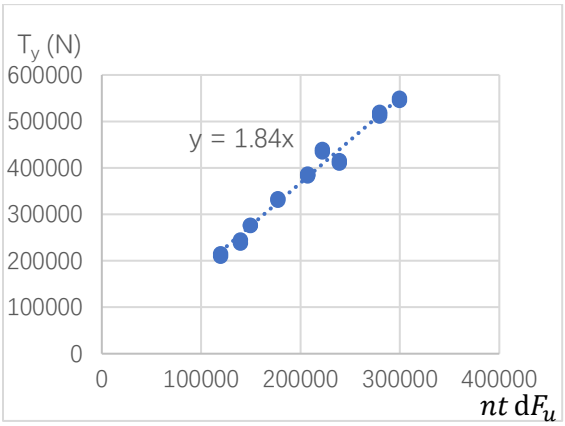

(a) $ntdF_u$ vs T_y

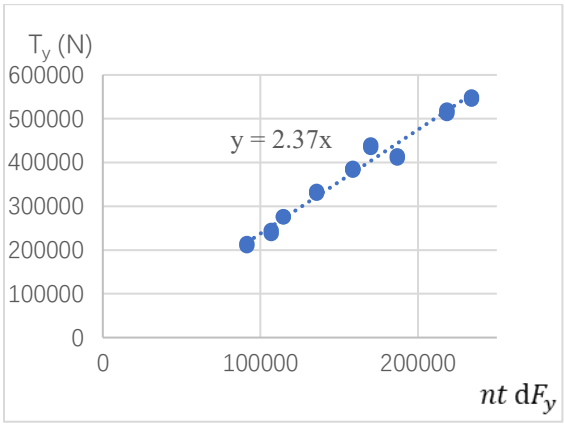

(b) $ntdF_y$ vs T_y

Figure 5.3 Determination of T_y

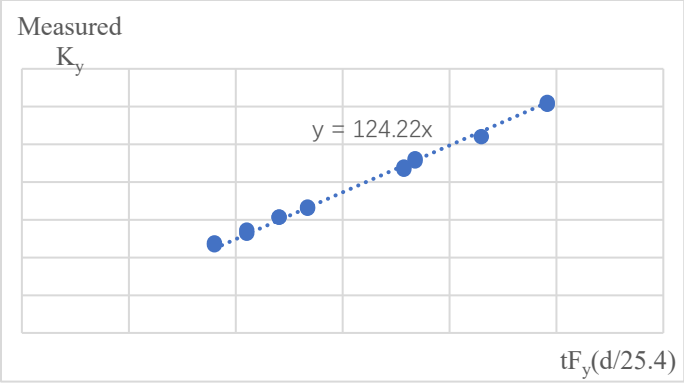

Figure 5.4 Determination of K_y

The data points in Figure 5.4 are based on Abaqus models only; i.e., the data from the tested specimens are not included in the regression analysis.

From Table 5.1, Figures 5.3 and 5.4, the effective yield tensile strength T_y and effective elastic stiffness K_y can be obtained as:

$$T_y = 2.37nt\,dF_y \quad \text{or} \tag{5.1}$$

$$T_y = 1.84nt\,dF_u \tag{5.2}$$

$$K_y = 124tF_y(d/25\text{mm}) \tag{5.3}$$

where n is the number of bolts; t is the thickness of tab plate; the bolt diameter d in Equation (5.3) must be in unit of mm.

Note that the stiffness K_y of Equation (5.3) is based on the finite element models only. For the tested 6 specimens, the average elastic stiffness is

$$K_{yt} = 52tF_y(d/25\text{mm}), \tag{5.4}$$

This discrepancy is mainly attributed to the uneven bearing between the bolt shank and the tab plate through the thickness direction and the deformation from the upper loading arm. The uneven bearing was caused by: 1) the bending of the bolt shank, and 2) the imperfect fitting between the shank and the hole, including that the hole surface was not flat due to punching and the bolts might not come to bearing simultaneously.

Combining Equations (5.3) and (5.4) and considering the number of bolts, the effective elastic stiffness K_y is obtained as

$$K_y = 62\lambda ntF_y(d/25.4\text{mm}) \tag{5.5}$$

where 62 is equal to 124 divided by 2 bolts; λ is a calibration factor, which is equal to 0.42 for the

tested specimens, and is equal to 1.0 for the specimens of finite element models.

The effective yield deformation Δ_y is calculated as T_y/K_y, i.e.,

$$\Delta_y = \frac{2.37nt\,dF_y}{62\lambda ntF_y(d/25\text{mm})} = \frac{0.038d}{\lambda(d/25\text{mm})} \tag{5.6}$$

where (d/25mm) is the normalized dimensionless bolt diameter. Δ_y has the same unit as the d in the numerator of the equation.

5.3 Determination of T_u and Δ_u

In this study, all the specimens were loaded to the rupture of shear tabs. The failure of the connection is thus defined as various forms of rupture of steel materials. Note that the rupture failure of bolts and welds were precluded from the test specimens through capacity design. In total, there are three kinds of rupture modes.

1) Block shear failure. From the tests, it is possible to have tensile fracture across A-B before rupture on the shear plane A-D and B-C, and this kind of failure is called block shear failure (Figure 5.5). The capacity can be obtained from the following equation:

$$T_1 = [A_n F_u + 0.6\,A_{gv}(F_y + F_u)/2] \tag{5.7}$$

where A_n is net area; F_u is the ultimate strength of steel material; A_{gv} is gross area in shear; and F_y is yielding stress of steel material.

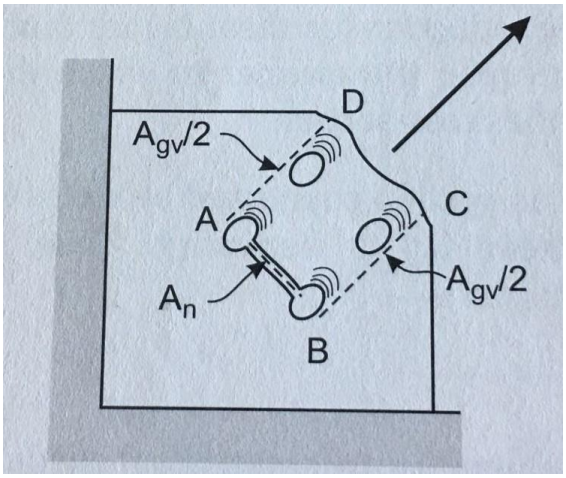

Figure 5.5 Block shear failure

2) Net-section rupture. This strength limit state is the rupture of steel material at the net section,

where the cross section is reduced by bolt holes. The strength equation is

$$T_2 = A_n F_u \tag{5.8}$$

where A_n is the net tensile area and F_u is the ultimate strength of steel material.

3) Bearing tear-out. In this case, a bolt bears against the edge of the hole. The bearing force is limited by the shear strength of the hole edge (i.e. tear-out of the edge). The strength equation is

$$T_3 = 0.6\,[(F_y + F_u) / 2]\,A_{gv} \tag{5.9}$$

where F_y is yield strength of steel material; F_u is the ultimate strength of steel material; and A_{gv} is gross sectional area in shear, which is equal to the plate thickness times the sectional length in the direction of the tear-out.

Table 5.2 and 5.3 show the calculation results of the 10 lab tests and 15 simulations. The predicted strength of a connection is taken as the minimum value among the strengths obtained from Equations (5.7), (5.8) and (5.9). It can be seen that the predicted strengths match the test results very well.

Table 5.2 Calculation results of the 10 lab tests

Specimen ID	T95-45-1a	T95-45-1b	T95-57-1a	T95-57-1b	T127-45-1a
t (mm)	9.41	9.41	9.38	9.44	12.43
L (mm)	152.30	152.63	152.24	152.55	152.08
l (mm)	76.11	76.35	75.72	75.76	75.50
c (mm)	45.19	45.63	57.68	56.97	43.90
d_h (mm)	23.55	23.44	23.43	23.50	23.70
F_y (MPa)	376	376	376	376	387
F_u (MPa)	491	491	491	491	495
T_1 (kN)	464	468	522	522	608
T_2 (kN)	486	489	485	489	645
T_3 (kN)	443	447	563	560	578
T_c (kN)	443	447	485	489	578
T_t (kN)	419	426	491	470	523
T_t/T_c	0.95	0.95	1.01	0.96	0.90

Specimen ID	T127-45-1b	T95-45-2a	T95-45-2b	T127-45-2a	T127-45-2b
t (mm)	12.33	9.38	9.37	12.39	12.38
L (mm)	151.71	152.48	152.27	152.09	152.08
l (mm)	75.42	75.29	75.50	75.31	74.75
c (mm)	43.99	121.14	121.65	121.16	121.18
d_h (mm)	23.48	23.54	23.53	23.64	23.62
F_y (MPa)	387	376	376	387	387
F_u (MPa)	495	491	491	495	495
T_1 (kN)	605	830	832	1112	1108
T_2 (kN)	640	485	484	643	643
T_3 (kN)	574	1183	1186	1590	1589
T_c (kN)	574	485	484	643	643
T_t (kN)	524	474	471	628	631
T_t/T_c	0.91	0.98	0.97	0.98	0.98

Note: t: plate thickness; L: plate length; l: distance between the two holes; c: edge distance, measured from the center of the bolt hole to the side edge; d_h: bolt hole diameter; T_c: predicted ultimate tensile strength; T_t: ultimate tensile strength from the test; the number highlighted in yellow is the minimum of three failure modes

Table 5.3 Calculation results of the 15 simulations

Specimen ID	T95-38-1	T95-48-1	T95-51-1	T95-64-1	T64-45-1
t (mm)	9.50	9.50	9.50	9.50	6.40
L (mm)	152.00	152.00	152.00	152.00	152.00
l (mm)	76.00	76.00	76.00	76.00	76.00
c (mm)	38.00	48.00	51.00	64.00	45.00
d_h (mm)	20.60	20.60	25.40	25.40	23.80
F_y (MPa)	376	376	376	376	376
F_u (MPa)	491	491	491	491	491
T_1 (kN)	446	496	488	552	314
T_2 (kN)	517	517	472	472	328
T_3 (kN)	376	474	504	633	300
T_c (kN)	376	474	472	472	300
T_t (kN)	352	440	490	512	284
T_t/T_c	0.94	0.93	1.04	1.08	0.95

Specimen ID	T64-57-1	T64-38-1	T64-48-1	T64-51-1	T64-64-1
t (mm)	6.40	6.40	6.40	6.40	6.40
L (mm)	152.00	152.00	152.00	152.00	152.00
l (mm)	76.00	76.00	76.00	76.00	76.00
c (mm)	57.00	38.00	48.00	51.00	64.00
d_h (mm)	23.80	20.60	20.60	25.40	25.40
F_y (MPa)	376	376	376	376	376
F_u (MPa)	491	491	491	491	491
T_1 (kN)	354	300	334	329	372
T_2 (kN)	328	348	348	318	318
T_3 (kN)	380	253	320	340	426
T_c (kN)	328	253	320	318	318
T_t (kN)	352	236	300	324	334
T_t/T_c	1.07	0.93	0.94	1.02	1.05

Specimen ID	T127-38-1	T127-48-1	T127-51-1	T127-64-1	T127-57-1
t (mm)	12.70	12.70	12.70	12.70	12.70
L (mm)	152.00	152.00	152.00	152.00	152.00
l (mm)	76.00	76.00	76.00	76.00	76.00
c (mm)	38.00	48.00	51.00	64.00	57.00
d_h (mm)	20.60	20.60	25.40	25.40	23.80
F_y (MPa)	387	387	387	387	387
F_u (MPa)	495	495	495	495	495
T_1 (kN)	604	671	661	748	711
T_2 (kN)	697	697	636	636	656
T_3 (kN)	511	645	686	860	766
T_c (kN)	511	645	636	636	656
T_t (kN)	480	594	628	636	672
T_t/T_c	0.94	0.92	0.99	1.00	1.02

Note: t: plate thickness; L: plate length; l: distance between the two holes; c: edge distance, measured from the center of the bolt hole to the side edge; d_h: bolt hole diameter; T_c: predicted ultimate tensile strength; T_t: ultimate tensile strength from the test; ; the number highlighted in yellow is the minimum of three failure modes

Therefore, the ultimate strength of a connection T_u is obtained as:

$$T_u = \text{Min}\ \{\ T_1, T_2, T_3\ \} \tag{5.10}$$

Whether a connection fails by the rupture of net section or the bearing tear-out is dependent upon which mode has a smaller tensile capacity. Using Equations (5.8) and (5.9), we can obtain the following criterion for a net section rupture failure:

$$A_n F_u < 0.6\, A_{gv}\, (F_u + F_y)/\, 2 \tag{5.11}$$

where $A_{gv}=2ct$ for one bolt hole, and net area $A_n=t(l - d_h)$ for one bolt. Equation (5.11) is rewritten as

$$\frac{c}{d_h} \geq \frac{1.67\left(\frac{l}{d_h}-1\right)}{1+\frac{F_y}{F_u}} \tag{5.12}$$

where l is the distance between the two holes or bolt pitch; d_h is the hole diameter; c is the edge distance.

For example, given t = 9.5 mm, d_h = 23.8 mm, l = 76 mm, F_y = 376 MPa, F_u = 491MPa, we have c/d_h = 2.07. Table 5.4 shows value of c/d_h from Equation (5.12) for 6 lab tests and 15 finite element simulations. It can be seen that the equations correctly predict the failure modes.

Table 5.4 Determination of the ultimate deformation

Specimen ID	Δ_u (mm)	Failure mode	d_h (mm)	d (mm)	Actual c/d_h	Actual c/d	c/d_h Eq.(5.12)
T95-45-1-a	13.2	B tear	23.8	22.20	1.89	2.03	2.07
T95-45-1-b	12.9	B tear	23.8	22.20	1.89	2.03	2.07
T95-57-1-a	14.9	N rupture	23.8	22.20	2.39	2.57	2.07
T95-57-1-b	14.6	N rupture	23.8	22.20	2.39	2.57	2.07
T127-45-1-a	9.6	B tear	23.8	22.20	1.89	2.03	2.05
T127-45-1-b	10.3	B tear	23.8	22.20	1.89	2.03	2.05
T95-38-1	9.6	B tear	20.6	19.00	1.84	2.00	2.54
T95-48-1	15.6	B tear	20.6	19.00	2.33	2.53	2.54
T95-51-1	15.7	B tear	25.4	23.80	2.00	2.14	1.88
T95-64-1	15.1	N rupture	25.4	23.80	2.52	2.69	1.88
T64-45-1	10.5	B tear	23.8	22.20	1.89	2.03	2.07
T64-57-1	20.3	N rupture	23.8	22.20	2.39	2.57	2.07
T64-38-1	10.1	B tear	20.6	19.00	1.84	2.00	2.54
T64-48-1	13.3	B tear	20.6	19.00	2.33	2.53	2.54
T64-51-1	15.1	B tear	25.4	23.80	2.00	2.14	1.88
T64-64-1	13.4	N rupture	25.4	23.80	2.52	2.69	1.88
T127-38-1	9.9	B tear	20.6	19.00	1.84	2.00	2.52
T127-48-1	17.1	B tear	20.6	19.00	2.33	2.53	2.52
T127-51-1	14.3	B tear	25.4	23.80	2.00	2.14	1.86
T127-64-1	14.3	N rupture	25.4	23.80	2.52	2.69	1.86
T127-57-1	21.0	N rupture	23.8	22.20	2.39	2.57	2.05

Note: l=76 mm for all the connections; Δ_u values exclude bolt slippage; B tear=bearing tear-out failure; N rupture=Net section rupture failure. The connections highlighted in yellow would have net section rupture failure based on Equation (5.12) criterion, but the finite element models predicted bearing tear-out failure.

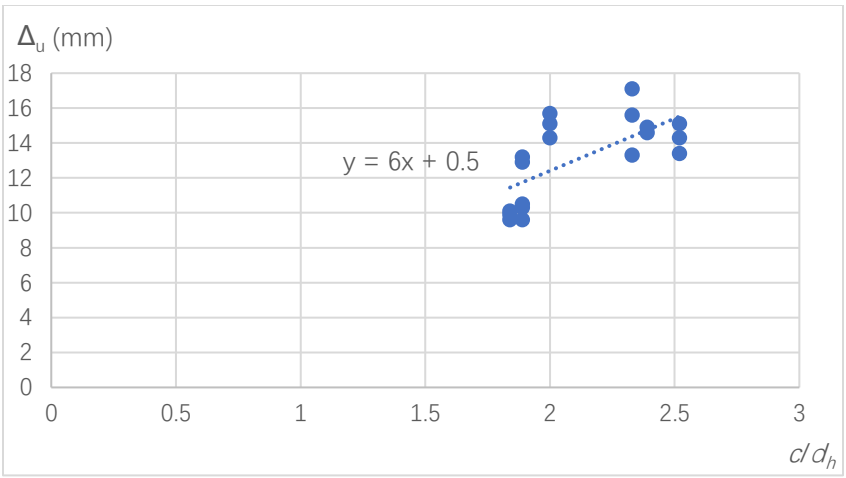

(a) Δ_u vs c/d_h

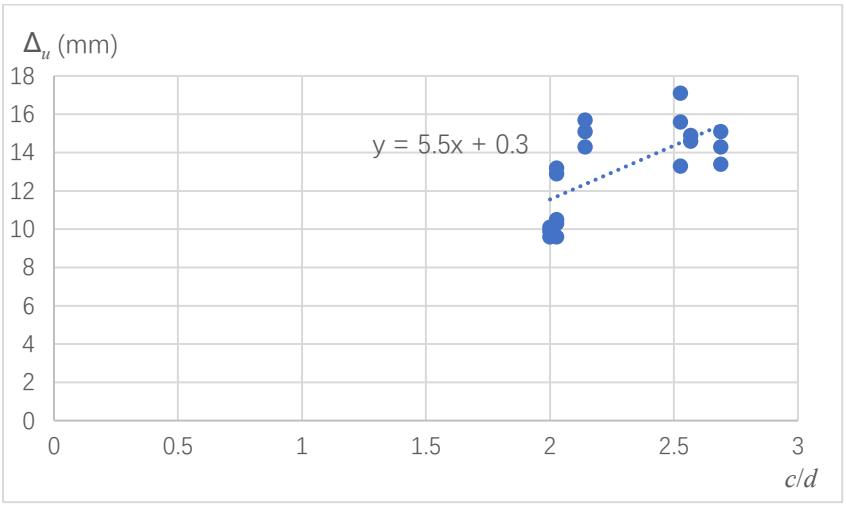

(b) Δ_u vs c/d

Figure 5.6 Determination of Δ_u

From Table 5.4 and Figures 5.6, the ultimate deformation Δ_u can be obtained as:

$$\Delta_u = \frac{6c}{d_h} + 0.5 \text{ mm, or} \quad (5.13)$$

$$\Delta_u = \frac{5.5c}{d} + 0.3 \text{ mm} \quad (5.14)$$

where c is edge distance, d_h is bolt hole diameter; d is bolt diameter.

Note that the data of T64-57-1 and T127-57-1 were excluded in Figure 5.6. Table 5.5 shows the calculation results of Equation (5.13) and (5.14).

Table 5.5 Calculation results of Equation (5.13) and (5.14)

Specimen ID	Δ_u (mm)	Actual c/d_h	Actual c/d	Eq.(5.13) (mm)	Eq.(5.13)/ Δ_u	Eq.(5.14) (mm)	Eq.(5.14)/Δ_u
T95-45-1-a	13.2	1.89	2.03	11.84	0.90	11.47	0.87
T95-45-1-b	12.9	1.89	2.03	11.84	0.92	11.47	0.89
T95-57-1-a	14.9	2.39	2.57	14.84	1.00	14.44	0.97
T95-57-1-b	14.6	2.39	2.57	14.84	1.02	14.44	0.99
T127-45-1-a	9.6	1.89	2.03	11.84	1.23	11.47	1.19
T127-45-1-b	10.3	1.89	2.03	11.84	1.15	11.47	1.11
T95-38-1	9.6	1.84	2.00	11.54	1.20	11.30	1.18
T95-48-1	15.6	2.33	2.53	14.48	0.93	14.22	0.91
T95-51-1	15.7	2.00	2.14	12.50	0.80	12.07	0.77
T95-64-1	15.1	2.52	2.69	15.62	1.03	15.10	1.00
T64-45-1	10.5	1.89	2.03	11.84	1.13	11.47	1.09
T64-57-1	20.3	2.39	2.57	14.84	0.73	14.44	0.71
T64-38-1	10.1	1.84	2.00	11.54	1.14	11.30	1.12
T64-48-1	13.3	2.33	2.53	14.48	1.09	14.22	1.07
T64-51-1	15.1	2.00	2.14	12.50	0.83	12.07	0.80
T64-64-1	13.4	2.52	2.69	15.62	1.17	15.10	1.13
T127-38-1	9.9	1.84	2.00	11.54	1.17	11.30	1.14
T127-48-1	17.1	2.33	2.53	14.48	0.85	14.22	0.83
T127-51-1	14.3	2.00	2.14	12.50	0.87	12.07	0.84
T127-64-1	14.3	2.52	2.69	15.62	1.09	15.10	1.06
T127-57-1	21.0	2.39	2.57	14.84	0.71	14.44	0.69

Note: l=76 mm for all the connections; Δ_u values exclude bolt slippage.

From Table 5.5, the predicted ultimate deformation Δ_u of a connection from Equations (5.13) and (5.14) are acceptable comparing with the Δ_u from test or model.

5.4 Determination of T_r and Δ_r

From Table 5.6 and Figure 5.7, the residual strength T_r of a connection can be obtained approximately as:

$$T_r = 0.7T_u \tag{5.15}$$

Table 5.6 Determination of T_r

Specimen ID	d (mm)	T_u for 2 bolts (N)	T_r for 2 bolts (N)	Eq.(5.15) (N)	Eq.(5.15)/ T_r
T95-45-1-a	22.20	385000	258100	269500	1.04
T95-45-1-b	22.20	386000	262550	270200	1.03
T95-57-1-a	22.20	440000	302600	308000	1.02
T95-57-1-b	22.20	426000	289250	298200	1.03
T127-45-1-a	22.20	476000	347100	333200	0.96
T127-45-1-b	22.20	474000	373800	331800	0.89
T95-38-1	19.00	352000	258100	246400	0.95
T95-48-1	19.00	440000	298150	308000	1.03
T95-51-1	23.80	490000	338200	343000	1.01
T95-64-1	23.80	512000	311500	358400	1.15
T64-45-1	22.20	284000	231400	198800	0.86
T64-57-1	22.20	352000	235850	246400	1.04
T64-38-1	19.00	236000	169100	165200	0.98
T64-48-1	19.00	300000	258100	210000	0.81
T64-51-1	23.80	324100	280350	226870	0.81
T64-64-1	23.80	334000	255875	233800	0.91
T127-38-1	19.00	480000	448000	336000	0.75
T127-48-1	19.00	594100	556000	415870	0.75
T127-51-1	23.80	628000	544000	439600	0.81
T127-64-1	23.80	636100	467250	445270	0.95
T127-57-1	22.20	672000	502850	470400	0.94

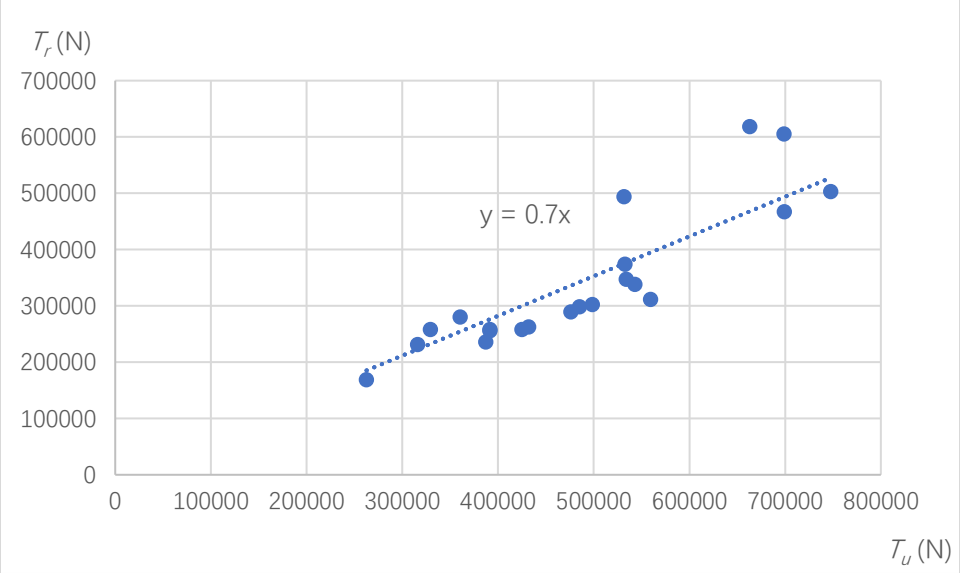

Figure 5.7 Determination of T_r

Table 5.7 Determination of Δ_r

Specimen ID	Δ_r (mm)	Actual c/d_h	Actual c/d	Eq.(5.16) (mm)	Eq.(5.16)/ Δ_r	Eq.(5.17) (mm)	Eq.(5.17)/Δ_r
T95-45-1-a	17.3	1.89	2.03	16.01	0.93	15.73	0.91
T95-45-1-b	17.6	1.89	2.03	16.01	0.91	15.73	0.89
T95-57-1-a	17.0	2.39	2.57	18.26	1.07	18.05	1.06
T95-57-1-b	16.3	2.39	2.57	18.26	1.12	18.05	1.11
T127-45-1-a	13.3	1.89	2.03	16.01	1.20	15.73	1.18
T127-45-1-b	13.9	1.89	2.03	16.01	1.15	15.73	1.13
T95-38-1	13.4	1.84	2.00	15.78	1.18	15.60	1.16
T95-48-1	21.7	2.33	2.53	17.99	0.83	17.88	0.82
T95-51-1	18.2	2.00	2.14	16.50	0.91	16.20	0.89
T95-64-1	18.6	2.52	2.69	18.84	1.01	18.57	1.00
T64-45-1	18.3	1.89	2.03	16.01	0.87	15.73	0.86
T64-57-1	23.1	2.39	2.57	18.26	0.79	18.05	0.78
T64-38-1	13.3	1.84	2.00	15.78	1.19	15.60	1.17
T64-48-1	20.8	2.33	2.53	17.99	0.86	17.88	0.86
T64-51-1	17.4	2.00	2.14	16.50	0.95	16.20	0.93
T64-64-1	15.5	2.52	2.69	18.84	1.22	18.57	1.20
T127-38-1	10.7	1.84	2.00	15.78	1.47	15.60	1.46
T127-48-1	17.7	2.33	2.53	17.99	1.02	17.88	1.01
T127-51-1	15.4	2.00	2.14	16.50	1.07	16.20	1.05
T127-64-1	18.3	2.52	2.69	18.84	1.03	18.57	1.01
T127-57-1	24.9	2.39	2.57	18.26	0.73	18.05	0.72

Note: l=76 mm for all the connections; Δ_r values exclude bolt slippage.

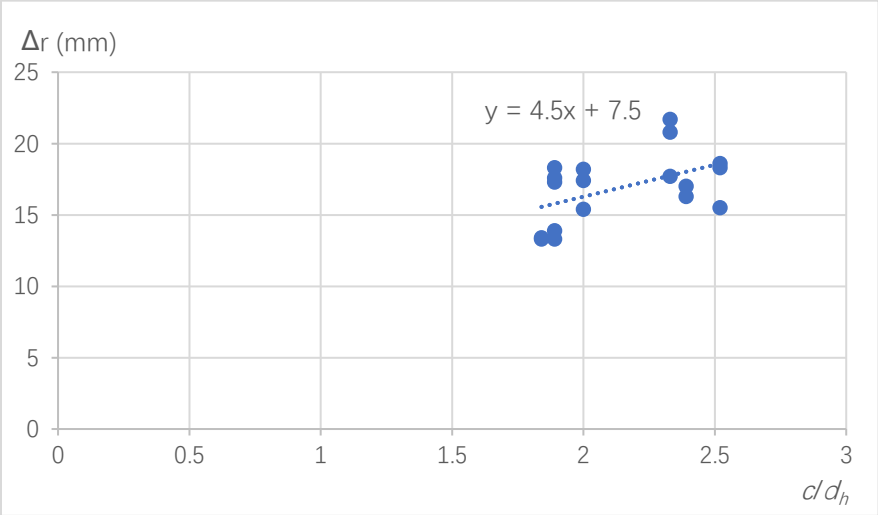

(a) Δ_r vs. c/d_h

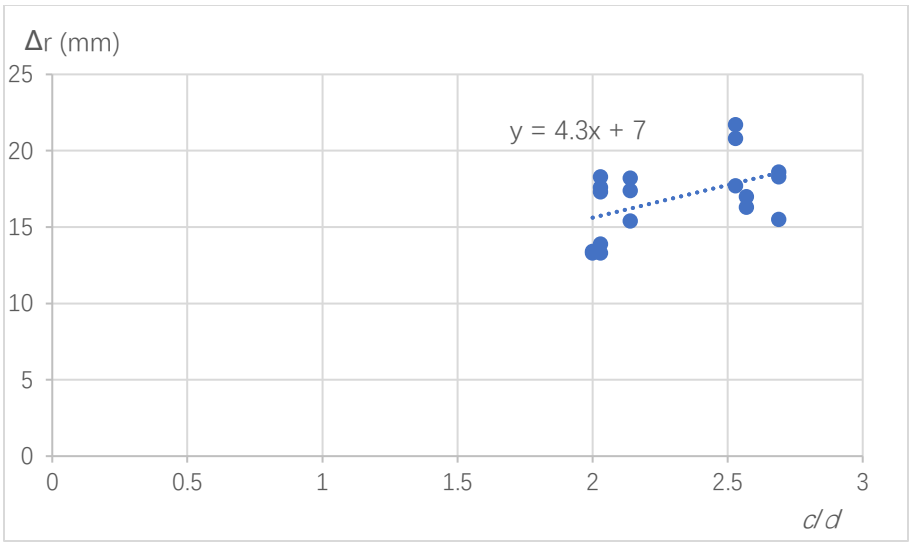

(b) Δ_r vs. c/d

Figure 5.8 Determination of Δ_r

From Table 5.7 and Figure 5.8, deformation Δ_r of a connection can be calculated as:

$$\Delta_r = \frac{4.5c}{d_h} + 7.5 \quad \text{mm}, \quad \text{or} \tag{5.16}$$

$$\Delta_r = \frac{4.3c}{d} + 7 \quad \text{mm} \tag{5.17}$$

From the calculation results in Tables 5.5 and 5.6, the predicted residual strength T_r from Equation (5.15) and its corresponding deformation Δ_r from Equations (5.16) and (5.17) are acceptable comparing with the T_r and Δ_r from the test or finite element models.

Chapter 6 Conclusions and future works

This chapter summarizes the research work of this thesis and provides some recommendations for future studies.

6.1 Summary and conclusions

This thesis consists of four parts: lab test, finite element modeling, parametric study, and load-deformation curve.

First, the test of two series of coupons and ten shear tab connections under a pure tension load were performed. The coupon test results included the material properties such as yield strength, ultimate strength and necking initiation strain. The shear tab connection test results included the failure modes and the load-deformation curves.

Second, software Abaqus was used to simulate the pure tension test of the shear tab connections. The test load-deformation curves and failure modes were used to calibrate the finite element models.

Third, the verified finite element models were employed to conduct a parametric study. Four parameters, i.e., plate thickness, edge distance, bolt diameter and shear load, were studied, which resulted in 15 simulations.

Last, a tri-linear curve was developed to predict the load versus deformation relationship of a shear tab connection having one-column bolts.

The following conclusions can be drawn from this research work:

1) Tensile rupture of the net section and bearing tear-out of the bolt hole side edge were the typical failure modes of the tested shear tab connections, for which the rupture of bolts or welds was precluded by a capacity design principle.

2) All the connections exhibited good ductility, i.e., experienced large plastic deformation before a rupture failure.

3) When the accompanying shear load was less than 45 percent of the tensile load, the impact of the shear load on the tensile strength and the tensile deformation of the shear tab connections could be ignored.

4) The actual load-deformation curves of the shear tab connections could be represented by a tri-linear curve, whose values at the three critical points are given by Equations (5.1) and (5.6),

Equations (5.10) and (5.14), and Equations (5.15) and (5.17), respectively.

Note that the developed tri-linear curve is valid under the following assumptions: (1) the bolt size ranges from 19 mm (3/4 in) to 25 mm (1 in); (2) the tab plate thickness ranges from 6.4 mm (1/4 in) to 12.7 mm (1/2 in); (3) the side edge distance of bolt holes ranges from 2 to 2.5 of the bolt diameter; (4) the pitch of the bolts is 76 mm (3 in); and (5) the distance between the boltline and the weldline is 80 mm.

6.2 Future works

The finite element models for the shear tab connections having two-column bolts need to be further calibrated to achieve a satisfactory accuracy.

When the shear load V was larger than $0.45T$, the preliminary simulation showed different failure modes (Figure 6.1), which could be investigated further.

A parametric study including bolt pitch and the distance between the boltline and the weldline should be conducted in a future study.

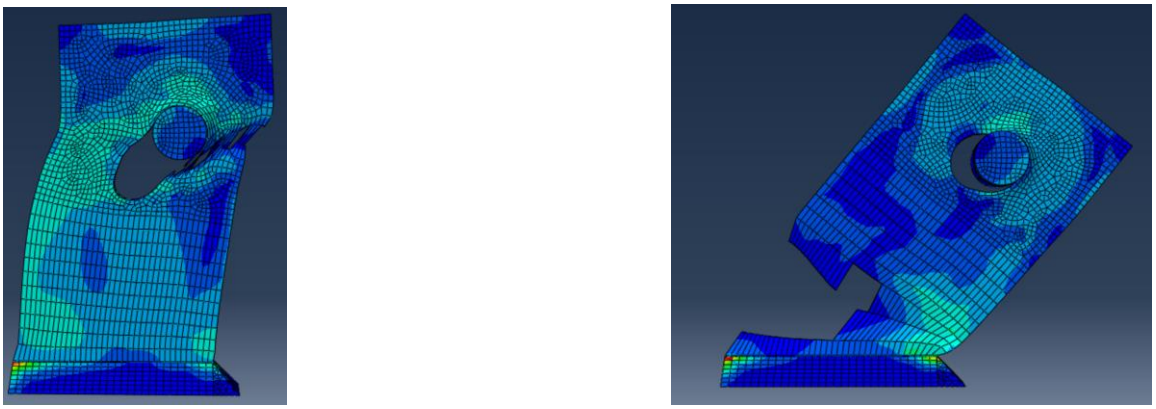

(a) (b)

Figure 6.1 Failure modes when $V > 0.45T$

References

Arasaratnam, P., Sivakumaran, K. S., & Tait, M. J. (2011). True stress-true strain models for structural steel elements. *ISRN Civil Engineering*, 2011, 1-11.

Ashakul, A. (2004). *Finite Element Analysis of Single Plate Shear Connections* (Doctoral dissertation, Virginia Tech).

Astaneh-Asl, A., McMullin, K.M., & Call, S. M. (1993). Behavior and design of steel single plate shear connections. *Journal of Structural Engineering,* 119(8), 2421-2440.

Canadian Institute of Steel Construction. (2014). CAS/S16-14 Design of steel structure. Canadian Standards Association, Toronto, *ON, Canada.*

Daneshvar H. & Driver R. G. (2011). Behavior of shear tab connections under column removal scenario. *In Structures Congress* 2011 (pp. 2905 -2916).

Daneshvar, H., & Driver, R. G. (2017). Behaviour of shear tab connections in column removal scenario. *Journal of Constructional Steel Research,* 138, 580-593.

Ehlers, S., & Varsta, P. (2009). Strain and stress relation for non-linear finite element simulations. *Thin-Walled Structures,* 47(11), 1203-1217.

Ferrell, M. T. (2003). Designing with single plate connections. *Modern Steel Construction,* 43(4), 51-53.

Gong, Y. (2009). Design moment of shear connections at the ultimate limit state. *Journal of Constructional Steel Research,* 65(10-11), 1921-1930.

Gong, Y. (2010). Analysis and design for the resilience of shear connections. *Canadian Journal of Civil Engineering,* 37(12), 1581-1589.

Gong, Y. (2014). Ultimate tensile deformation and strength capacities of bolted-angle connections. *Journal of Constructional Steel Research,* 100, 50-59.

Gong, Y. (2017). Test, modeling and design of bolted-angle connections subjects to column removal. *Journal of Constructional Steel Research,* 139, 315-326.

Guravich, S. J., & Dawe, J. L. (2006). Simple beam connections in combined shear and tension, *Canadian Journal of Civil Engineering,* 33(4), 357-372.

Hibbeler, R. C. (2014). *Mechanics of Materials.* US: Pearson Prentice Hall.

Hibbitt, K & Sorensen, I. (2000). *ABAQUS/CAE User's Manual*. US: Boston.

Kiran, R., & Khandelwal, K. (2014). A triaxiality and Lode parameter dependent ductile fracture criterion. *Engineering Fracture Mechanics,* 128, 121-138.

Levanger, H. (2012). *Simulating Ductile Fracture in Steel Using the Finite Element Mothed: Comparison of Two Models for Describing Local Instability due to Ductile Fracture* (Master's thesis).

Lipson, S. L. (1968, February). Single-angle and single-plate beam framing connections. *In Canadian Structural Engineering Conference, Toronto, Ontario* (pp. 141-162).

Logan, D. L. (2006). *A First Course in the Finite Element Method*. US: Chris Carson.

Mirzaei, A. (2014). *Steel Shear Tab Connections Subjected to Combined Shear and Axial Forces* (Doctoral dissertation: McGill University).

Oosterhof, S. A. & Driver, R. G. (2011). Performance of Steel Shear Connections under Combined Moment, Shear, and Tension. *Journal of Structural Engineering,* ASCE, University of Alberta, AB.

Oosterhof, S. A., & Driver, R. G. (2014). Behavior of steel shear connections under column-removal demands. *Journal of Structural Engineering,* ASCE, 141(4), 04014126.

Oosterhof, S. A., & Driver, R. G. (2016). Shear connection modelling for column removal analysis. *Journal of Constructional Steel Research,* 117, 227-242.

Rex, C. O., & Easterling, W. S. (1996). *Behavior and modeling of partially restrained composite beam-girder connections* (Virginia Polytechnic Institute and State University).

Rex, C. O., & Eastering, W. S. (2003). Behavior and modeling of a bolt bearing on a single plate. *Journal of Structural Engineering,* 129(6), 792-800.

Roddis, W. K., & Blass, D. (2013). Tensile capacity of single-angle shear connections considering prying action. *Journal of Structural Engineering,* 139(4), 504-514.

Sancho, A., Cox, M. J., Cartwright, T., Aldrich-Smith, G. D., Hooper, P. A., Davies, C. M., & Dear, J. P. (2016). Experimental techniques for ductile damage characterization. *Procedia Structural Integrity,* 2, 966-973.

Thompson, S. L. (2009). *Axial, Shear and Moment Interaction of Single Plate "Shear Tab" Connections* (Doctoral dissertation, Milwaukee School of Engineering).

Torrentallé Dot, M. (2015). *High strength steel fracture: fracture initiation analysis by the essential work of fracture concept* (Bachelor's thesis, Universitat Politècnica de Catalunya).

Yang, B., & Tan, K. H. (2013). Robustness of bolted-angle connections against progressive collapse: Experimental tests of beam-column joints and development of component-based models. *Journal of Structural Engineering,* ASCE*,* 139(9), 1498-1514.